

Iron Catalyzed Hydrogenation of Heavy Crude Oil Model Compounds

by

Benjamin Antwi Peprah

A thesis submitted in partial fulfillment of the requirements for the degree of

Doctor of Philosophy

In

Chemical Engineering

Chemical and Materials Engineering

University of Alberta

© Benjamin Antwi Peprah, 2023

Abstract

The development of economically viable processes for processing and transporting of heavy crude oil and bitumen are critical for continued development in the Canadian oil sands. Current technologies for preparing such crudes for transport to market include full upgrading to synthetic crude oil, or dilution before transport. An emerging family of technologies collectively referred to as partial upgrading can convert low-API gravity heavy crude oil into a refinery- and pipeline-grade product, with lower capital and operating expenses relative to current processes such as full upgrading or dilution. The processing goal of these technologies is to reduce both viscosity and density to enhance bitumen transportability while significantly reducing or avoiding the use of diluents. One key process in partial upgrading is the selective hydrogenation of the complex polycyclic aromatic molecules found in the asphaltene fraction. This approach alters the heavy oil structure, and thus reduces the viscosity and density of the oil, potentially resulting in a pipeline-ready product.

Developing efficient, practical, and economically viable catalytic processes for partial hydrogenation of heavy crude oils is an important research priority. Iron-based catalysts systems are ideal in this regard. Iron is earth-abundant, non-toxic, and inexpensive, making its utilization in heavy crude oil upgrading more attractive. Iron catalysts are usually less active than cobalt, nickel, or platinum-group transition metals for hydrogenation of aromatic molecules, but this is an advantage in partial upgrading. Selective hydrogenation and limited defunctionalization are preferred to more complete reactions mediated by commercially available hydroprocessing catalysts.

In this thesis, I explored partial hydrogenation and limited desulfurization reactions mediated by known air-stable, petroleum-soluble, and well-defined diiron sulfido complex, $\text{Fe}_2\text{S}_2(\text{CO})_6$.

Several polycyclic aromatic and heteroaromatic compounds were hydrogenated and desulfurized using $\text{Fe}_2\text{S}_2(\text{CO})_6$ as a precatalyst in a batch microreactors coupled with an agitator. The behavior of the catalyst system was evaluated over a wide range of temperatures, gas pressures, solvent systems, catalyst supports and metal loadings. The active phase, consisting of iron sulfide nanoparticles, was prepared from purified $\text{Fe}_2\text{S}_2(\text{CO})_6$ in toluene; no sulfur additive is required. The precatalyst is simple to prepare and recyclable, while the behavior of the system is highly reproducible. The results demonstrate that $\text{Fe}_2\text{S}_2(\text{CO})_6$ precatalyst leads to partial hydrogenation of polycondensed aromatics under moderate conditions using a carbon support. The reactivity trends show self-consistent substrate dependence, varying with the resonance energy stabilization of the starting compounds and partially saturated intermediates coupled with the surface adsorption enthalpy of the aromatic ring system.

Selective hydrogenation and defunctionalization of carbocyclic and heterocyclic aromatic heavy oil model compounds were also explored using unsupported $\text{Fe}_2\text{S}_2(\text{CO})_6$ exclusively. The reactivity of the anthracene series is governed by stereoelectronic effects imposed by the phenyl substituents, decreasing in the order anthracene > 9-phenylanthracene > 9,10-diphenylanthracene. Nitrogen- and sulfur-containing heterocycles are partially hydrogenated, with limited heteroatom removal for benzothiophene, showing that the unsupported iron sulfide catalyst is well-suited for the selective partial hydrogenation and limited defunctionalization, which are key for catalytic partial upgrading of heavy petroleum. The unsupported iron sulfide also catalyzes hydrogenation of mixed “feeds” comprising combinations of model compounds, demonstrating that carbocyclic and heterocyclic molecules can be processed simultaneously with little self-inhibition in overall activity, a key requirement for compositionally challenging bitumen feeds.

Hydrogen donor solvents can be substituted for hydrogen gas in these partial upgrading reactions. Unsupported iron sulfide catalysts derived from $\text{Fe}_2\text{S}_2(\text{CO})_6$ mediate transfer hydrogenation of carbocyclic- and N-heterocyclic aromatic compounds for the first time. Readily available hydrogen donors, including tetralin, 2-propanol, indane, indoline, and tetrahydroquinoline were tested. Using tetralin, indane or 2-propanol resulted in only limited hydrogenation of the target molecules, while indoline and tetrahydroquinoline hydrogen donors afforded near quantitative conversions. The thermodynamically favorable adsorption of N-heterocycles to the catalyst surface leads to facile dehydrogenation and hydrogen atom transfer to the substrate. The results demonstrate that a dual hydrogen donor system outperforms single donor systems to permit efficient transfer hydrogenation of various polycyclic aromatic and heteroaromatic compounds under moderate reaction conditions with good tolerance for alkyl and aryl substituents. Partially hydrogenated products are obtained in high yields with no “oversaturated” side products formed. This approach provides a cost-effective and viable catalytic protocol for partial upgrading of the challenging asphaltene fraction present in heavy crude oil, which requires partial saturation but limited heteroatom removal.

Preface

Two chapters of this work have been previously published and a third is ready to be submitted for publication. Chapter 2 of this thesis has been published as B. Antwi Peprah, O. Brown, J. M. Stryker, W. C. McCaffrey, “Sulfided Homogeneous Iron Precatalyst for Partial Hydrogenation and Hydrodesulfurization of Polycyclic Aromatic Model Asphaltenes”, *Energy & Fuels*, 34 (12), 2020, 16532-16541. I was responsible for the conceptualization, experimental design, precatalyst synthesis and purification, data collection and analysis, as well as the writing of original manuscript draft. Dr. O. Brown was supervisory author and was involved in the concept formation, precatalyst synthesis and purification, data interpretation, as well as editing of the manuscript first draft. Prof. J. M. Stryker was supervisory author and responsible for manuscript reviewing and editing, data interpretation, funding acquisition, and resources. Prof. W. C. McCaffrey was the supervisory and corresponding author and was involved in the conceptualization, data interpretation, and editing of the manuscript, as well as funding acquisition and resources. Dr. Jing Shen assisted with TEM imaging and XPS analysis. Dr. Asama Leduc helped with precatalyst synthesis and purification. Katie Nichols at the Department of Earth & Atmospheric Sciences assisted with XRD analysis. SEM analysis was done by a technician at the University of Alberta nanoFAB Fabrication and Characterization Centre. I presented this paper at the 258th American Chemical Society (ACS) Fall 2019 National Meeting & Exposition in San Diego, CA, USA.

Chapter 3 of this thesis has been published as B. Antwi Peprah, O. Brown, J. M. Stryker, W. C. McCaffrey, “Selective Hydrogenation and Defunctionalization of Heavy Oil Model Compounds Using an Unsupported Iron Catalyst”, *Fuel*, 333, 2023, 126184. I was responsible for the conceptualization, experimental design, data collection and analysis, as well as original manuscript composition. Dr. O. Brown was the supervisory and corresponding author and was involved in the concept formation, data interpretation, as well as editing of the manuscript first draft. Prof. J. M. Stryker was supervisory author and responsible for manuscript reviewing and editing, funding acquisition, and resources. Prof. W. C. McCaffrey was the supervisory author and was involved in data interpretation, editing of the manuscript, as well as funding acquisition. Katie Nichols at the Department of Earth & Atmospheric Sciences assisted with XRD analysis. TEM and SEM analyses were done by a technician at the University of Alberta nanoFAB Fabrication and Characterization Centre.

Chapter 4 of this thesis would be submitted for publication to *Industrial & Engineering Chemistry Research* as B. Antwi Peprah, O. Brown, J. M. Stryker, W. C. McCaffrey, “Efficient Unsupported Iron Catalyst for Transfer Hydrogenation of Carbocyclic and Heterocyclic Aromatic Compounds Using Mixed Hydrogen Donors”. I was responsible for the conceptualization, experimental design, data collection and analysis, as well as the writing of original manuscript draft. Dr. O. Brown was the supervisory author and was involved in the concept formation, data interpretation, as well as editing of the manuscript first draft. Prof. J. M. Stryker was supervisory author and responsible for manuscript reviewing and editing, funding acquisition, and resources. Prof. W. C. McCaffrey was the supervisory and corresponding author and was involved in data interpretation and editing of the manuscript, as well as funding acquisition.

Dedication

To my parents: Mr. Kwadwo Peprah Mensah and Mrs. Paulina Peprah Mensah.

Acknowledgements

I am incredibly thankful to *Prof. William C. McCaffrey* and *Prof. Jeffrey M. Stryker* for allowing me the opportunity to work on this research project and for seeing me through this thesis. Their inspiration and willingness to explain things in a clear and simple way have greatly influenced my way of thinking and approach to doing research. Thank you for sharing with me your thoughts about science and, more importantly, about life. I feel very fortunate to have had the opportunity to work with both professors.

My profound gratitude goes to *Dr. Orain Brown*, a complete description of a “true scientist” and a “brother”, for all the supervision and extremely helpful discussions throughout my PhD studies. When I was entirely lost in my PhD program, he came to my rescue and helped me synthesize the iron complex which is the backbone of my entire research work. He was responsible for conceptualization, project administration, writing (reviewing and editing), and supervision. I am forever grateful, *Dr. Brown*.

My sincere thanks to my thesis committee members *Prof. Natalia Semagina*, *Prof. Vinay Prasad*, *Prof. Hani Henein*, and *Prof. Jorge Ancheyta*.

Special thanks to *Daniel Palys*, *Dr. Cedric Laborde-Boutet*, *Dr. Shaofeng Yang*, *Anirban Chakraborty*, *Dr. Jing Shen*, *Dr. Robin Hamilton*, *Katie Nichols*, *Dr. Asama Vorapattanapong*, and technicians at the University of Alberta nanoFAB Fabrication and Characterization Centre.

To *Bridget*, thank you for all the love, encouragement, understanding, sacrifices, and prayer support. Thanks for giving me faith when I lost it, for being my strength and for trusting and believing in me since day one.

Also, I wish to express my deepest appreciation to my family: my parents, Mr. and Mrs. Peprah Mensah and siblings who were my greatest source of inspiration. Your continued prayers made the biggest difference in my life.

Most importantly, I'm forever grateful to Almighty God for giving me the strength to pursue my PhD.

Table of Contents

| | |
|--|------|
| List of Tables | xiii |
| List of Figures | xiv |
| Chapter 1: Introduction | 1 |
| 1.1. Background | 1 |
| 1.2. Research goals and thesis organization | 20 |
| 1.3. References | 21 |
| Chapter 2: Sulfided Homogeneous Iron Precatalyst for Partial Hydrogenation and Hydrodesulfurization of Polycyclic Aromatic Model Asphaltenes | 30 |
| 2.1. Introduction | 30 |
| 2.2. Experimental section | 32 |
| 2.2.1. Materials | 32 |
| 2.2.2. Precatalyst preparation | 32 |
| 2.2.3. Characterization techniques | 33 |
| 2.2.3.1. Thermogravimetric analysis (TGA) | 33 |
| 2.2.3.2. Elemental analysis | 34 |
| 2.2.3.3. Fourier transform infrared spectroscopy (FT-IR) | 34 |
| 2.2.3.4. X-ray diffraction (XRD) | 34 |
| 2.2.3.5. X-ray photoelectron spectroscopy (XPS) | 34 |
| 2.2.3.6. Scanning transmission electron microscopy (STEM) | 35 |
| 2.2.3.7. Scanning electron microscopy (SEM) | 35 |
| 2.2.4. Catalytic activity determinations | 36 |
| 2.3. Results and discussion | 37 |
| 2.3.1. Precatalyst characterization | 37 |
| 2.3.2. Catalyst characterization | 38 |
| 2.3.3. Catalytic activity | 41 |
| 2.3.4. Optimization and scope of catalytic arene hydrogenations | 45 |
| 2.3.4.1. Influence of iron concentration on the hydrogenation of pyrene (1) | 45 |
| 2.3.4.2. Influence of pressure and temperature on hydrogenation rate and conversion | 47 |
| 2.3.4.3. Scope of aromatic hydrogenation | 49 |
| 2.3.4.4. Hydrodesulfurization of benzothiophene | 50 |
| 2.4. Conclusions | 52 |
| 2.5. References | 53 |

| | |
|--|-----|
| 2.6. Associated content | 58 |
| Chapter 3: Selective Hydrogenation and Defunctionalization of Heavy Oil Model Compounds Using an Unsupported Iron Catalyst | 59 |
| 3.1. Introduction | 59 |
| 3.2. Experimental section | 63 |
| 3.2.1. Materials | 63 |
| 3.2.2. Methods | 64 |
| 3.2.3. Precatalyst preparation | 64 |
| 3.2.4. Catalytic procedures, product, and catalyst recovery | 65 |
| 3.2.5. Liquid product characterization | 66 |
| 3.2.6. Catalytic solids characterization techniques | 67 |
| 3.2.6.1. Scanning electron microscopy | 67 |
| 3.2.6.2. Transmission electron microscopy | 67 |
| 3.2.6.3. X-ray diffraction | 67 |
| 3.3. Results and discussion | 68 |
| 3.3.2. Hydrogenation of anthracenes over unsupported $\text{Fe}_2\text{S}_2(\text{CO})_6$ | 69 |
| 3.3.3. Mixed feeds: carbocyclic and N- and S-heterocyclic compounds | 73 |
| 3.3.4. Hydrotreating phenoxathiin and acridine | 75 |
| 3.3.5. Effects of extraneous sulfur | 77 |
| 3.3.6. Effects of precatalyst on anthracene hydrogenation | 78 |
| 3.4. Conclusions | 80 |
| 3.5. References | 81 |
| 3.6. Associated content | 85 |
| Chapter 4: Efficient Unsupported Iron Catalyst for Transfer Hydrogenation of Carbocyclic and Heterocyclic Aromatic Compounds Using Mixed Hydrogen Donors | 86 |
| 4.1 Introduction | 86 |
| 4.2. Experimental section | 89 |
| 4.2.1. Materials | 89 |
| 4.2.2. Precatalyst preparation | 89 |
| 4.2.3. Transfer hydrogenation reactions | 89 |
| 4.3. Results and discussion | 91 |
| 4.3.1. Scope of catalytic transfer arene hydrogenations | 97 |
| 4.3.2 Catalyst recycling | 101 |
| 4.4. Conclusions | 102 |

| | |
|--|-----|
| 4.5. References | 103 |
| Chapter 5: Conclusions and Recommendations for Future Work | 107 |
| 5.1. Conclusions | 107 |
| Bibliography | 110 |
| Appendix A: Chapter 2 Supporting Information | 133 |
| A.1. Product ranks and reaction network schemes | 133 |
| Appendix B: Chapter 3 Supporting Information | 137 |

List of Tables

| | |
|--|-----|
| Table 1.1. Common bond dissociation energies in upgrading (McMillen and Golden data, 1982). | 6 |
| Table 1.2. Summary of industrial non-catalytic thermal processing technologies (Rana et al., 2007; Gray, 2015). | 7 |
| Table 1.3. Summary of the various iron sulfide phases (Rickard and Luther, 2007; Ning et al., 2013). | 13 |
| Table 1.4. Summary of various iron sulfide catalyst systems in crude oil processing. | 17 |
| Table 1.5. Petroleum upgrading using hydrogen donors. | 19 |
| Table 2.1. Catalytic effects of iron precatalysts and elemental sulfur on pyrene hydrogenation. | 43 |
| Table 3.1. Hydrogenation of anthracene over iron precatalysts. | 79 |
| Table 4.1. Screening of optimal reaction conditions. | 93 |
| Table 4.2. Substrate scope of carbocyclic and heterocyclic aromatic compounds under unsupported iron-catalyzed transfer hydrogenation using mixed hydrogen donors. | 98 |
| Table 4.3. Unsupported iron-catalyzed transfer hydrogenation of quinoline derived substrates using mixed hydrogen donors. | 100 |

List of Figures

| | |
|---|----|
| Figure 1.1. Heavy crude oil comparison based on density and viscosity (adapted from ref 10). | 3 |
| Figure 1.2. Generic process flow diagram for a typical bitumen upgrader (adapted from ref 14) | 4 |
| Figure 1.3. Diluent cost in transporting bitumen (adapted from ref 34). | 9 |
| Figure 1.4. Flow diagram of bitumen production to the refinery: Two paths for Alberta's diluted bitumen (adapted from ref 14) | 10 |
| Figure 1.5. Cubic pyrite unit cell (adapted from ref 74). | 15 |
| Figure 1.6. NiAs-like unit cell, common for all pyrrhotites (adapted from ref 88). | 16 |
| Figure 2.1. Model heavy crude oil compounds used to evaluate hydrogenation using $\text{Fe}_2\text{S}_2(\text{CO})_6$. | 31 |
| Figure 2.2. Schematic illustration of the synthesis of $\text{Fe}_2\text{S}_2(\text{CO})_6$. Colors are approximate. | 35 |
| Figure 2.3. TGA of $\text{Fe}_2\text{S}_2(\text{CO})_6$. | 37 |
| Figure 2.4. FT-IR spectrum of $\text{Fe}_2\text{S}_2(\text{CO})_6$. | 38 |
| Figure 2.5. (a-d) SEM, EDX mapping images, and corresponding size distribution as well as (e-g) TEM and HR-TEM images coupled with particle size distribution of the FeS nanoparticles produced at 300 °C and 5000 ppm Fe. Inset: fast Fourier transform (FFT) pattern. | 39 |
| Figure 2.6. XRD patterns of carbon-supported FeS nanocatalyst produced at 300 °C, 6 MPa cold H_2 , and 5000 ppm Fe. | 40 |
| Figure 2.7. XPS spectra for (a) Fe 2p _{3,2} and (b) S 2p _{3,2} from the FeS nanocatalyst produced at 300 °C and 5000 ppm Fe. | 41 |
| Figure 2.8. Structures of the products from pyrene hydrogenation. | 42 |
| Figure 2.9. Relationship between $\text{Fe}_2\text{S}_2(\text{CO})_6$ loading and product distribution of pyrene. Reaction conditions: temperature, 300 °C; cold H_2 , 6 MPa; activated carbon, 0.1 g; time, 60 min. | 46 |
| Figure 2.10. Ratio of pyrene conversion and iron mass against Fe loading. Reaction conditions: temperature, 300 °C; cold H_2 , 6 MPa; activated carbon, 0.1 g; time, 60 min. | 47 |
| Figure 2.11. (a) Pyrene pressure profile and influence of temperature on (b) pyrene (c) phenanthrene and (d) naphthalene hydrogenation over $\text{Fe}_2\text{S}_2(\text{CO})_6$. Reaction conditions: temperature; 250-350 °C; cold H_2 , 2-10 MPa; activated carbon, 0.1 g; time, 60 min. | 48 |
| Figure 2.12. Phenanthrene and naphthalene hydrogenation products. | 49 |

| | |
|---|----|
| Figure 2.13. (a) Benzothiophene hydrodesulfurization products and (b) relationship between temperature and product distribution for the hydrodesulfurization of benzothiophene over $\text{Fe}_2\text{S}_2(\text{CO})_6$. Reaction conditions: temperature, 250-350 °C; cold H_2 , 6 MPa; activated carbon, 0.1 g; time, 60 min. | 51 |
| Figure 3.1. Heavy crude oil model compounds used to evaluate hydrogenation using unsupported catalyst from $\text{Fe}_2\text{S}_2(\text{CO})_6$. | 63 |
| Figure 3.2. Graphical representation of the methods used for experimentation | 64 |
| Figure 3.3. Schematic diagram of the batch microreactor. | 65 |
| Figure 3.4. (a-d) SEM, EDX mapping images, and corresponding size distribution as well as (e) TEM and (f) HR-TEM images of the FeS nanocatalyst at 300 °C and 60 min. | 68 |
| Figure 3.5. XRD pattern of unsupported FeS nanoparticles at 300 °C and 60 min. | 69 |
| Figure 3.6. Conversion time profiles of (a) anthracene, 9-phenylanthracene, and 9,10-diphenylanthracene as well as their product distribution (b-d), respectively. Reaction conditions: temperature, 300 °C; cold H_2 , 6 MPa; substrate to active metal (Fe) molar ratio, 1.67 mol/mol; time, 15-180 min. | 71 |
| Figure 3.7. Structures of the products from the hydrogenation of anthracene, 9-phenylanthracene and 9,10-diphenylanthracene. | 73 |
| Figure 3.8. Effect of combining carbocycles with (a) quinoline and (b) benzothiophene on hydrogenation under unsupported $\text{Fe}_2\text{S}_2(\text{CO})_6$. Reaction conditions: temperature, 300 °C; cold H_2 , 6 MPa; substrate to Fe molar ratio, 1.67 mol/mol; time, 60 min. | 74 |
| Figure 3.9. 1,2,3,4-tetrahydroquinoline, 2,3-dihydrobenzothiophene, and ethylbenzene. | 75 |
| Figure 3.10. Conversion of (a) quinoline and (b) benzothiophene in the presence of either anthracene, 9-phenylanthracene, or 9,10-diphenylanthracene. Reaction conditions: temperature, 300 °C; cold H_2 , 6 MPa; substrate to active metal (Fe) molar ratio, 1.67 mol/mol; time, 60 min. | 75 |
| Figure 3.11. Phenoxathiin hydrodesulfurization and acridine hydrogenation products. | 76 |
| Figure 3.12. Effect of sulfur concentration on the catalytic hydrogenation of 9-phenylanthracene and 9,10-diphenylanthracene. Reaction conditions: temperature, 300 °C; cold H_2 , 6 MPa; time, 60 min. Standard error values are one standard deviation. | 78 |
| Figure 4.1. (a) Anthracene conversion as a function of temperature using tetralin as hydrogen donor and (b) tetralin conversion with temperature in the absence of a hydrogen acceptor. Reaction conditions: temperature, 200-350°C; cold N_2 , 6 MPa; $\text{Fe}_2\text{S}_2(\text{CO})_6$ (Fe, 0.12 mmol); Substrate to Fe molar ratio, 1.67 mol/mol; time, 30 min; anthracene, 0.2 mmol; toluene, 2.5 mL; tetralin, 2.5 mL in (a) and 0.20 mmol in (b). | 92 |

Figure 4.2. Iron-catalyzed dehydrogenation of various hydrogen donor compounds. Reaction conditions: temperature, 350 °C; cold N₂, 6 MPa; Fe₂S₂(CO)₆ (Fe, 0.12 mmol); Hydrogen donor to Fe molar ratio, 1.67 mol/mol; time, 30 min; hydrogen donor, 0.20 mmol; toluene, 2.5 mL. 95

Figure 4.3. Anthracene conversion as a function of (a) indoline concentration at 350 °C and (b) temperature. Reaction conditions: temperature, 250-350 °C; cold N₂, 6 MPa; anthracene, 0.2 mmol; toluene, 2.5 mL; tetralin, 2.0 mL; indoline, 0.05-0.5 mL; Fe, 0.12 mmol; time, 30 min. 96

Figure 4.4. Catalyst recycling for the transfer hydrogenation of quinoline to tetrahydroquinoline. Reaction conditions: substrate, 0.2 mmol; temperature, 325 °C; cold N₂, 6 MPa; toluene, 2.5 mL; tetralin, 2.0 mL; indoline, 0.2 mL; Fe₂S₂(CO)₆ (Fe, 0.12 mmol); time, 30 min. 102

Figure A1. First-rank Delplots of (a) pyrene and (b) phenanthrene, and (c) benzothiophene. Second-rank Delplots of (d) pyrene, (e) phenanthrene, and (f) benzothiophene. Reaction conditions: temperature; 250-350 °C; cold H₂, 6 MPa; activated carbon, 0.1 g; time, 60 min. 134

Figure A2. Reaction networks proposed for (a) pyrene, (b) phenanthrene, and (c) naphthalene, hydrogenation, and (d) benzothiophene hydrodesulfurization over Fe₂S₂(CO)₆. Structures: 4,5-dihdropyrene (**5**), 4,5,9,10-tetrahydropyrene (**6**), 1,2,3,3a,4,5-hexahdropyrene (**7**), 1,2,3,6,7,8-hexahdropyrene (**8**), 9,10-dihydrophenanthrene (**9**), 1,2,3,4-tetrahydrophenanthrene (**10**), 1,2,3,4-tetrahydronaphthalene (**11**), 2,3-dihydrobenzothiophene (**12**), and ethylbenzene (**13**). 135

Figure B1. Reaction networks proposed for (a) anthracene and (b) 9-phenylanthracene hydrogenation over unsupported Fe₂S₂(CO)₆. Structures: anthracene (**1**), 9-phenylanthracene (**2**), 9,10-dihydroanthracene (**8**), 1,2,3,4-tetrahydroanthracene (**9**), 9,10-dihydrophenylanthracene (**10**), 1,4-dihydrophenylanthracene (**11**), and 1,2,3,4-tetrahydrophenylanthracene (**12**). 137

Figure B2. Reaction networks for hydrogenation (a) 9,10-diphenylanthracene (b) quinoline as well as hydrodesulfurization of (c) benzothiophene over unsupported Fe₂S₂(CO)₆. Structures: 9,10-diphenylanthracene (**3**), quinoline (**4**), benzothiophene (**5**), trans-9,10-dihydro-9,10-diphenylanthracene (**13**), cis-9,10-dihydro-9,10-diphenylanthracene (**14**), 1,2,3,4-tetrahydrodiphenylanthracene (**15**), 1,4-dihydrodiphenylanthracene (**16**), 1,2,3,4-tetrahydroquinoline (**17**), 2,3-dihydrobenzothiophene (**18**), and ethylbenzene (**19**). 138

Figure B3. Reaction networks for hydrotreating of (a) phenoxathiine and (b) acridine.1,2 Structures: phenoxathiin (**6**), acridine (**7**), diphenyl ether (**20**), 9,10-dihydroacridine (**21**), 1,2,3,4-tetrahydroacridine (**22**), 1,2,3,4,4a,9,9a,10-octahydroacridine (**23**), and 1,2,3,4,5,6,7,8- octahydroacridine (**24**). 139

Figure B4. Structures of 1,2,3,4,4a,9,9a,10-octahydroanthracene (**25**) and 1,2,3,4,5,6,7,8-octahydroanthracene (**26**). 139

Figure B5. XRD pattern of unsupported catalyst derived from $\text{Fe}(\text{CO})_5$ at 300 °C and 60 min. It is ascribed to iron carbide phase (Jade 9.0 PDF No. 00-036-1248).

140

Chapter 1: Introduction

1.1. Background

Crude oil is the most widely used and one of the most reliable energy sources in the world. Despite an intensifying transition to more renewable fuels sources, the International Energy agency (IEA) projects that crude oil use is expected to increase by 21% before 2040. This will largely be driven by continued growth in the economies of developed countries coupled with rising standards of living and consumption in emerging economies.¹ This increasing demand for crude oil in conjunction with stringent regulations on emissions of greenhouse gases from the petrochemical industry will drive significant innovations in extraction and processing of crude oil globally.

Of the global total estimated crude oil reserves more than half are described as unconventional crude oil deposits.² This means that development and utilization of these unconventional petroleum resources is crucial for meeting current and the future global energy demand. Unconventional crude includes resources which require enhanced methods of extraction and processing beyond the typical well to pipeline to refinery routine. Examples include bitumen, heavy and extra-heavy crude oil, oil sands, and oil shale.² These unconventional crude oil reserves are predominantly found in Canada, the United States of America, Venezuela, Asia, and Russia.³⁻⁵ Ongoing geopolitical instability makes resource development in Russia and Venezuela financially risky and thus less attractive. Canadian oil sands which represent the third-largest proven oil reserves in the world, enjoy an ideal combination of relative insulation from geopolitical conflicts and relatively low cost of development and extraction.^{3,6,7} In 2020, production in the Canadian oil sands contributed 4.04 million barrels of crude oil per day to the global market.⁸ This amount is increasing with Canadian crude oil production rising by 2.6 million barrels per day over the last three decades, largely because of the continuous growth in supply from the oil sands.

Oil sands are a natural mixture of water, mineral solids (clays and quartz), and bitumen.^{9,10} Canada oil sands have three main deposits located across Alberta and Saskatchewan, namely Athabasca, Cold Lake, and Peace River. Although majority of the oil is found deeper underground, some is located within 70 meters (200 ft) of the surface. The method of extraction depends on the depth of the oil deposits. For deeper deposits, wells are drilled, and the oil pumped to the surface, usually with the assistance of heated fluids to reduce viscosity and improve flow. Shallow deposits are mined and then the oil is separated from the sandy matrix in which it is entrained. About 80% of the oil in the Canadian oil sands is extracted by the drilling, while the remaining 20% is surface mined using large shovels and trucks.

The recovery, processing, and transportation of Alberta crude to refineries presents a series of challenges for the petroleum industry.¹¹ This is principally due to the density, viscosity, API gravity, and chemical composition of the petroleum deposits.¹⁰ Classification of the various crude oil based on these key properties is shown in Figure 1.1. Compared to the most important North American benchmark crude, the West Texas Intermediate (WTI), oil sands crude oils are denser and more viscous. As a result, oil sands crude typically trades at a significant discount relative to WTI. More importantly the natural density and viscosity of oil sands crude are much greater than the maximum pipeline specifications, and so further processing is required before transportation through established pipeline networks.

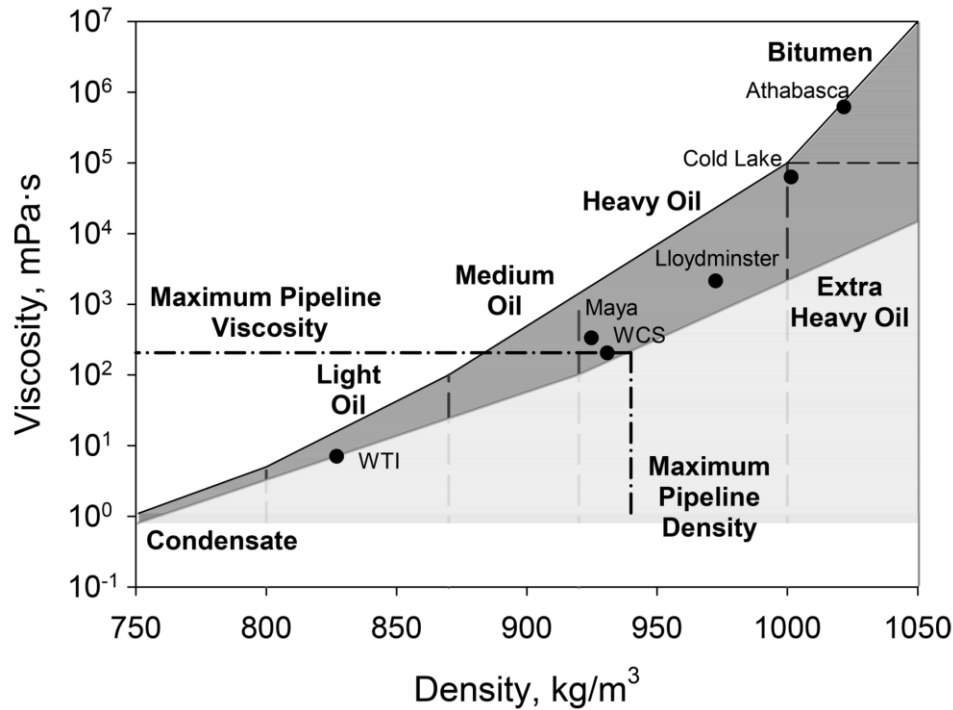


Figure 1.1. Heavy crude oil comparison based on density and viscosity (adapted from ref 10).

To meet pipeline specifications for transport to refineries, heavy crude oils must be upgraded in an energy- and greenhouse gas-intensive process to produce less dense and less viscous products. The Alberta Energy Regulator (AER) estimates that in 2020 about 1.3 million barrels of bitumen were transported for upgrading in Canada each day. This represents 42% of total bitumen production.⁵ The remaining 58% of crude is blended with diluents to achieve pipeline specifications, then transported to refineries. Developing more economical and environmentally friendly processing technologies for the upgrading of heavy crude oil is critical for supporting continued growth in oil sands production to meet both Canada's and global energy demands.

The main aim of heavy oil/ bitumen upgrading is to increase the hydrogen to carbon atomic ratio (H/C) thus lowering viscosity and density. To accomplish this task, various upgrading technologies have been developed and are classified as separation, carbon rejection, or hydrogen addition

processes (Figure 1.2). The degree to which any of these processes is done determines whether the bitumen is fully or partially upgraded, and the choice is usually based on prevailing economic factors.^{12,13}

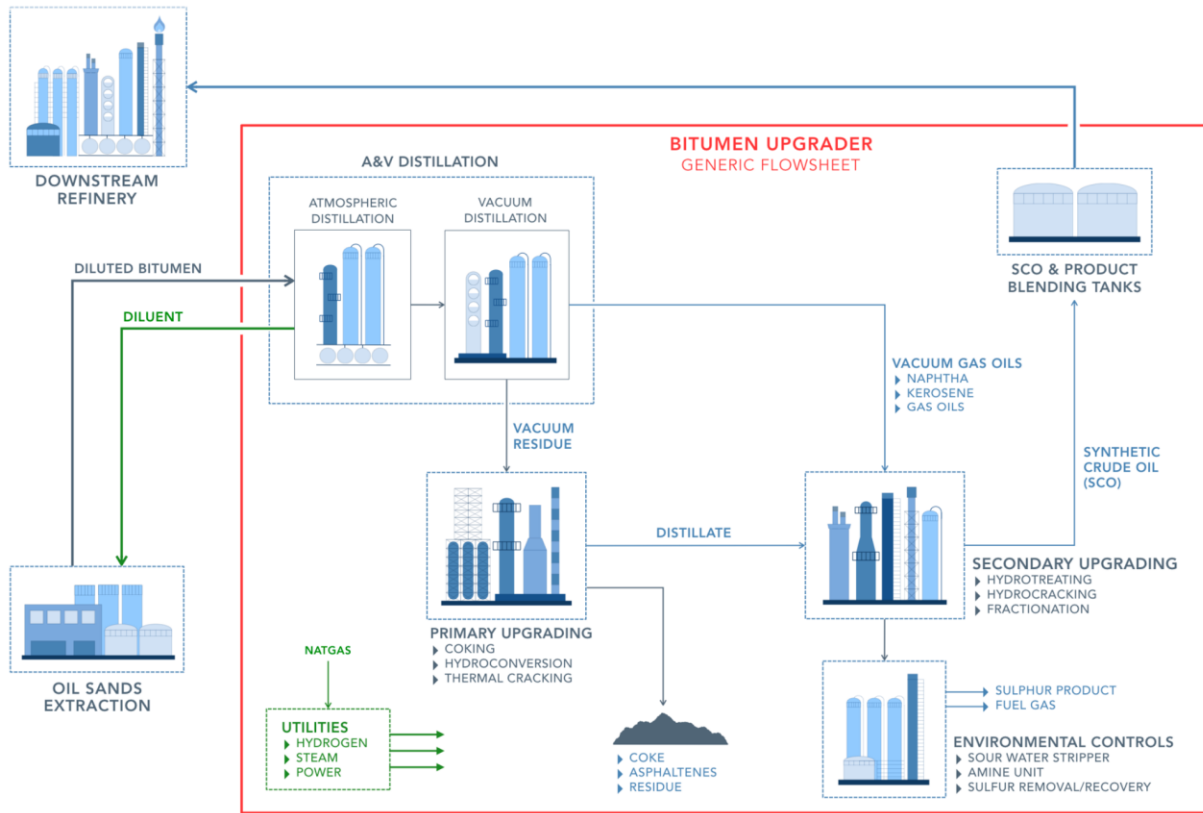


Figure 1.2. Generic process flow diagram for a typical bitumen upgrader (adapted from ref 14)

Separation processes are used largely to remove the heaviest and most problematic fraction from heavy crude oils: asphaltenes. For analysis, crude oils can be divided into several components based on polarity, saturates, aromatics, resins and asphaltenes. The saturates and aromatics fraction consists of low polarity aliphatic and small aromatic molecules. Resins and asphaltenes contain polar substituents with the distinction between the two fractions being that resins are miscible with pentane and *n*-heptane; asphaltenes are not. Asphaltenes contain the heaviest and most polar

fraction of crude oil. This fraction is soluble in aromatic solvents, such as benzene and toluene, and insoluble in linear *n*-alkanes, such as *n*-pentane and *n*-heptane.¹⁵ The high polarity and complex composition of asphaltenes results in a highly aggregated supramolecular structure which easily forms precipitates and is difficult to unravel. As a result, precipitated asphaltenes are responsible for blocking pipelines, deactivating catalysts, and causing deposition on the internal surface of reservoirs.¹⁶ Understanding the chemical structure and behavior of asphaltenes remains crucial for improving production processes of heavy crude oil. Asphaltenes are typically removed from crude oil by precipitation in the presence of paraffinic solvents. The yield of asphaltenes during precipitation is influenced by temperature, pressure, solvent polarity, molecular weight, ratio of solvents to asphaltenes, aromaticity (presence of polynuclear aromatic compounds), and precipitation time.¹⁷ Mitchell and Speight¹⁸ extracted asphaltenes from Athabasca bitumen via precipitation using various solvents and their blends and reported that the different yields of the asphaltene fraction correlated linearly with the variations in the solubility parameter of the solvents. Importantly, asphaltenes were removed from bitumen by addition of 40 volumes of the solvent. To produce high asphaltene yields, it is important to make use of the following parameters: *n*-pentane or *n*-heptane as solvents, 8-10 h contact time, minimum of 30 mL solvent per gram feedstock, and employ a precipitation sequence to remove any adsorbed resin from the asphaltene fraction.¹⁹

The second method for upgrading heavy crude oil is carbon rejection. Carbon rejection uses thermal processes to separate heavy crudes into coke and lighter crude oil. These processes have been used in the petroleum industries since 1913 and includes catalytic thermal cracking (fluid catalytic cracking, FCC) and non-catalytic cracking (delayed coking, visbreaking, and fluid coking).^{10,20} They are also used to upgrade vacuum residue; the fraction remaining after heavy oil

is processed by a vacuum distillation column. Thermal conversion is the oldest but still the most popular choice used globally to process bitumen and vacuum residue owing to its relatively low operating costs. An increasing focus on greenhouse gas emissions and the associated carbon pricing regimes can change these economics significantly.

Thermal cracking relies on high temperatures ($> 400^{\circ}\text{C}$) to convert large molecules into smaller more volatile fragments via a complex free-radical chain reaction mechanism.²¹ Thermodynamics governs bonds breakage and the minimum energy required to cleave a stable chemical bond is shown in Table 1.1.

Table 1.1. Common bond dissociation energies in upgrading²²

| Chemical bond | Energy, kJ/mol |
|----------------------|-----------------------|
| C-C (aliphatic) | 344 |
| C-H (primary) | 411 |
| C-H (secondary) | 398 |
| C-H (aromatic) | 464 |
| C-S | 307 |
| C-N | 342 |
| C-O | 344 |

Fluid catalytic cracking is a process used for cracking high-boiling distillates to gasoline and diesel fuel in the presence of a fine-powdered catalyst in fluid beds. This process is limited to good quality feedstock mainly due to rapid catalyst deactivation by asphaltene rich feeds.^{10,23}

Visbreaking is a mild thermal, non-catalytic cracking process in which heavy oil is heated in a furnace ($450\text{-}500^{\circ}\text{C}$ at furnace outlet) with a residence time of 1-3 minutes to reduce its viscosity.^{24,25} The severity is controlled to favor low coke formation and avoid sediment deposition during storage.²⁶ Delayed coking is a semi-batch process used to transform various oil feeds into

gases, distillates, and coke at long reaction times and temperatures up to 500°C. Although it produces significant yields of coke, it is the most widely used technology for refiners to convert residues principally due to its simplicity, good feed flexibility, and relatively low capital expenditure and operating costs.²³ Fluid coking is a continuous process operated at a short reaction time relative to delayed coking and uses hot coke particles to increase the feed temperature up to about 510-550°C. Unfortunately, the process liberates significant amounts of sulfur dioxide from combustion of coke particles.¹⁰ Detailed operating conditions for the various non-catalytic thermal processes is illustrated in Table 1.2.

Table 1.2. Summary of industrial non-catalytic thermal processing technologies^{10,23}

| Technology | Temperature (°C) | Pressure (MPa) | Capital cost | Severity | Conversion |
|-------------------|-------------------------|-----------------------|---------------------|-----------------|-------------------|
| Visbreaking | 450-500 | 0.3-2.1 | low | low | low |
| Delayed coking | 450-500 | 0.6 | low | high | high |
| Fluid coking | 510-560 | 0.7 | medium | high | high |

The final class of upgrading technologies is hydrogen addition. Adding hydrogen converts heavy crude into higher value oil at the expense of increased hydrogen costs. Adding hydrogen is achieved by using either hydroconversion, hydrocracking, or hydrotreating processes. Hydroconversion uses high temperature (> 410°C) and catalyst to promote thermal cracking and aromatics hydrogenation while suppressing coke formation. Hydrocracking processes use catalyst along with high-pressure hydrogen to induce significant cracking of chemical bonds along with hydrogenation of unsaturated molecules. Hydrotreating typically operates at lower temperatures (< 410°C) which prevent significant cracking reactions. Instead, a catalyst and a high partial pressure of hydrogen promote removal of heteroatoms (S, N, and O) and metals (Ni and V) from

feeds.²⁷⁻²⁹ This process lowers the polarity and hence aggregation in the feed, leading to a less viscous product. Fixed-bed, ebullated-bed, and slurry phase reactors are all used in hydroprocessing with the selection depending on the process objective, feedstock characteristics, operating conditions, and refinery requirements.^{30,31}

A combination of the technologies described so far can convert raw bitumen to synthetic crude oil (SCO) (Figure 1.2), a high-grade product resembling light crude oil. Typically, SCO is produced via feed separation (distillation, desalting, and desasphalting), primary upgrading (thermal cracking, coking, and hydroconversion), and secondary upgrading (hydrotreating and hydrocracking).¹⁰ Generally, SCO production is capital intensive, and the product competes in a crowded marketplace dominated by light crude producers in the United States of America.³² In 2017, nearly 40% of raw bitumen was sent for upgrading,³³ however, the existing full upgrading facilities are complex and expensive to operate. The estimated cost in 2013 of the proposed Suncor Voyager Full Upgrader, a 60,000 bbl/day facility was \$11.5 billion.³⁴ The project was eventually cancelled. Similarly, the operation of CNOOC's upgrader at the Long Lake in situ project was suspended in 2016 after an accident damaged the facility.³² Currently, there are only four full upgraders operating in Alberta, which processes 42% of crude produced in the province. Because of high costs investing in new facilities adjacent to bitumen extraction sites is economically unattractive.

The majority of heavy crude oil that is not upgraded in Alberta is blended with natural gas condensate, naphtha, or SCO prior to transporting to petroleum refineries. Most of the bitumen shipped to U.S refining markets via pipelines is diluted bitumen (dilbit). The cost of diluent used to transport bitumen to the U.S Gulf Coast (USGC) in the second quarter of 2017 was about

US\$14/bbl of bitumen (Figure 1.3). The current cost of natural gas condensate is US\$84 in November, 2022.³⁵

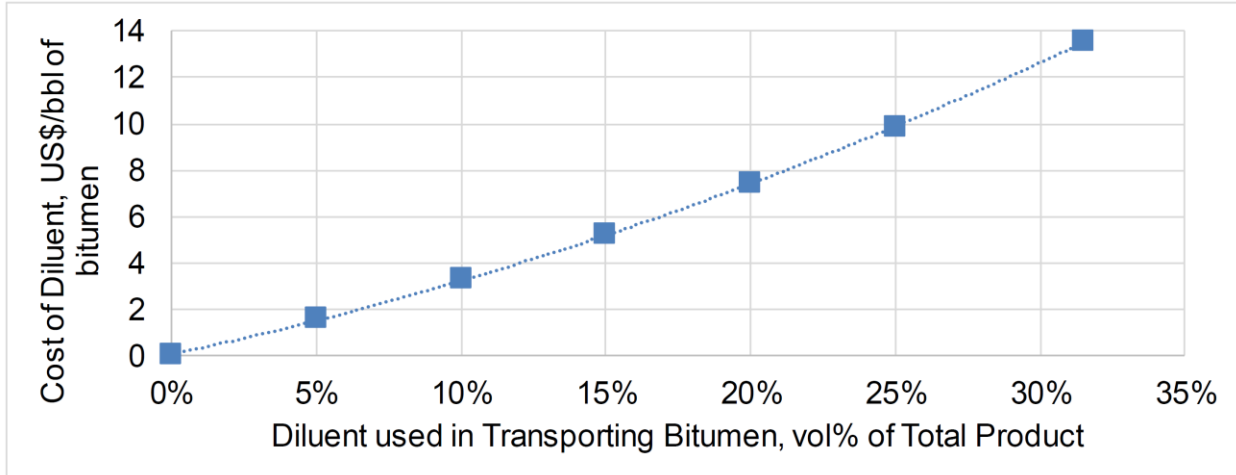


Figure 1.3. Diluent cost in transporting bitumen (adapted from ref 34).

Additionally, diluent occupies 30-50% of pipeline effective volume, limiting transportable bitumen and costs of recovering and recycling the diluents is high. Dilution is therefore costly and unattractive though necessary approach to transporting heavy crude oil (Figure 1.4).³⁴ To address the economic constraints of both full upgrading and dilution, a new set of technologies have been proposed which avoids the high capital costs of full upgraders and the high ongoing costs and complex logistics of dilution. This new direction is referred to as partial upgrading.

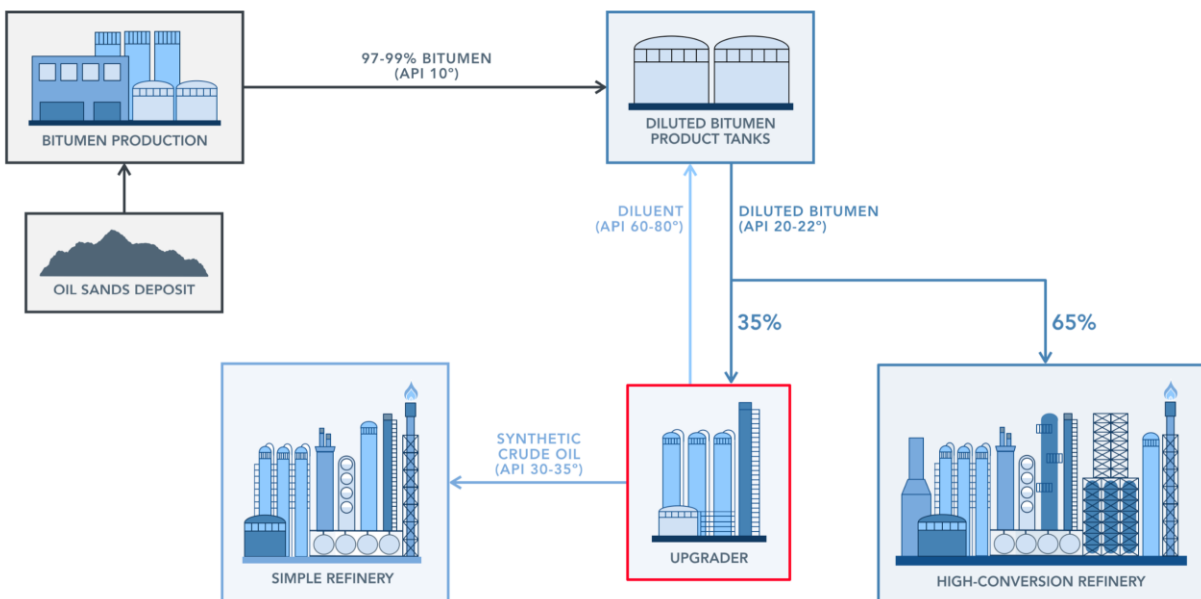


Figure 1.4. Flow diagram of bitumen production to the refinery: Two paths for Alberta’s diluted bitumen (adapted from ref 14)

Ideally, partial upgrading technologies convert bitumen to stable and pipeline-ready oil with high liquid yields, but at lower costs relative to either diluted bitumen or SCO.^{12,36} The primary processing goal of partial upgrading is the reduction of viscosity and density to enhance bitumen transportability while avoiding the use of diluents.³⁴ The minimum pipeline specifications are as follows: viscosity (<350 cst at 7°C), API gravity (>19°API), density (<940 kg/m), and total olefin content (<1 wt% 1-decene equivalence, based on ¹H NMR test methods).^{13,37,38} Achieving the technical requirements via an economically viable process requires significant research and investment. The potential benefits associated with this technology are enormous. Partially upgraded bitumen is less expensive and greenhouse gas-intensive to process and its higher quality relative to heavy crude or diluted bitumen translates into a higher commodity price. Because partially upgraded bitumen can be transported by pipeline, marine or rail networks with zero or

minimal dilution, this process permits shipping of higher volumes of bitumen through the existing pipeline network, thus lowering pipeline tolls per barrel of extracted bitumen and allowing for more oil to be shipped by reducing the volumes of diluent.^{12,39}

Despite the clear advantages of partial upgrading, the associated technology has not yet been commercialized. Uncertainty associated with a new technology and the current petroleum averse social and regulatory climate limit the capital investments needed. Nevertheless, investments from the Provincial Government of Alberta, particularly through its Energy Diversification Act (2018) and Petroleum Marketing Act (2000), is supporting development of new partial upgrading capacity.³⁹ Currently, there are several partial upgrading technologies in different stages of development. Canadian based companies including MEG Energy, Expander Energy, Field Upgrading, Value Creation Inc., Fractal Systems Inc., and ETX Systems Inc. are all exploring or developing partial upgrading projects in the Alberta oil sands.

Although majority of the emerging partial upgrading technologies are based on either thermal conversion⁴⁰⁻⁴³ or partial deasphalting,⁴⁴⁻⁴⁶ such technologies suffer from notable limitations. Thermal cracking proceeds via a free radical mechanism and produces olefins,²¹ resulting in unstable liquid products. Furthermore, for the product to have improved density, significant coking is necessary. This naturally reduces volumetric yield of the process. Removing a portion of asphaltene results in reduced viscosity and density, but the volume loss is significant.

Hydroprocessing under moderate conditions^{47,48} represents a better approach to bitumen upgrading. Hydroprocessing involves the use of low-cost catalysts and hydrogen gas under relatively mild conditions to convert bitumen to meet flow properties. It offers advantages such as coke reduction, increased liquid yield, viscosity and density reduction, and significant decrease in olefins formation. Conversion of the bitumen during partial upgrading must be limited to what is

necessary for meeting viscosity, density, and olefins content requirements. In one prominent example of this process, raw bitumen was converted to refinery- and pipeline-grade product using NiMo/Al₂O₃ catalyst under moderate (400°C and 6.9 MPa H₂) hydroprocessing in a fixed-bed reactor.⁴⁷ While the product was desirable, the catalyst resulted in elevated hydrogen consumption levels due to its high affinity for hydrodesulfurization (HDS) and hydrodenitrogenation (HDN). This NiMo/Al₂O₃, can be modified to limited defunctionalization activity under similar reaction conditions, producing transportable product without excessive use of hydrogen consumption.⁴⁸

While there are many mature hydroprocessing methods, widespread use of this method for partial requires costs reduction. An important element in hydroprocessing is the type of catalyst used. Existing catalysts used for heavy oil hydroprocessing are mostly made of transition metals such as Ni,^{49,50} Mo,⁵¹⁻⁵³ W,^{54,55} Fe,⁵⁶⁻⁶⁰ Co,^{61,62} Pt,⁶³ or Pd.^{64,65} However, the high cost of noble metals (Pd and Pt) coupled with their continuous deactivation by heteroatoms in petroleum feedstocks makes them undesirable catalyst for deployment in bitumen upgrading. The ideal hydroprocessing catalysts for partial upgrading must be cost-effective and possess sufficient hydrogenation activity to suppress coke formation and reduce liquid density, but with limited hydrodesulfurization and hydrodenitrogenation activity. Although iron is much less active than most metals,^{58,60,66} it fits these criteria. Iron is highly abundant, not toxic, exhibits excellent arenes hydrogenation activity,^{67,68} and its ore is significantly less expensive (\$81.19/ton) than nickel (\$11,800/ton), molybdenum (\$14,500/ton), cobalt (\$29,200/ton), and platinum-group metals (\$13,500,000/ton).⁶⁹

Whether iron or any another transition metal is used as a hydroprocessing catalyst in petroleum upgrading, metal sulfidation is indispensable. Iron sulfides have been studied by physicists, chemists, biologists, engineers, and material scientists for many decades.⁷⁰ They usually exhibit a wide range of chemical, physical, and electronic properties and find applications in

electromagnetic devices,⁷¹ solar cells,⁷² crude oil upgrading,⁵⁸ and wastewater treatment.⁷³ Currently, iron sulfide compounds have at least nine known discrete crystallographic phases via the formation of different stoichiometric ratios: mackinawite (FeS_{1-x}), amorphous iron sulfide, (FeS), troilite (FeS), cubic iron sulfide (FeS), smythite ($\text{Fe}_{3+x}\text{S}_4$), greigite (Fe_3S_4), marcasite (FeS_2 , orthorhombic), pyrite (FeS_2 , cubic), pyrrhotite (Fe_{1-x}S) (Table 1.3). Of these, pyrite and pyrrhotite are the most abundant in nature and important for catalysis. Marcasite is only common in hydrothermal systems and sedimentary rocks, amorphous FeS does not exist naturally, and mackinawite can only be formed from solution under inert atmosphere since it oxidizes rapidly upon exposure to air therefore requiring special handling.^{74,75}

Table 1.3. Summary of the various iron sulfide phases^{74,75}

| Phase | Composition | Crystal structure | Properties |
|---------------|-----------------------------|-------------------------------|---|
| Mackinawite | FeS_{1-x} | Tetragonal, 2D layer | Metastable, initial observed corrosion product. |
| Amorphous FeS | FeS | Nanocrystalline/ amorphous | Unstable, converts smoothly into mackinawite. |
| Troilite | FeS | Hexagonal | Stoichiometric end member of the Fe_{1-x}S group. |
| Cubic FeS | FeS | Cubic | Unstable, transforms to pyrite, mackinawite, or pyrrhotite. |
| Smythite | $\text{Fe}_{3+x}\text{S}_4$ | Trigonal-hexagonal | Metastable, sub-phase from Fe_{1-x}S group. |
| Greigite | Fe_3S_4 | Cubic | Metastable, contains both Fe^{2+} and Fe^{3+} ions. |
| Marcasite | FeS_2 | Orthorhombic | Metastable, commonly observed in hydrothermal systems and sedimentary rocks |

| | | | |
|------------|---------------------|-------------------------|---|
| Pyrite | FeS ₂ | Cubic | Thermodynamically stable, stoichiometric iron disulfide. |
| Pyrrhotite | Fe _{1-x} S | Monoclinic or hexagonal | Thermodynamically stable, nonstoichiometric iron-deficient monosulfide. |

Under certain conditions, such as high temperature and/or pressure, transformation from one phase to another can occur and some of these phases become unstable, acting as transition states.⁷⁶ The crystal structures and phase transitions of iron-sulfur compounds are complex and dynamic. For example, pyrite the most abundant form of iron sulfide on the earth's surface is converted to either hematite (Fe₂O₃) or magnetite (Fe₃O₄) in air, it is transformed to pyrrhotite under inert atmosphere between 500°C and 600°C, and remains stable as pyrrhotite even at 900°C. However, under CO₂ an intermediate pyrrhotite is first formed at low pressure, and further transformed to magnetite and hematite, mainly due to dissociation of CO₂ into CO and O₂.⁷⁷ Mackinawite can convert to other crystal structures under H₂S environment; the transition sequence at 120 °C is as follows: mackinawite → troilite → pyrrhotite → pyrite.⁷⁸ The thermodynamic data predicts the stable phases (pyrite and pyrrhotite) to predominate eventually (Table 1.3). This discussion is limited to pyrite and pyrrhotite because they are most widely studied for petroleum upgrading.⁷⁹⁻⁸⁴

Pyrite is an iron (II) disulfide with structure similar to rock salt (NaCl). While Fe atoms occupy the corners and face centers of the units, the two sulfur atoms form a dumbbell-shaped [S₂]²⁻ structure and are positioned at the cube center and the midpoints of cube edges. Each sulfur atom is bonded to its dimer and three Fe²⁺ ions, while each Fe²⁺ cation in the bulk is coordinated to six sulfur atoms forming a distorted octahedral (Figure 1.5). The pyrite unit cell comprises four FeS₂ formula units, which is characterized by the cell parameter or cell wall length, a_0 and the S coefficient, u , characterizing the coordinates of each S atom in the unit cell. The unit cell

parameters are now generally accepted as $a_0 = 0.5417$ nm and $u = 0.0385$ nm. Average Fe-S distance is 0.2259 nm. Pyrite stability is attributed to the strong S-S bond and the symmetric cubic crystal structure.^{73,74,85}

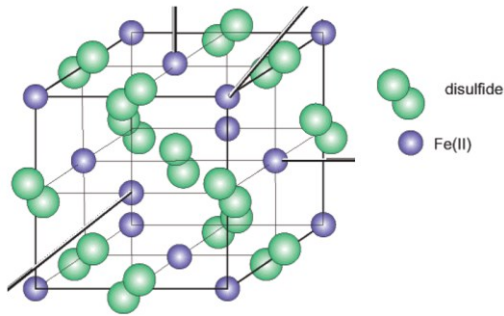


Figure 1.5. Cubic pyrite unit cell (adapted from ref 74).

Pyrrhotite is a set of iron sulfides commonly found in nature with the general formula $Fe_{1-x}S$, where x ranges from 0 (FeS, troilite) to 0.125 (Fe_7S_8). It adopts various superstructures based on the NiAs structure, which depicts a hexagonal closed packing structure, and exhibits nonstoichiometric composition due to a system of ordered vacancies within the iron lattice (Figure 1.6). Two basic subgroups are known: hexagonal pyrrhotite, an iron-rich group (47.4-48.3 at.%) generally denoted as $Fe_{10}S_{11}$, and monoclinic pyrrhotite, a less iron-rich crystal structure (46.5-46.8 at.%) with general formula Fe_7S_8 . The average Fe-S distance is 0.250 nm.^{74,86,87} Both pyrrhotite and pyrite minerals are ubiquitous and utilized mainly in mining industries.

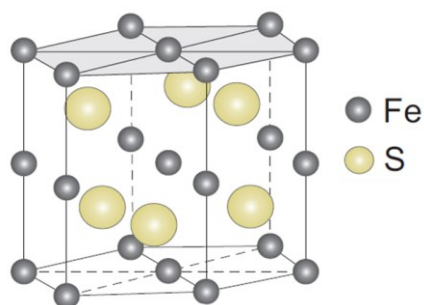


Figure 1.6. NiAs-like unit cell, common for all pyrrhotites (adapted from ref 88).

There are several iron sulfide catalyst systems that have been studied for petroleum processing and Table 1.4 shows their various operating conditions and feeds used. The majority of the reactions in these studies were conducted at temperatures above the onset of coking ($> 400^{\circ}\text{C}$) and usually require a sulfiding agent to convert the catalyst precursors to its active form prior to reaction. In heavy crude oil processing, catalyst sulfidation is indispensable for efficient upgrading.^{10,89} To address these problems, relevant parameters were considered in selecting the iron precatalyst including stoichiometric composition, thermal stability under reaction conditions, sulfiding state of the compound, solubility in petroleum feedstock, and effectiveness in ensuring broad dispersal of the resulting bitumen-supported heterogeneous catalysts.

The well-defined and air-stable dinuclear iron sulfide complex $\text{Fe}_2\text{S}_2(\text{CO})_6$ is a good fit and was selected for the study throughout this thesis. It exhibits high solubility in crude oil feedstock, possesses a predetermined Fe to S ratio, and is thermally stable only up to a temperature of 70°C .⁹⁰ Importantly, this stoichiometrically presulfided iron precatalyst is straightforward to prepare⁹¹ and can produce nanoparticles of active catalyst under solvothermal conditions,⁹² making it a good candidate for further development and use in petroleum processing.

Table 1.4. Summary of various iron sulfide catalyst systems in crude oil processing.

| Feed | Catalyst precursor | Support | Temp (°C) | Press (MPa) | Time (min) | Ref |
|--------------------------------|---------------------------------------|----------------------|------------------|--------------------|-------------------|------------|
| Mexican heavy crude | Iron (III) acetylacetonate | none | 380 | 4.41 | 60 | 56 |
| Liaohe vacuum residue | FeCl ₃ , NiCl ₂ | none | 430 | 7 | 60 | 57 |
| Saudi Arabian vacuum gas oil | Iron naphthenate | none | 420 | 8.5 | 60 | 58 |
| Belayin vacuum residue | Iron naphthenate | none | 410-460 | 8-20 | 1-120 | 66 |
| Coal, Athabasca bitumen | FeSO ₄ | none | 400-490 | 3.4-24.1 | - | 93 |
| Atmospheric and vacuum residue | Iron (III) oxide | alumina | 400-500 | 3.5-24 | - | 94 |
| 1,3,6,8-tetrahexylpyrene | Iron (III) nitrate nanohydrate | alumina, glass beads | 430 | 5 | 30 | 95 |
| Heavy crude | Iron (III) oxide | none | 355-425 | 1-5 | 20-80 | 96 |

Temp: temperature, Press: pressure, Ref: reference

In addition to focusing on less expensive and more efficient catalyst systems for partial upgrading, substantial research attention focuses on utilizing alternative sources of hydrogen. While typical hydrogenation, with molecular hydrogen, is widely used because of its simplicity and atom-efficiency, there are challenges with such systems. Molecular hydrogen is expensive and is often considered as a hazardous gas due to its extremely flammable nature,⁹⁷ particularly after the Tesoro Anacortes refinery disaster on April 2, 2010, that claimed the lives of seven (7) workers.⁹⁸ One

common alternative to molecular hydrogen is the use of hydrogen donor molecules to drive hydrogenation of unsaturated bonds. This process is referred to as transfer hydrogenation. While hydrogenation involves the reduction of multiple bonds using hydrogen gas and a catalyst,⁹⁹ transfer hydrogenation utilizes hydrogen-rich compounds to perform reduction reactions.¹⁰⁰ Ideal hydrogen donors are inexpensive and readily available small molecules that can be readily dehydrogenated under reaction conditions. Common hydrogen donor molecules include tetralin, acridine, indole, decalin, naphthalene, indoline, indane, 9,10-dihydroanthracene, ethanol, 1,2,3,4-tetrahydroquinoline, pyrene, and 9,10-dihydrophenanthrene.¹⁰¹ Dehydrogenating such compounds liberates hydrogen atoms that are transferred to heavy hydrocarbons in the crude oil, preventing the polymerization of the heavy molecules, therefore suppressing coke formation. A comprehensive review by Zhao et al.¹⁰² covers much of the accumulated knowledge on the role of hydrogen donors in upgrading heavy oil and bitumen.

Table 1.5 shows selected studies on crude oil upgrading using various hydrogen donors. Tetralin is ubiquitous in transfer hydrogenation reactions relevant to heavy crude oil processing. It is recognized that the presence of tetralin decreases coke forming tendency and promote both viscosity and API reduction.¹⁰³⁻¹⁰⁶ However, the literature lacks the extensive use of inexpensive and earth-abundant element such as iron in transfer hydrogenation reactions as well as the study of mixed hydrogen donors for petroleum processing. Chapter 4 of this thesis focuses on addressing these challenges.

Table 1.5. Petroleum upgrading using hydrogen donors.

| Feed | Hydrogen donor | Catalyst | Temp (°C) | Press (MPa) | Ref |
|----------------------|---|--|------------------|--------------------|------------|
| West Texas residue | Tetralin, decalin, benzene, cyclohexane | Al ₂ O ₃ -Cr ₂ O ₃ | 450 | 4.1-18.3 | 103 |
| Athabasca asphaltene | Tetralin | none | 195-390 | 0.1 | 104 |
| Athabasca bitumen | Tetralin, hydrogen | Ni-Mo/ gamma alumina | 400 | 8.4 | 105 |
| Mexican heavy crude | Tetralin, decalin, naphthalene | none | 420 | 1.1 | 106 |
| Polycyclic arenes | Tetralin, 9,10-dihydroanthracene | Sulfided ferric oxide | 425 | 6-8 | 107 |

Temp: temperature, Press: pressure, Ref: reference

For initial studies on catalyst effectiveness and during process optimization, it is often useful to study model petroleum systems before authentic crude feeds. Authentic crudes are complex mixture, which can undergo numerous changes under reaction conditions, making analysis of products recognizing the effects of the catalyst challenging. The model compounds must be chosen carefully to reflect the types of molecular architectures present in heavy crude oil. Because the asphaltenes in bitumen contain significant amount of polycyclic aromatic carbocycles and heterocycles, the model compounds selected for this study therefore are typically small polycyclic aromatic hydrocarbon substructures typically found in the non-distillable fraction of heavy crudes.

1.2. Research goals and thesis organization

The chapters that follow describe the use of well-defined iron catalyst for the hydrogenation of various polycyclic aromatic compounds, as well as hydrogenolysis of C-S and C-N bonds, which are key reactions for the partial upgrading of heavy crude oil. In chapter 2, the use of a hydrocarbon-soluble molecular iron sulfide precatalyst for partial hydrogenation of simple condensed arenes, which are representative of small polycyclic units dominant in lighter asphaltenes, is discussed. High conversions were only achieved by utilizing a support to effectively disperse the iron precatalyst. Chapter 3 explores the use of this iron precatalyst for hydrogenation and defunctionalization of some key structural units present in heavy crude oil, which do not require incorporation of a catalyst support. Chapter 4 addresses the alternatives to hydrogen gas for crude oil upgrading. In this study, the unsupported iron precatalyst and mixed hydrogen donors were employed to perform transfer hydrogenation and defunctionalization reactions of wide range of polyaromatic carbo- and heterocycles under nitrogen. Finally, chapter 5 summarizes the findings and key contributions from the studies above, as well as recommendations for future research.

1.3. References

1. IEA, 2021 World Energy Outlook. <https://iea.blob.core.windows.net/assets/4ed140c1-c3f3-4fd9-acae-789a4e14a23c/WorldEnergyOutlook2021.pdf> (accessed on March 16, 2022).
2. Demirbas, A.; Bafail, A.; Nizami, A. S. Heavy oil upgrading: Unlocking the Future Fuel Supply. *Pet. Sci. Technol.* **2016**, *34*, 303-308.
3. Hein, F. J. Geology of Bitumen and Heavy oil: An Overview. *J. Pet. Sci. Eng.* **2017**, *154*, 551-563.
4. Hills, D. J.; Hooks, C. H.; McIntyre-Redden, M. R.; Crooke, L. A.; Tew Jr, B. H.; Parks, K. Oil Sands in Alabama, USA: A Fresh Look at an Emerging Potential Resource. *Bull. Can. Petrol. Geol.* **2016**, *64*, 278-290.
5. AER, 2021. ST98:2021. Alberta Energy Outlook. <https://static.aer.ca/prd/documents/sts/ST98/2021/st98-2021-executivesummary.pdf> (accessed on March 15, 2022).
6. Meyer, R. F.; Attanasi, E. D.; Freeman, P. A. Heavy Oil and Natural Bitumen Resources in Geological Basins of the World. U.S. Geological Survey Open-File Report 2007, 1084, 1-42, <http://pubs.usgs.gov/of/2007/1084/> (accessed on March 16, 2022).
7. Greene, D. L.; Hopson, J. L.; Li, J. Running Out of and Into Oil: Analyzing Global Oil Depletion and Transition Through 2050. *Transp. Res. Rec.* **2004**, *1880*, 1-9.
8. Canadian Association of Petroleum Producers CAPP. *Crude Oil Forecast, Markets and Transportation 2021*. <https://www.capp.ca/publications-and-statistics/publications/320292> (accessed on March 16, 2022).
9. de Klerk, A.; Gray, M. R.; Zerpa, N. Unconventional oil and gas: Oilsands. *In Future Energy. Improved, Sustainable and Clean Options for Our Planet*, 2nd Edition; Letcher, T. M., Ed.; Elsevier: Amsterdam, 2014; pp 95-116.
10. Gray, M. R. *Upgrading Oilsands Bitumen and Heavy Oil*; University of Alberta Press: Edmonton, Alberta, Canada, 2015.
11. Hart, A. A Review of Technologies for Transporting Heavy Crude Oil and Bitumen via Pipelines. *J. Pet. Explor. Prod. Technol.* **2014**, *4*, 327-336.

12. de Klerk, A. Processing Unconventional Oil: Partial Upgrading of Oilsands Bitumen. *Energy Fuels* **2021**, *35*, 14343-14360.
13. Gray, M. R. Fundamentals of Partial Upgrading of Bitumen. *Energy Fuels* **2019**, *33*, 6843.
14. Oil Sands Magazine. <https://www.oilsandsmagazine.com/technical/bitumen-upgrading> (accessed on September 20, 2022).
15. Alshareef, A. H. Asphaltenes: Definition, Properties, and Reactions of Model Compounds. *Energy Fuels* **2020**, *34*, 16.
16. Kamkar, M.; Natale, G. A Review on Novel Applications of Asphaltenes: A Valuable Waste. *Fuel* **2021**, *285*, 119272.
17. Zuo, P.; Qu, S.; Shen, W. Asphaltenes: Separations, Structural Analysis and Applications. *J. Energy Chem.* **2019**, *34*, 186–207.
18. Mitchell, D. L.; Speight, J. G. The solubility of asphaltenes in hydrocarbon solvents. *Fuel* **1973**, *52*, 149–152.
19. Speight, J. G. Petroleum Asphaltenes-Part 1: Asphaltenes, resins and the structure of petroleum. *Oil Gas Sci. Technol.* **2004**, *59*, 467–477.
20. Castaneda, L. C.; Munoz, J. A.; Ancheyta, J. Current Situation of Emerging Technologies for Upgrading of Heavy Oils. *Catal. Today* **2014**, *220*, 248.
21. Gray, M. R.; McCaffrey, W. C. Role of Chain Reactions and Olefin Formation in Cracking, Hydroconversion, and Coking of Petroleum and Bitumen Fractions. *Energy Fuels* **2002**, *16*, 756–766.
22. McMillen, D. F.; Golden, D. M. Hydrocarbon Bond Dissociation Energies. *Annu. Rev. Phys. Chem.* **1982**, *33*, 493-532.
23. Rana, M. S.; Samano, V.; Ancheyta, J.; Diaz, J. A. I. A Review of Recent Advances on Process Technologies for Upgrading of Heavy Oils and Residua. *Fuel* **2007**, *86*, 1216.
24. Speight, J. G. New Approaches to Hydroprocessing. *Catal. Today* **2004**, *98*, 55-60.
25. Joshi, J. B.; Pandit, A. B.; Kataria, K. L.; Kulkarni, R. P.; Sawarkar, A. N.; Tandon, D.; Ram, Y.; Kumar, M. M. Petroleum Residue Upgradation via Visbreaking: A Review. *Ind. Eng. Chem. Res.* **2008**, *47*, 8960-8988.
26. Speight, J. G. Visbreaking: A Technology of the Past and the Future. *Sci. Iran.* **2012**, *19*, 569–573.

27. Marafi, A.; Albazzaz, H.; Rana, M. S. Hydroprocessing of Heavy Residual Oil: Opportunities and Challenges. *Catal. Today* **2019**, *329*, 125-134.
28. Prado, G. H.; Rao, Y.; de Klerk, A. Nitrogen Removal from Oil: A Review. *Energy Fuels* **2017**, *31*, 14-36.
29. Bello, S. S.; Wang, C.; Zhang, M.; Gao, H.; Han, Z.; Shi, L.; Su, F.; Xu, G. A Review on the Reaction Mechanism of Hydrodesulfurization and Hydrodenitrogenation in Heavy Oil Upgrading. *Energy Fuels* **2021**, *35*, 10998-11016.
30. Furimsky, E. Selection of catalysts and reactors for hydroprocessing. *Appl. Catal., A* **1998**, *171*, 177-206.
31. Ancheyta, J.; Rana, M. S.; Furimsky, E. Hydroprocessing of Heavy Petroleum Feeds: Tutorial. *Catal. Today* **2005**, *109*, 3-15.
32. Fellows, G. K.; Mansell, R.; Schlenker, R.; Winter, J. *Public-Interest Benefit Evaluation of Partial-Upgrading Technology*, SPP Research Papers AB; University of Calgary, The School of Public Policy: Calgary, 2017; Vol. 10.
33. AER, 2018. ST98:2018. Alberta's Energy Reserves & Supply/Demand Outlook. <https://www.aer.ca/providing-information/data-and-reports/statistical-reports/st98/archives> (accessed on April 2, 2022).
34. Keesom, W.; Gieseeman, J. *Bitumen Partial Upgrading 2018 Whitepaper AM0401A*; Alberta Innovates: Calgary, AB, **2018**; pp 152.
35. Eagle Ford Condensate Price Index. <https://www.barchart.com/cmdty/indexes/us-crude-oil/explore/CLPAUS133.CM> (accessed on November 17, 2022).
36. Colyar, J. I. M. Has the Time for Partial Upgrading of Heavy Oil and Bitumen Arrived? *Pet. Technol. Q.* **2009**, *Q14*, 43.
37. Ng, S. H.; Heshka, N. E.; Zheng, Y.; Ling, H.; Wang, J.; Liu, Q.; Little, E.; Wang, H.; Ding, F. Preliminary Assessment of a Strategy for Processing Oil Sands Bitumen to Reduce Carbon Footprint. *Energy Fuels* **2021**, *35*, 9489-9496.
38. Enbridge Quality Pooling. *Enbridge: Quality Pooling Specification Package*; Edmonton, 2022. https://www.enbridge.com/~/_media/Enb/Documents/Shippers/Quality_Pooling_Specification_Package.pdf?la=en (accessed April 28, 2022).

39. Winter, J.; Goodday, V.; Fellows, G. K. Enabling Partial Upgrading in Alberta: A Review of the Regulatory Framework and Opportunities for Improvement. *School Public Policy Publ.* 2019; 12: 0-47.
40. Yañez Jaramillo, L. M.; de Klerk, A. Partial Upgrading of Bitumen by Thermal Conversion at 150–300°C. *Energy Fuels* **2018**, 32, 3299-3311.
41. Kaminski, T.; Husein, M. M. Partial Upgrading of Athabasca Bitumen using Thermal Cracking. *Catalysts* **2019**, 9, 431.
42. Alvarez-Majmutov, A.; Gieleciak, R.; Chen, J. Enhanced Representation of Thermal Cracking Chemistry in the Context of Bitumen Partial Upgrading. *Energy Fuels* **2021**, 35, 12005-12018.
43. Salehzadeh, M.; Kaminski, T.; Husein, M. M. An Optimized Thermal Cracking Approach for Onsite Upgrading of Bitumen. *Fuel* **2022**, 307, 121885.
44. Díaz-Boffelli, G.; Ancheyta, J.; Muñoz, J. A. D.; Centeno, G. Experimental Study and Economic Analysis of Heavy Oil Partial Upgrading by Solvent Deasphalting–Hydrotreating. *Energy Fuels* **2018**, 32, 55–59.
45. Zachariah, A.; de Klerk, A. Partial Upgrading of Bitumen: Impact of Solvent Deasphalting and Visbreaking Sequence. *Energy Fuels* **2017**, 31, 9374.
46. Gholami, R.; Alvarez-Majmutov, A.; Chen, J. Process Modelling and Simulation of Bitumen Partial Upgrading: Analysis of Solvent Deasphalting-Thermal Cracking Configuration. *Can. J. Chem. Eng.* **2021**, 1-14.
47. Xing, T.; Alvarez-Majmutov, A.; Chen, J. Bitumen Partial Upgrading by Mild Hydroprocessing in a Fixed-bed Reactor. *Fuel* **2019**, 235, 696.
48. Gholami, R.; Alvarez-Majmutov, A.; Xing, T.; Chen, J. Bitumen Partial Upgrading Through Fixed-Bed Hydroprocessing: Examining Catalyst Stability. *Fuel* **2021**, 287, 119830.
49. Djimasbe, R.; Varfolomeev, M. A.; Al-Muntaser, A. A.; Yuan, C.; Feoktistov, D. A.; Suwaid, M. A.; Kirgizov, A. J.; Davletshin, R. R.; Zinnatullin, A. L.; Fatou, S. D.; Galeev, R. I. Oil Dispersed Nickel-Based Catalyst for Catalytic Upgrading of Heavy Oil Using Supercritical Water. *Fuel* **2022**, 313, 122702.

50. Schacht-Hernández, P.; Portales-Martínez, B.; Laredo, G. C.; Pérez-Romo, P.; Domínguez-Esquível, J. M. Homogeneous Catalyst for In-Situ Hydrotreating of Heavy Oils. *Appl. Catal., A* **2019**, *577*, 99-106.
51. Kim, S. H.; Kim, K. D.; Lee, Y. K. Effects of Dispersed MoS₂ Catalysts and Reaction Conditions on Slurry Phase Hydrocracking of Vacuum Residue. *J. Catal.* **2017**, *347*, 127-137.
52. Nguyen, T. S.; Tayakout-Fayolle, M.; Lacroix, M.; Gotteland, D.; Aouine, M.; Bacaud, R.; Afanasiev, P.; Geantet, C. Promotion Effects with Dispersed Catalysts for Residue Slurry Hydroconversion. *Fuel* **2015**, *160*, 50-56.
53. Kang, K. H.; Nguyen, N. T.; Seo, P. W.; Seo, H.; Kim, G. T.; Kang, N.; Lee, C. W.; Han, S. J.; Chung, M. C.; Park, S. Slurry-Phase Hydrocracking of Heavy Oil over Mo Precursors: Effect of Triphenylphosphine Ligands. *J. Catal.* **2020**, *384*, 106-121.
54. Schacht, P.; Díaz-García, L.; Aguilar, J.; Ramírez, S. Upgrading of Heavy Crude Oil with W-Zr Catalyst. *Adv. Chem. Eng. Sci.* **2014**, *4*, 250-257.
55. Jeong, H. R.; Lee, Y. K. Comparison of Unsupported WS₂ and MoS₂ Catalysts for Slurry Phase Hydrocracking of Vacuum Residue. *Appl. Catal., A* **2019**, *572*, 90-96.
56. Morelos-Santos, O.; de la Torre, A. R.; Melo-Banda, J. A.; Schacht-Hernández, P.; Portales-Martínez, B.; Soto-Escalante, I.; José-Yacamán, M. A Novel Direct Method in One-Step for Catalytic Heavy Crude Oil Upgrading using Iron Oxide Nanoparticles. *Catal. Today* **2022**, *392*, 60-71.
57. Luo, H.; Sun, J.; Deng, W.; Li, C.; Du, F. Preparation of Oil-Soluble Fe-Ni Sulfide Nanoparticles for Slurry-Phase Hydrocracking of Residue. *Fuel* **2022**, *321*, 124029.
58. Bdwi, E. A.; Ali, S. A.; Quddus, M. R.; Al-Bogami, S. A.; Razzak, S. A.; Hossain, M. M. Kinetics of Promotional Effects of Oil-Soluble Dispersed Metal (Mo, Co, and Fe) Catalysts on Slurry Phase Hydrocracking of Vacuum Gas Oil. *Energy Fuels* **2017**, *31*, 3132.
59. Suwaid, M. A.; Varfolomeev, M. A.; Al-Muntaser, A. A.; Yuan, C.; Starshinova, V. L.; Zinnatullin, A.; Vagizov, F. G.; Rakhmatullin, I. Z.; Emelianov, D. A.; Chemodanov, A. E. In-Situ Catalytic Upgrading of Heavy Oil using Oil-Soluble Transition Metal-Based Catalysts. *Fuel* **2020**, *281*, 118753.
60. Quitian, A.; Fernández, Y.; Ancheyta, J. Viscosity Reduction of Heavy Oil during Slurry-Phase Hydrocracking. *Chem. Eng. Technol.* **2019**, *42*, 148-155.

61. Kim, S. H.; Kim, K. D.; Lee, D.; Lee, Y. K. Structure and Activity of Dispersed Co, Ni, or Mo Sulfides for Slurry Phase Hydrocracking of Vacuum Residue. *Journal of Catalysis* **2018**, *364*, 131-140.
62. Al-Attas, T. A.; Zahir, M. H.; Ali, S. A.; Al-Bogami, S. A.; Malaibari, Z.; Razzak, S. A. Hossain, M. M. Novel (Co-, Ni)-p-tert-Butylcalix [4] Arenes as Dispersed Catalysts for Heavy Oil Upgrading: Synthesis, Characterization, and Performance Evaluation. *Energy Fuels* **2018**, *33*, 561-573.
63. Murray, A.; Omajali J.; Del Mastio, Y.; Hart A, Wood J.; Macaskie L. Potential for conversion of Waste Platinum Group Metals in Road Dust into Biocatalysts for Cracking Heavy Oil. *Adv. Mater. Res.* **2015**, *11306*, 623-626. Trans Tech Publ.
64. Hart, A.; Omajali, J. B.; Murray, A. J.; Macaskie, L. E.; Greaves, M.; Wood, J. Comparison of the Effects of Dispersed Noble Metal (Pd) Biomass Supported Catalysts with Typical Hydrogenation (Pd/C, Pd/Al₂O₃) and Hydrotreatment Catalysts (CoMo/Al₂O₃) for In-Situ Heavy Oil Upgrading with Toe-to-Heel Air Injection (THAI). *Fuel* **2016**, *180*, 367-376.
65. Hossain, M. M.; Al-Saleh, M. A.; Shalabi, M. A.; Kimura, T.; Inui, T. Pd–Rh Promoted Co/HPS Catalysts for Heavy Oil Upgrading. *Appl. Catal., A* **2004**, *278*, 65-71.
66. Panariti, N.; Del Bianco, A.; Del Piero, G.; Marchionna, M. Petroleum Residue Upgrading with Dispersed Catalysts: Part 1. Catalysts Activity and Selectivity. *Appl. Catal., A* **2000**, *204*, 203-213.
67. Fürstner, A. Iron Catalysis in Organic Synthesis: A Critical Assessment of What it Takes to Make This Base Metal a Multitasking Champion. *ACS Cent. Sci.* **2016**, *2*, 778-789.
68. Chakraborty, S.; Brennessel, W. W.; Jones, W. D. A Molecular Iron Catalyst for the Acceptorless Dehydrogenation and Hydrogenation of N-heterocycles. *J. Am. Chem. Soc.* **2014**, *136*, 8564-8567.
69. Kelly, T. D.; Matos, G. R. *Historical Statistics for Mineral and Material Commodities in the United States, 2015*; U.S. Geological Survey Data Series 140; <https://www.usgs.gov/centers/nmic/historical-statistics-mineral-and-material-commodities-united-states> (accessed on March 25, 2022).
70. Yuan, Y.; Wang, L.; Gao, L. Nano-Sized Iron Sulfide: Structure, Synthesis, Properties, and Biomedical Applications. *Front. Chem.* **2020**, *8*, 818.

71. Man, Z.; Li, P.; Zhou, D.; Wang, Y.; Liang, X.; Zang, R.; Li, P.; Zuo, Y.; Lam, Y. M.; Wang, G. Two Birds with One Stone: FeS₂@C Yolk–Shell Composite for High-Performance Sodium-Ion Energy Storage and Electromagnetic Wave Absorption. *Nano Lett.* **2020**, *20*, 3769-3777.
72. Chen, H.; Zhu, L.; Liu, H.; Li, W. Efficient Iron Sulfide Counter Electrode for Quantum Dots-Sensitized Solar Cells. *J. Power Sources* **2014**, *245*, 406-410.
73. Yang, Y.; Chen, T.; Sumona, M.; Gupta, B. S.; Sun, Y.; Hu, Z.; Zhan, X. Utilization of Iron Sulfides for Wastewater Treatment: A Critical Review. *Rev. Environ. Sci. Biotechnol.* **2017**, *16*, 289-308.
74. Rickard, D.; Luther, G. W. Chemistry of Iron Sulfides. *Chem. Rev.* **2007**, *107*, 514-562.
75. Ning, J.; Zheng, Y. G.; Young, D.; Brown, B.; Nesic, S. Thermodynamic Study of Hydrogen Sulfide Corrosion of Mild Steel. *Corrosion* **2014**, *70*, 375–389.
76. Bai, P.; Zheng, S.; Chen, C.; Zhao, H. Investigation of the Iron–Sulfide Phase Transformation in Nanoscale. *Cryst. Growth Des.* **2014**, *14*, 4295-4302.
77. Bhargava, S. K.; Garg, A.; Subasinghe, N. D. In Situ High-Temperature Phase Transformation Studies on Pyrite. *Fuel* **2009**, *88*, 988-993.
78. Gao, S.; Brown, B.; Young, D.; Singer, M. Formation of Iron Oxide and Iron Sulfide at High Temperature and Their Effects on Corrosion. *Corros. Sci.* **2018**, *135*, 167-176.
79. Anderson, R. R.; Bockrath, B. C. Effect of Sulphur on Coal Liquefaction in the Presence of Dispersed Iron or Molybdenum Catalysts. *Fuel* **1984**, *63*, 329-333.
80. Herrick, D. E.; Tierney, J. W.; Wender, I.; Huffman, G. P.; Huggins, F. E. Activity and Characterization of Coprocessing Catalysts Produced from an Iron Pentacarbonyl Precursor. *Energy Fuels* **1990**, *4*, 231.
81. Pradhan, V.; Herrick, D. E.; Tierney, J. W.; Wender, I. Finely Dispersed Iron, Iron-Molybdenum, and Sulfated Iron Oxides as Catalysts for Coprocessing Reactions. *Energy Fuels* **1991**, *5*, 712.
82. Huffman, G. P.; Ganguly, B.; Zhao, J.; Rao, K. R. P. M.; Shah, N.; Feng, Z.; Huggins, F. E.; Taghiei, M. M.; Lu, F. Structure and Dispersion of Iron-Based Catalysts for Direct Coal Liquefaction. *Energy Fuels* **1993**, *7*, 285.
83. Ogata, E.; Wei, X. Y.; Horie, K.; Nishijima, A.; Saito, I.; Ukegawa, K. Catalysis of Iron Sulfates on Hydroconversion of 1-methylnaphthalene. *Catal. Today* **1998**, *43*, 161-169.

84. Yang, L.; Sheng, J. J. Pyrite Effects on the Oxidation of In Situ Crude Oil. *J. Pet. Sci. Eng.* **2022**, *209*, 109812.
85. Murphy, R.; Strongin, D. R. Surface Reactivity of Pyrite and Related Sulfides. *Surf. Sci. Rep.* **2009**, *64*, 1–45.
86. Wang, H.; Salveson, I. A review on the Mineral Chemistry of the Non-stoichiometric Iron Sulfide, Fe_{1-x}S ($0 \leq x \leq 0.125$): Polymorphs, Phase Relations and Transitions, Electronic and Magnetic Structures. *Phase Transitions* **2005**, *78*, 547-567.
87. Belzile, N.; Chen, Y. W.; Cai, M. F.; Li, Y. A Review on Pyrrhotite Oxidation. *J. Geochem. Explor.* **2004**, *84*, 65-76.
88. Herbert, F. W. Mechanisms Governing the Growth, Reactivity and Stability of Iron Sulfides. Ph.D. Dissertation, Massachusetts Institute of Technology: Cambridge, Massachusetts, 2015.
89. Ramselaar, W. L. T. M.; Craje, M. W. J.; Hadders, R. H.; Gerkema, E.; de Beer, V. H. J.; van der Kraan, A. M. Sulfidation of Carbon-Supported Iron Oxide Catalysts. *Appl. Catal.* **1990**, *65*, 69-84.
90. Brandt, P. F.; Lesch, D. A.; Stafford, P. R.; Rauchfuss, T. B.; Kolis, J. W.; Roof, L. C. $\text{Fe}_2(\text{S}_2)(\text{CO})_6$ and $\text{Fe}_3\text{Te}_2(\text{CO})_{9,10}$. *Inorg. Synth.* **1997**, *31*, 112.
91. Seyferth, D.; Henderson, R. S.; Song, L. -C. Chemistry of μ -Dithio-bis(tricarbonyliron), a Mimic of Inorganic Disulfides. 1. Formation of Di- μ -thiolato-bis(tricarbonyliron) Dianion. *Organometallics* **1982**, *1*, 125.
92. Di Giovanni, C.; Wang, W. A.; Nowak, S.; Grenèche, J. M.; Lecoq, H.; Mouton, L.; Giraud, M.; Tard, C. Bioinspired Iron Sulfide Nanoparticles for Cheap and Long-Lived Electrocatalytic Molecular Hydrogen Evolution in Neutral Water. *ACS Catal.* **2014**, *4*, 681.
93. Ranganathan, R.; Denis, J. D.; Pruden, B. B. Hydrocracking of Heavy Oils Using Iron Coal Catalyst. U.S. Patent 4,214,977, 1980.
94. Bhattacharyya, A.; Mezza, B. J. Process for Using Catalyst with Rapid Formation of Iron Sulfide in Slurry Hydrocracking. Patent No. US 8,277,638 B2, 2012.
95. Habib, F. K.; Diner, C.; Stryker, J. M.; Semagina, N.; Gray, M. R. Suppression of Addition Reactions during Thermal Cracking Using Hydrogen and Sulfided Iron Catalyst. *Energy Fuels* **2013**, *27*, 6637.

96. Al-Marshed, A.; Hart, A.; Leeke, G.; Greaves, M.; Wood, J. Optimization of Heavy Oil Upgrading Using Dispersed Nanoparticulate Iron Oxide as a Catalyst. *Energy Fuels* **2015**, *29*, 6306-6316.
97. Dawood, F.; Anda, M.; Shafiullah, G. M. Hydrogen Production for Energy: An Overview. *Int. J. Hydrogen Energy* **2020**, *45*, 3847-3869.
98. Animation of Explosion at Tesoro's Anacortes Refinery 2010.
<https://www.youtube.com/watch?v=8vPaQYM-tWs> (accessed on November 17, 2022).
99. de Vries, J. G.; Elsevier, C. J. *The Handbook of Homogeneous Hydrogenation*; Wiley-VCH: Weinheim, 2007.
100. Wang, D.; Astruc, D. The Golden Age of Transfer Hydrogenation. *Chem. Rev.* **2015**, *115*, 6621-6686.
101. Alemán-Vázquez, L. O.; Torres-Mancera, P.; Ancheyta, J.; Ramírez-Salgado, J. Use of Hydrogen Donors for Partial Upgrading of Heavy Petroleum. *Energy Fuels* **2016**, *30*, 9050-9060.
102. Zhao, F.; Xu, T.; Zhu, G.; Wang, K.; Xu, X.; Liu, L. A Review on the Role of Hydrogen Donors in Upgrading Heavy Oil and Bitumen. *Sustainable Energy Fuels* **2022**, *6*, 1866-1890.
103. Carlson, C. S.; Langer, A. W.; Stewart, J.; Hill, R. M. Thermal hydrogenation. Transfer of Hydrogen from Tetralin to Cracked Residua. *Ind. Eng. Chem.* **1958**, *50*, 1067-1070.
104. Ignasiak, T. M.; Strausz, O. P. Reaction of Athabasca Asphaltene with Tetralin. *Fuel* **1978**, *57*, 617-621.
105. Sanford, E. C.; Xu, C. M. Relationship Between Solids Formation, Residuum Conversion, Liquid Yields and Losses During Athabasca Bitumen Processing in the Presence of a Variety of Chemicals. *Can. J. Chem. Eng.* **1996**, *74*, 347-352.
106. Alemán-Vázquez, L. O.; Cano-Domínguez, J. L.; García-Gutiérrez, J. L. Effect of Tetralin, Decalin and Naphthalene as Hydrogen Donors in the Upgrading of Heavy Oils. *Procedia Eng.* **2012**, *42*, 532-539.
107. Li, L.; Hou, Y.; Wu, W.; Liang, S.; Ren, S. Behaviors of Tetralin and 9,10-dihydroanthracene as Hydrogen Donor Solvents in the Hydrogenolysis of Coal-Related Model Compounds. *Fuel Process. Technol.* **2019**, *191*, 202-210.

Chapter 2: Sulfided Homogeneous Iron Precatalyst for Partial Hydrogenation and Hydrodesulfurization of Polycyclic Aromatic Model Asphaltenes

Published in Energy & Fuels

2.1. Introduction

Hydrogenation of cyclic unsaturated hydrocarbons and polynuclear heteroaromatic compounds over homogeneous^{1,2} or heterogeneous catalysts³ has been studied intensively and used extensively for the production of commercial chemicals,⁴ refined petroleum and petrochemicals,⁵ and coal.⁶ In an appropriate matrix, i.e., support substructure or ligand sphere, transition metals make excellent catalysts for the catalytic hydrogenation of arenes,^{7,8} with noble metal catalysts (Pd, Pt, Rh, Ir, etc.) exhibiting the highest activity and best selectivity. However, platinum-group metals are very expensive, generally toxic, and easily poisoned by heteroatoms in petroleum streams, leading to minimal use in commercial applications on any substantial scale. Fundamental advances in the design of high-activity catalysts comprised of earth-abundant metals such as Mo, Fe, Co, and Ni promise reduced catalyst costs and reduced environmental footprints for many industries.⁹⁻¹¹

Although traditional iron-based catalysts are much less active than most metals, the potential use of this ubiquitous and nontoxic element has received extensive attention.^{6,11-15} Kelly and Matos¹⁶ reported a rough comparison of various bulk metal prices, showing that in 2015 iron ore (\$81.19/ton) was significantly more affordable than molybdenum (\$14500/ton), cobalt (\$29200/ton), nickel (\$11800/ton) and any of the platinum-group metals (~\$13500000/ton).

Many iron catalysts have been used for hydrogenation of condensed arenes, including simple Fe(III) salts (e.g., naphthenate, acetylacetonate, 2-ethylhexanoate, stearate, and nitrate)^{12,15} and

zero-valent organometallic precursors, principally $\text{Fe}(\text{CO})_5$.^{14,17} For petroleum upgrading, sulfided precatalysts are indispensable,^{18,19} leading us to pursue sulfided iron compounds for this purpose. To maximize catalyst dispersion and increase metal reactivity, very small metal sulfide nanoparticles were considered to be critical for the effective processing of heavy, highly aggregated crude oils and coal.^{20,21} To control chemical composition, structural morphology, and particle size of the active catalysts, we have investigated the use of hydrocarbon-soluble molecular iron sulfide precatalysts for partial hydrogenation of simple condensed arenes. We selected air-stable iron sulfido clusters of known Fe/S ratio, high solubility in hydrocarbon media, and relatively modest thermal stability to ensure efficient formation of an oil-supported nanocatalyst under reaction conditions. Four model compounds (Figure 2.1), which are representative of the small polycyclic aromatic hydrocarbon units dominant in lighter asphaltenes,²²⁻²⁴ were selected for this investigation of catalytic aromatic hydrogenation and hydrodesulfurization.

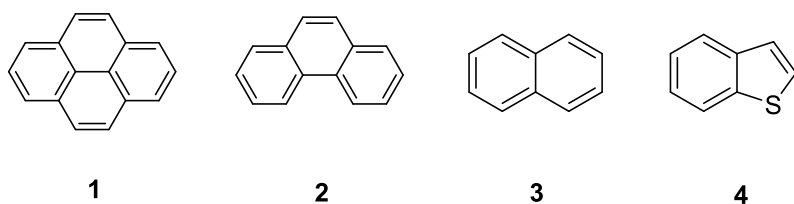


Figure 2.1. Model heavy crude oil compounds used to evaluate hydrogenation using $\text{Fe}_2\text{S}_2(\text{CO})_6$.

The known diiron sulfido complex, $\text{Fe}_2\text{S}_2(\text{CO})_6$, fits our criteria and was selected for the study. Wei and Dahl²⁵ first isolated $\text{Fe}_2\text{S}_2(\text{CO})_6$ from the reaction of elemental sulfur and $\text{Fe}(\text{CO})_5$; the structure was determined by X-ray crystallography and is comprised of a disulfide (S_2) ligand symmetrically bridged between two $\text{Fe}(\text{CO})_3$ units. The complex is isolated as red-brown air-stable crystals, which sublimes at room temperature under high vacuum and dissolves readily in nonpolar solvents.^{26,27} A low melting solid (46 °C), the precatalyst decomposes conveniently at 70 °C. Although $\text{Fe}_2\text{S}_2(\text{CO})_6$ has been used for electrocatalytic molecular hydrogen evolution from

neutral water,²⁸ to the best of our knowledge, this is the first reported use of this complex for catalytic hydrogenation of condensed aromatic and heteroaromatic compounds under heavy oil upgrading conditions.

2.2. Experimental section

2.2.1. Materials

Pyrene (98%), phenanthrene (98%), naphthalene (>99%) and benzothiophene (98%) were obtained from Sigma-Aldrich and used without further purification. Toluene (reagent grade, Fisher Scientific) was used as solvent for all experiments. Commercial ethylbenzene (99.8%), FeS (95%), 9,10-dihydrophenanthrene (94%), 1,2,3,4-tetrahydronaphthalene (99%), 1,2,3,6,7,8-hexahdropyrene (97%), and 1-methylnaphthalene (95%) were purchased from Sigma-Aldrich, as was iron pentacarbonyl (>99.99%), and elemental sulfur ($\geq 99.5\%$). Methanol, hexane, ammonium chloride, and magnesium sulfate (all reagent grade) were purchased from Caledon. High-purity silica gel and γ -alumina were obtained from Sigma-Aldrich. Activated carbon was obtained from Strem.

2.2.2. Precatalyst preparation

$\text{Fe}_2\text{S}_2(\text{CO})_6$ was synthesized according to published procedures.^{26,27,29} A two-necked, 2 L round-bottom flask fitted with a mechanical stirrer was connected to a N_2 inlet adapter and sealed with a septum. About 25 mL (0.190 mol) of $\text{Fe}(\text{CO})_5$ [*Caution: carbon monoxide!*] was introduced into the nitrogen-purged flask, followed by 125 mL of degassed methanol and 75 mL of degassed 50% aq KOH. The resulting orange-red solution was stirred vigorously for 30 min, cooled to 0 °C in an ice bath, and treated with 32.67 g (1.02 mol) of sulfur over 5 min, leading to formation of a dark-

brown mixture, which was allowed to stir for 1 h. The mixture was quenched with 300 mL of degassed distilled water, 750 mL of degassed hexane, and 84.5 g (1.58 mol) of NH_4Cl . An Extra precaution was taken to manage the evolution of gaseous H_2S . Subsequently, the ice bath was removed and the reaction mixture was allowed to stir at room temperature for 16 h, forming a dark oily aqueous phase and a brownish-red hexane layer. The hexane fraction was collected using a separatory funnel. Remaining organics were exhaustively extracted from the aqueous phase using fresh hexane in 200 mL portions until the aqueous fraction was nearly colorless (1.2 L of hexane in total). The combined organic fractions were filtered through celite and rinsed with 200 mL of fresh hexanes. The solution was washed with an equal volume of deionized water, dried over anhydrous MgSO_4 , and gravity-filtered to produce a dark red solution. The volatiles were removed under reduced pressure and the crude solid was purified by sublimation (room temperature, 10^{-5} Torr). $\text{Fe}_2\text{S}_2(\text{CO})_6$ was obtained as the red-brown crystalline sublimate [9.7 g; 30% based on $\text{Fe}(\text{CO})_5$]. A schematic illustration of this procedure is presented in Figure 2.2.

2.2.3. Characterization techniques

2.2.3.1. Thermogravimetric analysis (TGA)

TGA was conducted on a Mettler Toledo thermogravimetric analyzer (TGA)/ Differential Scanning Calorimeter (DSC) 1 Star System. Between 6 and 8 mg of the precursor was placed in the sample holder heated at $10\text{ }^\circ\text{C}/\text{min}$ from 25 to $600\text{ }^\circ\text{C}$ with nitrogen ($60\text{ mL}/\text{min}$) as a purge gas.

2.2.3.2. Elemental analysis

Combustion analysis (CHNS) was conducted on a Thermo Scientific Flash 2000 elemental analyzer. The run time was 12 min, and the Eager Xperience software package generated the area count data was used to calculate the percentage of carbon and sulfur in the precursor.

2.2.3.3. Fourier transform infrared spectroscopy (FT-IR)

IR spectra were recorded on a Nicolet 8700 Fourier transform infrared (FT-IR) spectrometer at ambient temperature, 650-4000 cm^{-1} at a resolution of 4 cm^{-1} .

2.2.3.4. X-ray diffraction (XRD)

Powder X-ray diffraction (XRD) analysis was performed using a Rigaku Ultima IV diffractometer (38 kV, 38 mA) equipped with a D/Tex ultra detector, Co $K\alpha$ radiation source ($\lambda = 1.78900 \text{ \AA}$) and 2θ ranging from 5° to 90° , operating at a scanning rate of 2° min^{-1} and a step size of 0.0200° . XRD peak identification and baseline correction were done using JADE 9.0 software coupled with the ICDD database.

2.2.3.5. X-ray photoelectron spectroscopy (XPS)

XPS measurements were performed using a Kratos Axis 165 X-ray photoelectron spectrometer with mono Al $K\alpha$ radiation as the excitation source, operating at 15 mA and 14 kV. Background subtraction (Shirley-type), smoothing, and peak fitting were carried out using the CasaXPS software package. All binding energies were corrected with the C 1s peak at 284.7 eV. Electron flood neutralizer was applied to compensate sample charging.

2.2.3.6. Scanning transmission electron microscopy (STEM)

Recovered in situ-generated catalyst was characterized by scanning transmission electron microscopy (STEM) and high-resolution STEM (HR-STEM) using a JEOL JEM-ARM200cF scanning transmission electron microscope operating at the 200 kV accelerating voltage.

2.2.3.7. Scanning electron microscopy (SEM)

A Hitachi S-2700 scanning electron microscope operating at an accelerating voltage of 200 kV was employed to image recovered catalysts. EDX mapping was conducted by SEM equipped with a Princeton Gamma-Tech (PGT) IMIX digital imaging system and a PGT PRISM Intrinsic Germanium (IG) detector.

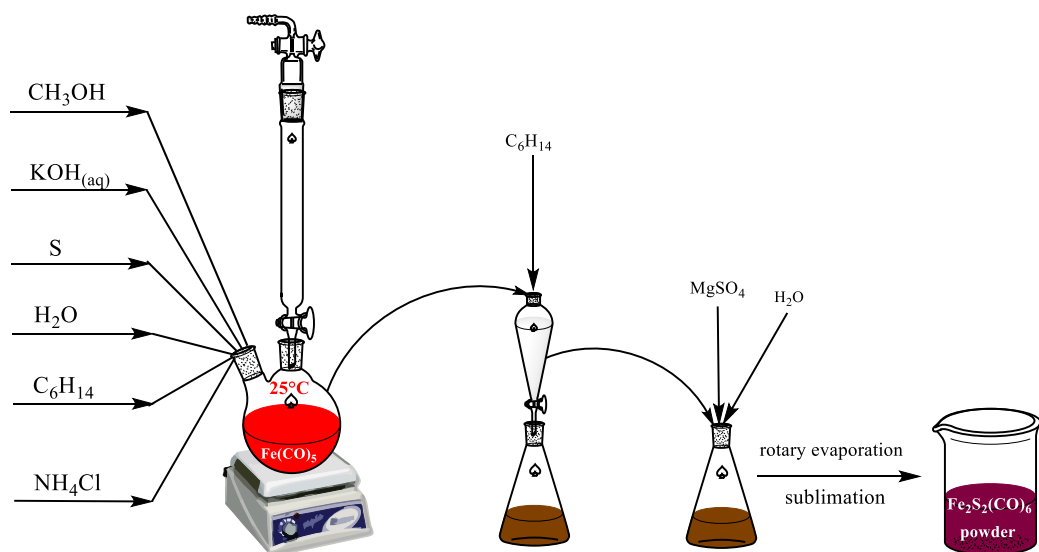


Figure 2.2. Schematic illustration of the synthesis of $\text{Fe}_2\text{S}_2(\text{CO})_6$. Colors are approximate.

2.2.4. Catalytic activity determinations

Both control experiments and catalytic reactions were conducted in a 20 cm³ stainless-steel tubular batch microreactor, coupled to a high-temperature Swagelok severe-service Bonnet needle valve. For each experiment, the reactor was charged with 5 mL of a solution containing about 2.9 wt % of the reactant dissolved in toluene, followed by addition of 0.1 g of activated carbon. The precatalyst loading was varied between 1000 and 8000 ppm Fe. After leak testing, the microreactor was purged five times with hydrogen to ensure that the reactor was devoid of oxygen. The reactor was pressurized (2–10 MPa) at room temperature, sealed, and immersed in a preheated agitated sand bath to ensure hydrogen saturation, efficient mass-transfer, and uniform temperature profile. The interior of the reactor reached reaction temperature (250–350 °C) within 5 min, as determined by a thermocouple. The transformation of the catalyst precursor to dispersed iron sulfide occurs rapidly. After the reaction period, the microreactor was cooled to room temperature by a cold air circulator to suppress further reaction. Each experiment was conducted at least in duplicate; data reproducibility was quite good.

Solid and liquid products were separated by filtration. Reaction products and unreacted substrate were identified by gas chromatography/mass spectrometry (GC/MS, Agilent 6850) equipped with an HP-5 (5% phenyl)-methylpolysiloxane capillary column (Agilent). Quantification of product distribution was achieved by GC with flame ionization detection (GC-FID, Agilent 6890N), also using the HP-5 (5% phenyl)-methylpolysiloxane column (Agilent). Yields were determined relative to 1-methylnaphthalene, used as the internal standard.

2.3. Results and discussion

2.3.1. Precatalyst characterization

The thermal behavior of the iron precatalyst was studied using TGA (Figure 2.3). As reported, the complex is thermally unstable above 70 °C,²⁶ decomposing in a single-stage process over the range 70–125 °C. The mass loss of 48.9 wt % corresponds exactly with the desorption of all CO ligands in the complex $\text{Fe}_2\text{S}_2(\text{CO})_6$. Heating beyond 125 °C does not lead to a further decrease in mass, indicating that the iron sulfide produced in situ is thermally stable at higher temperatures.

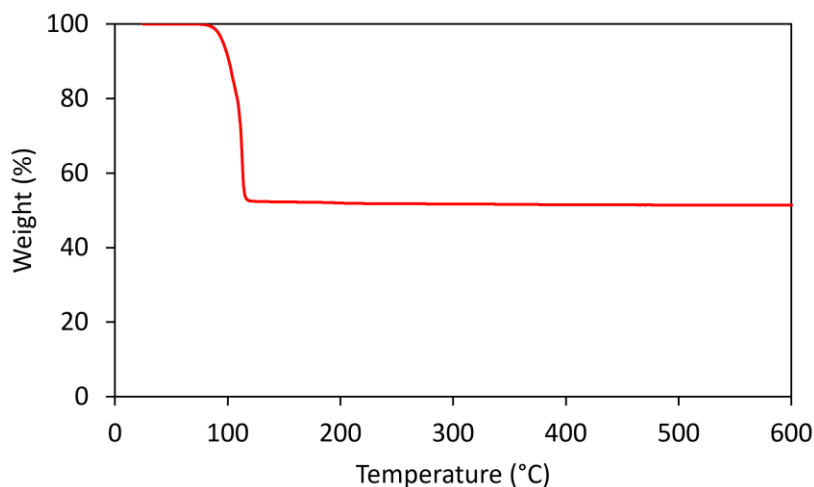


Figure 2.3. TGA of $\text{Fe}_2\text{S}_2(\text{CO})_6$.

The elemental composition determined by CHNS analysis confirms the data obtained from TGA. The weight percent of C and S in the solid catalyst, 21.12 and 19.08 wt % respectively, again corresponds to the complete loss of CO from $\text{Fe}_2\text{S}_2(\text{CO})_6$. The solution Fourier transform infrared (FT-IR) spectrum of $\text{Fe}_2\text{S}_2(\text{CO})_6$ in toluene reveals three distinct, strong absorptions in the carbonyl region, at 2083, 2036, and 1987 cm^{-1} (Figure 2.4), consistent with previous reports.^{26,29}

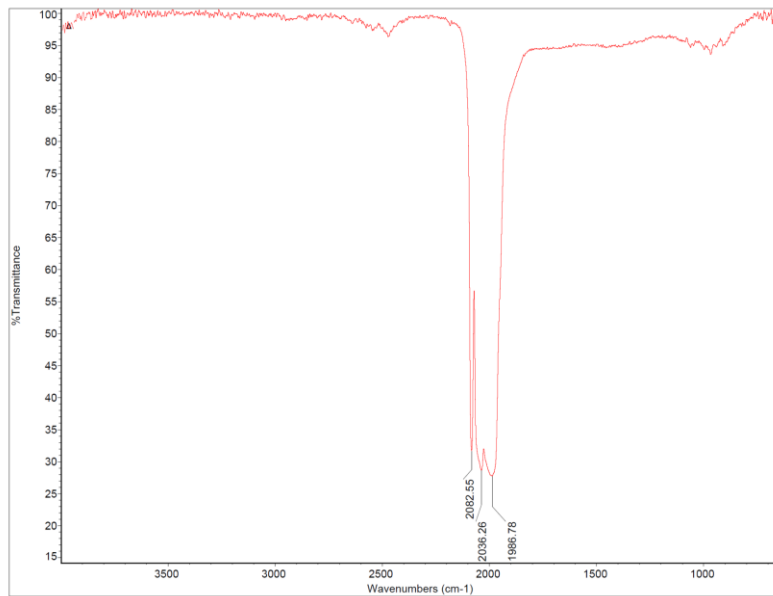


Figure 2.4. FT-IR spectrum of Fe₂S₂(CO)₆.

2.3.2. Catalyst characterization

Iron sulfide nanoparticles obtained from thermal decomposition of Fe₂S₂(CO)₆ were analyzed by TEM and SEM. Solvothermal synthesis of unsupported FeS nanoparticles from Fe₂S₂(CO)₆ using octylamine as both reaction solvent and particle growth regulator has been reported to produce polydisperse hexagonal FeS nanoparticles with sizes ranging from 50 to 500 nm.²⁸ Under our modified solvothermal synthesis conditions, however, we obtained roughly spherical FeS nanoparticles on a carbon support with sizes ranging from 45 to 110 nm (Figure 2.5a,d). The nanoparticles were generated under reaction conditions and were therefore deposited in-situ on the activated carbon. Transmission electron microscopy imaging revealed the formation of irregularly shaped polydisperse iron sulfide nanoparticles ranging from 42 nm to 106 nm in size (Figure 2.5e,g). The SEM-EDX mapping images (Figure 2.5b,c) show that the nanoparticles consisted primarily of Fe and S, despite the absence of an added source of sulfur in the system. The

distribution of the signals for iron and sulfur is strongly correlated, confirming the presence of a uniform iron sulfide phase.

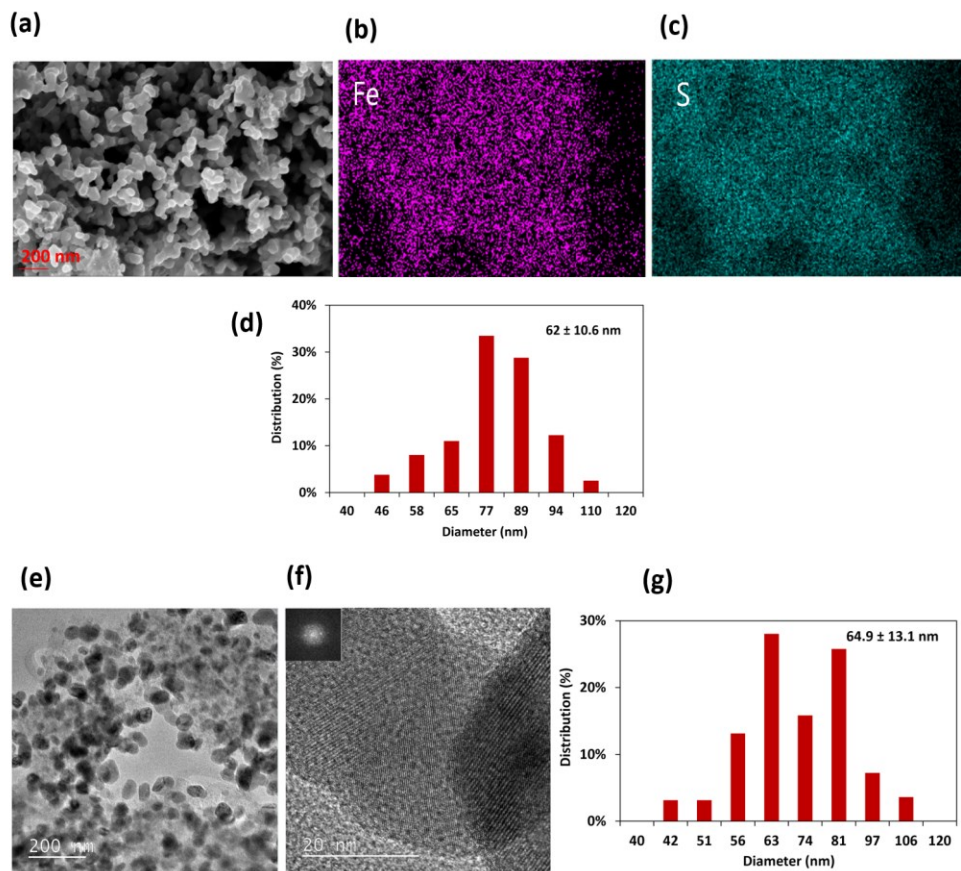


Figure 2.5. (a-d) SEM, EDX mapping images, and corresponding size distribution as well as (e-g) TEM and HR-TEM images coupled with particle size distribution of the FeS nanoparticles produced at 300 °C and 5000 ppm Fe. Inset: fast Fourier transform (FFT) pattern.

Powder X-ray diffraction (XRD) provided further insights into the structure of the iron sulfide particles formed from the solvothermal treatment of $\text{Fe}_2\text{S}_2(\text{CO})_6$. The iron sulfide deposited is highly crystalline (Figure 2.6) with key reflections at 35, 39.7, 51.6, and 62.8°, indicating the presence of a pyrrhotite (Fe_{1-x}S) phase (Jade 9.0 PDF No. 98-000-0368). High-resolution transmission electron microscopy (HR-TEM) imaging also confirms the crystallinity of the

deposited iron sulfide (Figure 2.5f). The strong reflection having 2θ value of 30.9° results from the underlying carbon support (Jade 9.0 PDF No. 98-000-0231). The importance of pyrrhotite phases in iron sulfide catalysis has been well established in the literature, with several reports suggesting that the common pyrite phase of iron sulfide is inactive and must be converted to the active pyrrhotite phase by loss of H_2S before catalytic hydrogenation and hydrocracking reactions can proceed.^{12,19}

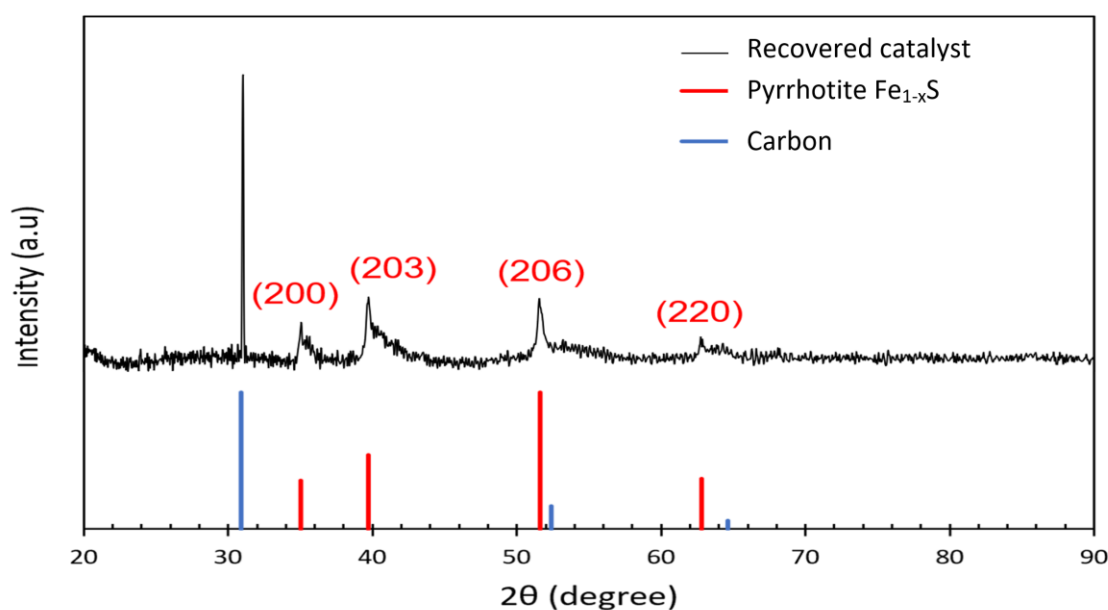


Figure 2.6. XRD patterns of carbon-supported FeS nanocatalyst produced at 300°C , 6 MPa cold H_2 , and 5000 ppm Fe.

Further insight into the chemical composition and structure of the iron sulfide nanoparticles was obtained using X-ray photoelectron spectroscopy. XPS spectra reveal iron and sulfur in a variety of chemical environments, with Fe(II) (707.0 eV) and Fe(III) (710.0 eV and 711.7 eV) being the most prominent species in the Fe $2p_{3,2}$ spectrum (Figure 2.7a). In the S $2p_{3,2}$ spectrum, S^{2-} (161.0 eV) and S_2^{2-} (162.3 eV) dominate, although a small proportion of polysulfide(s) (163.7 eV) was also indicated (Figure 2.7b). The presence of Fe(III) may be ascribed to surface oxidation during

sample handling, but the relatively high concentration of iron in this chemical environment suggests that the Fe(III) is actually integral part of the bulk structure of the particles.³⁰⁻³² XPS analysis of comparable FeS nanoparticles has revealed similar patterns, with Fe(III) signals persisting even after extensive surface etching under an inert atmosphere.³³ Similarly, disulfides and polysulfides are anticipated to be important core structural elements in the nanoparticles, rather than surface artifacts.^{30,33,34}

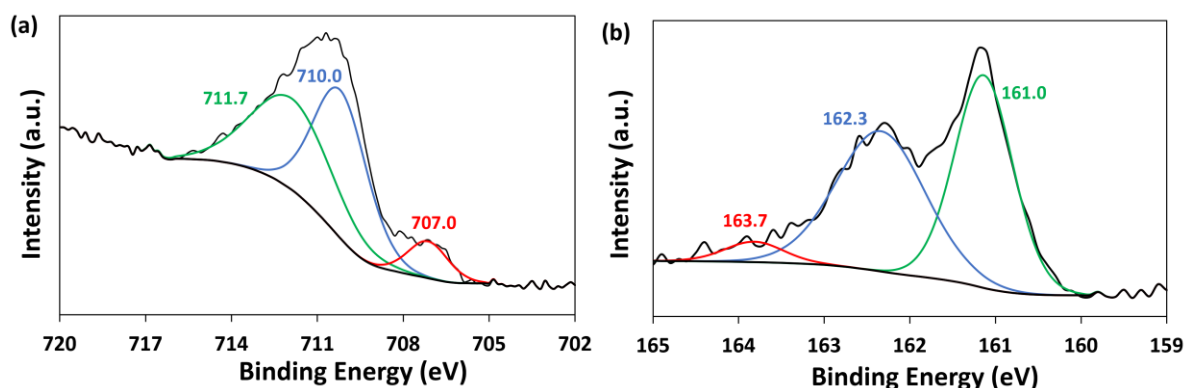


Figure 2.7. XPS spectra for (a) Fe 2p_{3,2} and (b) S 2p_{3,2} from the FeS nanocatalyst produced at 300 °C and 5000 ppm Fe.

2.3.3. Catalytic activity

The iron sulfide nanocatalyst was investigated for the partial hydrogenation of unsubstituted polycyclic arenes with varying aromatic stabilization energies and cleavage of thiophenic carbon-sulfur bonds. Pyrene hydrogenation was initially assessed, the products of which were readily identified (Figure 2.8).³⁵⁻³⁷ Reductions were run under uniform conditions, with pyrene (2.9 wt % solution in toluene) heated to 300 °C for 60 min under 6 MPa (cold) hydrogen pressure in the presence of the iron precatalyst (5000 ppm Fe). The solvent is inert to hydrogenation under the reaction conditions.

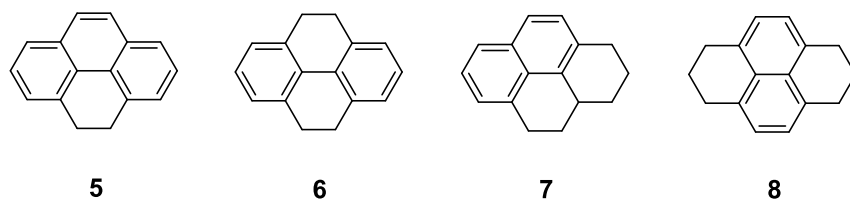


Figure 2.8. Structures of the products from pyrene hydrogenation.

Using $\text{Fe}_2\text{S}_2(\text{CO})_6$ as the catalyst precursor, 13.1 % conversion of pyrene (**1**) was observed, giving mostly 4,5-dihydropyrene **5** (11.6 mol %), along with minor amounts of more saturated products **6-8** (Table 2.1, entry 2). By contrast, the use of $\text{Fe}(\text{CO})_5$ in the absence of added sulfur gave just 3.6 % conversion (entry 3). No conversion is obtained upon heating in the absence of the catalyst (entry 1) indicating that the walls of the reactor had negligible catalytic activity. The importance of an iron sulfide phase in active hydrogenation catalysts is demonstrated by in situ sulfidation of $\text{Fe}(\text{CO})_5$ using elemental sulfur (entry 4), which gave 46.5 % conversion, a significant improvement. This dramatic increase relative to unsulfided $\text{Fe}(\text{CO})_5$ alone is consistent with the literature, which clearly establishes the key role that sulfur plays in catalytic arene hydrogenation.^{14,15,17} Although the active catalyst derived from $\text{Fe}(\text{CO})_5$ (entry 6) is slightly better than that from $\text{Fe}_2\text{S}_2(\text{CO})_6$ (entry 5) on comparable conditions (1:1 equivalence of Fe to S), $\text{Fe}(\text{CO})_5$ is air-sensitive, generates equilibrium concentrations of higher clusters and CO gas even on short-term storage, and requires special handling procedures to use on any scale. For end users in chemical- or oil-processing industries, an air- and thermally stable, low-toxicity, one-step, and easy-to-handle precatalyst is highly desirable.

Table 2.1. Catalytic effects of iron precatalysts and elemental sulfur on pyrene hydrogenation.

| Entry | Catalyst precursor | Conversion (%) | Yield (%) | | |
|-------|---|----------------|------------|-----------|------------|
| | | | 5 | 6 | (7 + 8) |
| 1 | None | 0.0 | 0.0 | 0.0 | 0.0 |
| 2 | Fe ₂ S ₂ (CO) ₆ | 13.1 (0.1) | 11.6 (0.4) | 0.5 (0.1) | 0.8 (0.1) |
| 3 | Fe(CO) ₅ | 3.6 (0.5) | 2.9 (0.1) | 0.0 | 0.3 (0.1) |
| 4 | Fe(CO) ₅ -S ^b | 46.5 (2.6) | 34.7 (2.0) | 3.2 (0.4) | 8.4 (0.3) |
| 5 | Fe ₂ S ₂ (CO) ₆ ^a | 29.0 (1.1) | 23.9 (0.5) | 0.8 (0.1) | 4.0 (0.2) |
| 6 | Fe(CO) ₅ -S ^{a,c} | 36.7 (2.9) | 27.6 (1.1) | 2.3 (0.8) | 6.3 (1.1) |
| 7 | Fe(CO) ₅ -S ^{a,b} | 59.7 (1.9) | 43.7 (0.9) | 4.6 (0.1) | 11.2 (1.0) |
| 8 | Fe(CO) ₅ ^a | 11.8 (0.9) | 10.0 (0.9) | 0.3 (0.1) | 1.0 (0.1) |
| 9 | FeS ^a | 2.3 (0.2) | 2.1 (0.1) | 0.0 | 0.0 |
| 10 | Fe ₂ S ₂ (CO) ₆ ^d | 27.0 (1.2) | 22.5 (1.6) | 0.7 (0.1) | 3.7 (0.5) |
| 11 | Fe ₂ S ₂ (CO) ₆ ^e | 28.8 (1.4) | 24.4 (0.8) | 0.9 (0.1) | 3.0 (0.1) |

Reaction conditions: temperature, 300 °C, Fe loading, 5000 ppm; initial H₂, 6 MPa; 2.9 wt % pyrene in toluene; time, 60 min. ^aActivated carbon, 0.1 g added. ^bFe/S molar ratio, 0.333 mol/mol. ^cFe/S molar ratio, 1.0 mol/mol. ^dAlumina, 0.1 g added. ^eSilica, 0.1 g added. Data are mean values for n = 2. Standard error values in parenthesis are one standard deviation.

Switching from an unsupported catalyst to the use of FeS nanoparticles dispersed on activated carbon provided a dramatic enhancement in conversion. For Fe₂S₂(CO)₆, pyrene conversion more than doubles (entry 5), presumably reflecting a greater number of active sites in the dispersed catalysts. A similar trend is evident when Fe(CO)₅ is used as the precatalyst, both in the presence (entry 6,7) and absence (entry 8) of added sulfur. An iron sulfide active phase, however, remains crucial to achieving high conversions (entries 5,6); a high concentration of the sulfiding agent increases the effectiveness of the catalyst derived from Fe(CO)₅ (entry 7). Finally, unmodified commercial iron sulfide is a poor catalyst for the hydrogenation of pyrene (entry 9), likely a result of significantly lower dispersion coupled with the presence of inactive crystalline phases.¹⁷ Physical pretreatment or milling of this ‘bulk’ iron sulfide prior to use is anticipated to yield

smaller, higher-surface-area catalyst particles, but $\text{Fe}_2\text{S}_2(\text{CO})_6$ remains our preferred precatalyst because the hydrocarbon solubility of the precursor should allow the creation of even smaller nanosized particles than milling would allow, with superior dispersion into a complex asphaltene matrix. It is noteworthy that $\text{Fe}_2\text{S}_2(\text{CO})_6$ is the first arene hydrogenation precatalyst of iron that does not require an external sulfiding agent to produce highly active catalyst. The distribution of products from the partial hydrogenation of pyrene is typical for hydrogenation catalysis, with 4,5-dihydropyrene (**5**) as the major product. While our data are not sufficient to establish a conclusive pathway for further hydrogenation, 4,5,9,10-tetrahydropyrene (**6**) and 1,2,3,3a,4,5-hexahydropyrene (**7**) are present,³⁷⁻³⁹ as is 1,2,3,6,7,8-hexahydropyrene (**8**), which can be formed directly from pyrene or by olefin isomerization of **7**.^{17,40} Indeed, the purified hexahydropyrene **7** isomerizes primarily to **8** under the reaction conditions, also returning a minor amount of disproportionation products pyrene **1** and dihydropyrene **5**. We conclude that the thermodynamically driven isomerization^{35,40} of **7** is the principal source of **8** in our reaction. The high yield of dihydropyrene **5** relative to other products is unusual. The hydrogenation of pyrene to the dihydropyrene intermediate is thermodynamically favorable, but further hydrogenation to 4,5,9,10-tetrahydropyrene **6** is also thermodynamically driven;⁴¹ the total resonance stabilization energy increases as pyrene is hydrogenated to the biphenyl core tetrahydropyrene.^{35,36} At that point, further hydrogenation is kinetically prohibitive, but the products continue to equilibrate by dehydrogenation/rehydrogenation and nonhydrogenative alkene migration, giving the observed product distribution.³⁷ Ting et al.³⁷ further suggests that the torsional strain energy in the skew-chair saturated rings of tetrahydropyrene **6** lowers the activation barrier to isomerization and further hydrogenation to the hexahydropyrenes **7** and **8**.

The higher activity observed for supported catalysts derived from $\text{Fe}_2\text{S}_2(\text{CO})_6$ remains consistent across several dispersants (Table 2.1, entries, 5, 10, and 11), suggesting that the increase in catalytic activity is due to smaller particle size and resistance to sintering rather than metal-support synergies.⁴² Other unsupported Fe precursors have been used to reduce pyrene at temperatures ranging from 380 to 425 °C,¹⁵ but the highest conversion is reported to be 12 %. Much higher conversion (31 %) was reported by Suzuki et al.¹⁷ from the combination of $\text{Fe}(\text{CO})_5$, elemental sulfur and activated carbon, which was reproduced as a control for this study. Previous studies⁴³⁻⁴⁵ have asserted that the support plays a critical role, mediating metal-free hydrogenation of some PAHs. The data suggest otherwise; no background support-induced hydrogenation was detected in the absence of an iron source.

2.3.4. Optimization and scope of catalytic arene hydrogenations

2.3.4.1. Influence of iron concentration on the hydrogenation of pyrene (1)

Prior to addressing the scope of arene hydrogenations using the presulfided iron catalyst, the effects of operating conditions on the activity of the supported catalyst were assessed, beginning with studying the effects of catalyst concentration on pyrene hydrogenation. The conversion of pyrene is directly dependent on catalyst loading, but only to a point (Figure 2.9). The relationship between substrate conversion and catalyst loading is a key indicator of mass-transfer limitations in heterogeneous catalysis.³⁸ The reactor used in this study is a vibrating-type batch reactor that was operated at 14 Hz with a relatively long amplitude of 17.5 mm. When operated in this mode, the vibrational pressure easily overcomes the hydrostatic pressure and enables excellent mixing within the vessel. Visualization experiments using a similar clear reactor showed chaotic mixing

with complete suspension of a powdered solid catalyst and incorporation of the gas phase into the mixture.⁴⁶ These types of systems have been shown to have very high gas-liquid mass-transfer rates.⁴⁷⁻⁴⁹ In this case, the proportional increase in conversion up to ~5000 ppm establishes that external mass-transfer limitations are likely negligible under typical catalyst loadings. Indeed, the small particle size (62 ± 10.6 nm) of the putative active FeS phase is expected to suffer but minimal internal mass-transfer limitations (Figure 2.5).⁵⁰

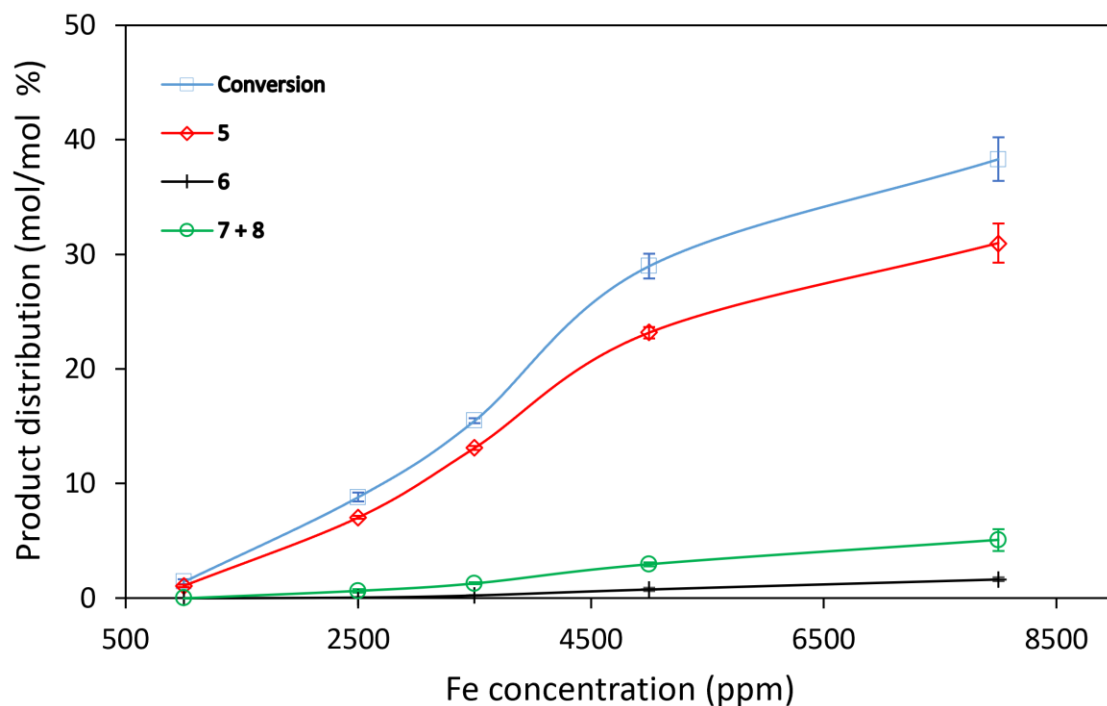


Figure 2.9. Relationship between $\text{Fe}_2\text{S}_2(\text{CO})_6$ loading and product distribution of pyrene. Reaction conditions: temperature, 300 °C; cold H_2 , 6 MPa; activated carbon, 0.1 g; time, 60 min.

The inflection point observed at ~4400 ppm and change in the slope reveals the onset of catalyst saturation or particle agglomeration to form larger, less active, superstructures. Beyond 5000 ppm Fe, the conversion per metal is suppressed (Figure 2.10), supporting the notion of iron mobility on

the surface of the support or by solvation/readsorption of molecular clusters at high temperatures.

A precatalyst loading of 5000 ppm was adopted for all subsequent experiments.

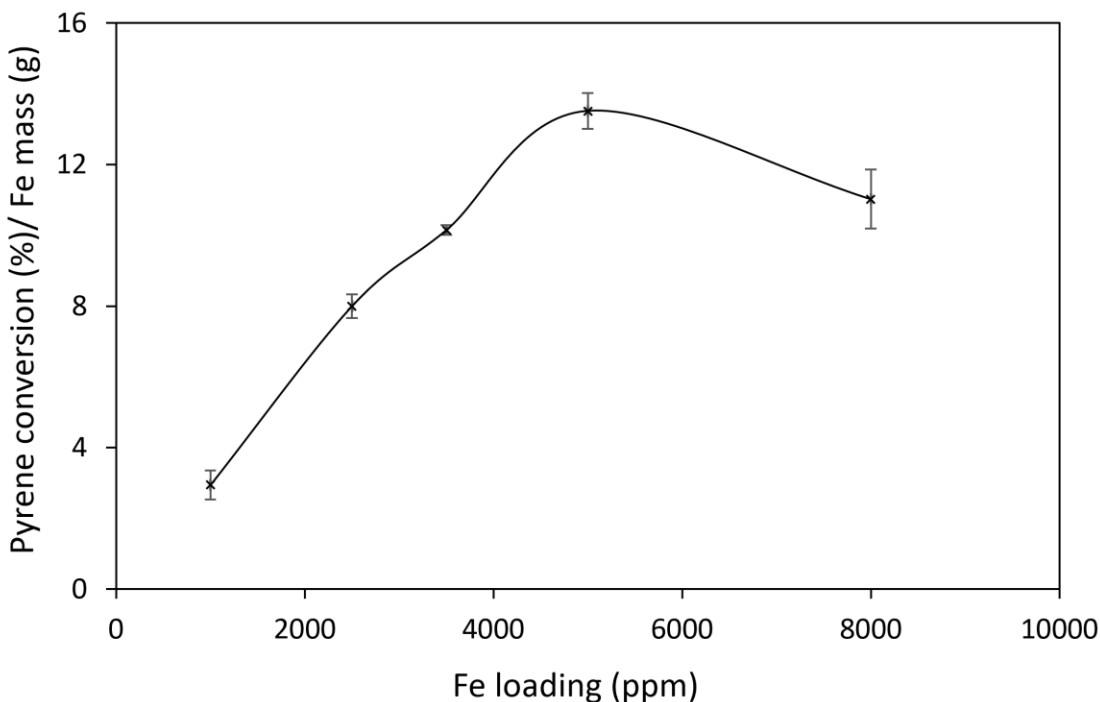


Figure 2.10. Ratio of pyrene conversion and iron mass against Fe loading. Reaction conditions: temperature, 300 °C; cold H₂, 6 MPa; activated carbon, 0.1 g; time, 60 min.

2.3.4.2. Influence of pressure and temperature on hydrogenation rate and conversion

The effect of initial hydrogen pressure on the conversion and product distribution obtained from pyrene hydrogenation is displayed in Figure 2.11a. As expected, pyrene conversion increases with increasing hydrogen partial pressure, rising from 11.7 to 40 % conversion with an increase from 2 and 10 MPa. Hydrogen gas dissolves in the liquid phase and adsorbs onto the catalyst surface more readily at higher H₂ pressure. Dissociation of the adsorbed gas produces an ample supply of hydrogen atoms to drive the reduction reactions forward. The effect of higher pressures on the

hydrogenation of pyrene diminishes beyond 6 MPa; the yield of **5** increased by 150 % (from 9.24 to 23.16 %) between 2 and 6 MPa but only by 35 % (from 23.16 to 31.62) between 6 and 10 MPa. It is likely that at higher H₂ pressure, there is competitive adsorption with the substrate, causing a decrease in substrate-catalyst coordination. Additional experimental work is required to verify this hypothesis, but based on these data, 6 MPa H₂ pressure was used for most reactions.

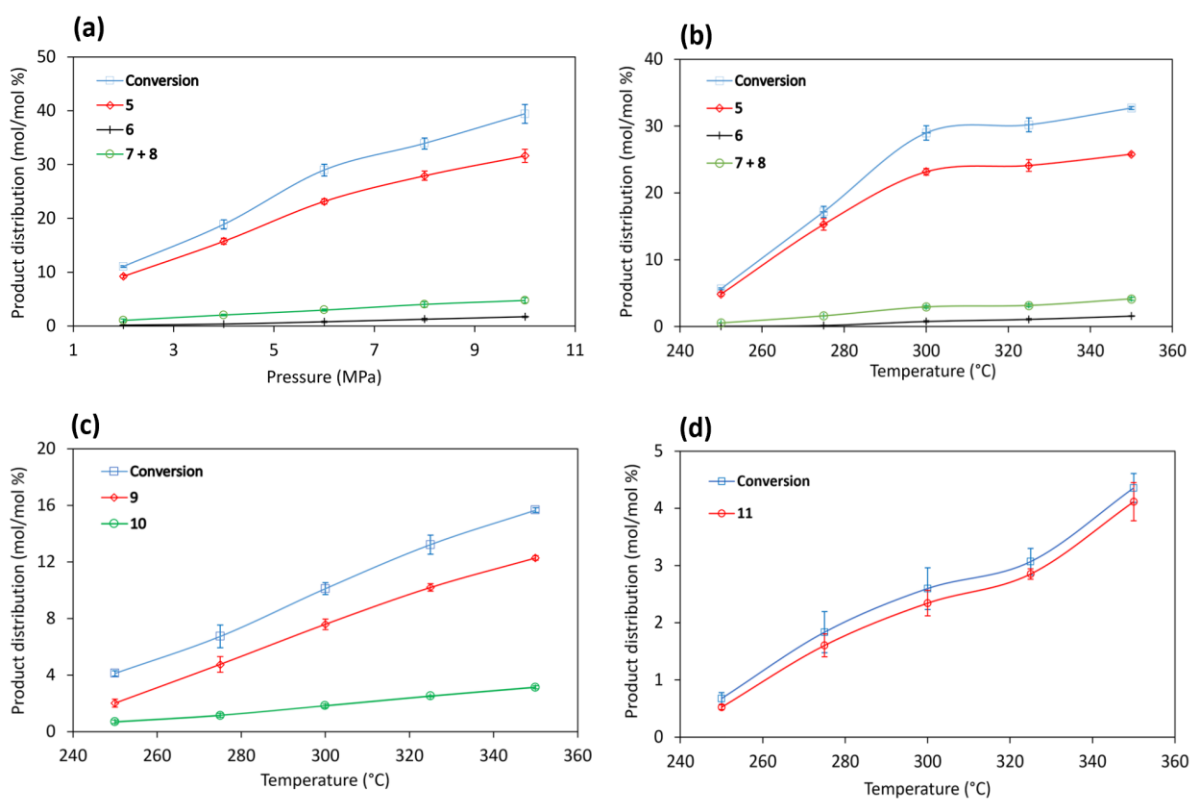


Figure 2.11. (a) Pyrene pressure profile and influence of temperature on (b) pyrene (c) phenanthrene and (d) naphthalene hydrogenation over Fe₂S₂(CO)₆. Reaction conditions: temperature; 250-350 °C; cold H₂, 2-10 MPa; activated carbon, 0.1 g; time, 60 min.

The catalytic hydrogenation responds to temperature variations in a typical fashion; very little conversion is observed at 250 °C, but conversion increases dramatically above this, increasing to 29 % at an optimal temperature of 300 °C. Higher conversions are obtained beyond this

temperature, but the plateau is severe (Figure 2.11b). This stagnation in conversion at very high temperatures is not uncommon and is generally attributed to competitive entropically driven dehydrogenation. Alternatively, it is also possible that a thermally induced shift in the Langmuir adsorption isotherm favors desorption of pyrene and/or molecular hydrogen. Similar observations have been reported by others,^{38,50} with some evidence supporting the competitive dehydrogenation option.

2.3.4.3. Scope of aromatic hydrogenation

The iron sulfide catalyst promotes hydrogenation of other polycyclic aromatic molecules, with mixed results (Figure 2.12). Phenanthrene is hydrogenated to 9,10-dihydrophenanthrene (**9**) as the major product, along with a very small quantity of 1,2,3,4-tetrahydrophenanthrene (**10**) (Figure 2.11c). It has been suggested that the dihydrophenanthrene **9** is formed first then subsequently converted to tetrahydrophenanthrene (**10**)⁵¹ but control reactions starting with **9** as a substrate show that it is more likely to revert to phenanthrene **2** by dehydrogenation.^{52,53} Mathematical modeling of first- and second-rank Delplots⁵⁴⁻⁵⁶ also confirms that tetrahydrophenanthrene is a primary product, derived directly from phenanthrene, not from an intermediate (Figure A1 in Appendix A).

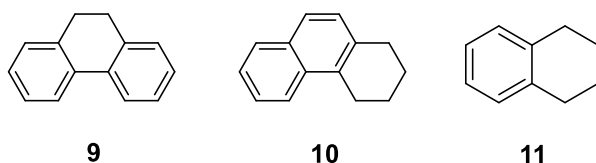


Figure 2.12. Phenanthrene and naphthalene hydrogenation products.

In contrast to pyrene and phenanthrene, naphthalene (**3**) strongly resists hydrogenation at any temperature (Figure 2.11d), giving low conversion (4.3 %) to 1,2,3,4-tetrahydronaphthalene (**11**) at 350 °C. This is as expected, given the high activation barrier for disruption of the aromaticity.

No dihydronaphthalene was detected, a consequence of rapid subsequent hydrogenation to 1,2,3,4-tetrahydronaphthalene, as verified by control reactions. Once formed, the isolated aromatic ring in 1,2,3,4-tetrahydronaphthalene strongly resists further hydrogenation, reflecting the intrinsic stability of the “perfectly aromatic” isolated benzene ring. Precious metal catalysts (e.g., Pd, Pt) are generally required to readily convert such rings to the saturated hydrocarbon.⁵⁷ The differences between naphthalene conversion and the yields of 1,2,3,4-tetrahydronaphthalene (Figure 2.11d) are not statistically significant within a 95% confidence interval.

2.3.4.4. Hydrodesulfurization of benzothiophene

Sulfur removal from petroleum is vital for meeting pipeline and refinery standards, as well as reducing harmful emissions from combustion.⁹ Desulfurization catalysts containing molybdenum, nickel, and cobalt are widely used in the industry, but low-cost iron hydrodesulfurization catalysts are highly desirable, if elusive.^{11,58} The iron sulfide nanoparticles described here catalyze both hydrogenation and subsequent hydrodesulfurization of benzothiophene to 2,3-dihydrobenzothiophene (**12**) and ethylbenzene (**13**) (Figure 2.13a).

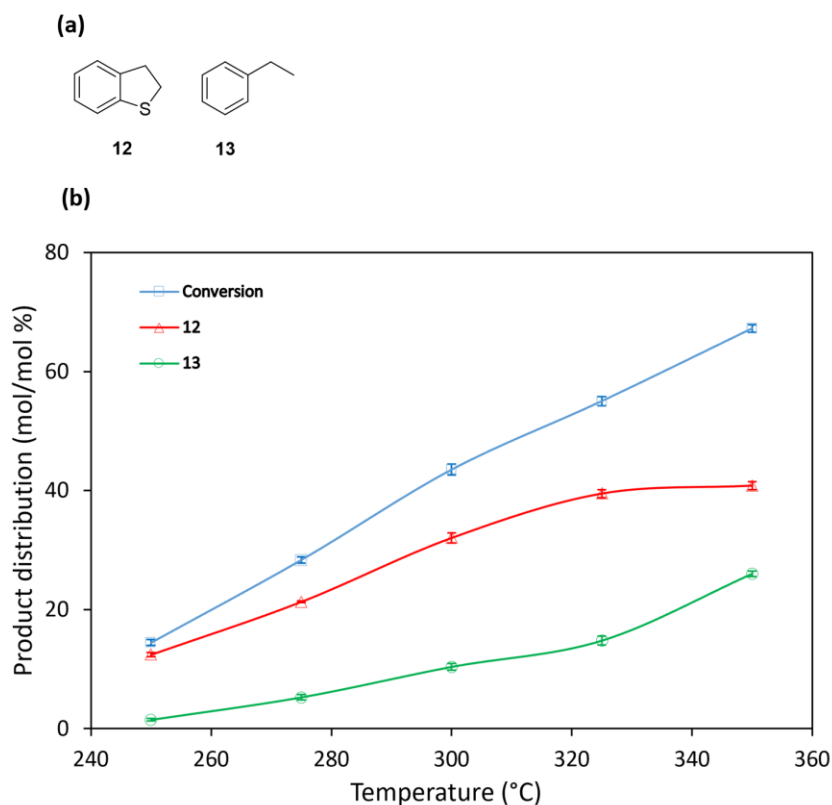


Figure 2.13. (a) Benzothiophene hydrodesulfurization products and (b) relationship between temperature and product distribution for the hydrodesulfurization of benzothiophene over $\text{Fe}_2\text{S}_2(\text{CO})_6$. Reaction conditions: temperature, 250-350 °C; cold H_2 , 6 MPa; activated carbon, 0.1 g; time, 60 min.

The temperature dependence of the reaction is typical, with the exception of the unusual rate acceleration for ethylbenzene formation simultaneously with the plateau in the yield of the simple hydrogenation product (Figure 2.13b). This suggests either a rapid conversion of 2,3-dihydrobenzothiophene to ethylbenzene at this temperature or alternatively a competitive direct desulfurization pathway. Both have been established for other catalysts.⁵⁹⁻⁶³ For comparison, while mineral pyrite from coal is active for hydrogenation of the heterocyclic ring in benzothiophene, it is much less effective for sulfur removal.⁶⁴ Both the trinuclear iron cluster $(\text{Fe}_3(\text{CO})_{12})$ ⁶⁵ and a sulfided iron naphthenate-derived catalyst⁵⁹ promote desulfurization of benzothiophene to ethylbenzene but require much more forceful conditions than required for the $\text{Fe}_2\text{S}_2(\text{CO})_6$

precatalyst. The present study results, along with past reports,^{11,58} strongly suggest that the development of inexpensive iron catalysts for direct desulfurization is indeed feasible.

2.4. Conclusions

In this work, we demonstrated that a synthetic “single-source” iron precatalyst is effective for the hydrogenation of condensed aromatic and heterocyclic compounds representative of heavy crude oil. The active pyrrhotite FeS nanoparticles are very selective for partial hydrogenation and limited desulfurization, making them suited for development in petroleum partial-upgrading processes. The ease of preparation and exceptional air stability of the "earth-abundant" metal precatalyst, coupled with the moderate hydroprocessing conditions, make iron catalysts good candidates for further development and use in petroleum processing. Further optimization and applications of the catalyst system to the hydroprocessing of authentic petroleum feeds is essential.

2.5. References

1. de Vries, J. G.; Elsevier, C. J. *The Handbook of Homogeneous Hydrogenation*; Wiley-VCH: Weinheim, 2007.
2. Han, B.; Ma, P.; Cong, X.; Chen, H.; Zeng, X. Chromium- and Cobalt-Catalyzed, Regiocontrolled Hydrogenation of Polycyclic Aromatic Hydrocarbons: A Combined Experimental and Theoretical Study. *J. Am. Chem. Soc.* **2019**, *141*, 9018.
3. Liu, Z. Q.; Wei, X. Y.; Liu, F. J.; Wang, B. J.; Zong, Z.M. Temperature-Controlled Hydrogenation of Anthracene over Nickel Nanoparticles Supported on Attapulgite Powder. *Fuel* **2018**, *223*, 222.
4. Hagen, J. *Industrial Catalysis: A Practical Approach*; Wiley-VCH: Weinheim, 2015.
5. Sánchez, J.; Moreno, A.; Mondragón, F.; Smith, K. J. Morphological and Structural Properties of MoS₂ and MoS₂-Amorphous Silica-Alumina Dispersed Catalysts for Slurry-Phase Hydroconversion. *Energy Fuels* **2018**, *32*, 7066.
6. Li, Y.; Ma, F., Su, X.; Shi, L.; Pan, B.; Sun, Z.; Hou, Y. Ultra-Large-Scale Synthesis of Fe₃O₄ Nanoparticles and Their Application for Direct Coal Liquefaction. *Ind. Eng. Chem. Res.* **2014**, *53*, 6718.
7. Stanislaus, A.; Cooper, B. H. Aromatic Hydrogenation Catalysis: A review. *Catal. Rev. Sci. Eng.* **1994**, *36*, 75.
8. Deng, W.; Lu, J.; Li, C. Hydrogenation Behavior of Bicyclic Aromatic Hydrocarbons in the Presence of a Dispersed Catalyst. *Energy Fuels* **2015**, *29*, 5600.
9. Tanimu, A.; Alhooshani, K. Advanced Hydrodesulfurization Catalysts: A Review of Design and Synthesis. *Energy Fuels* **2019**, *33*, 2810.
10. Giustra, Z. X.; Ishibashi, J. S.; Liu, S. Y. Homogeneous Metal Catalysis for Conversion between Aromatic and Saturated Compounds. *Coord. Chem. Rev.* **2016**, *314*, 134.
11. Li, H.; Liu, J.; Li, J.; Hu, Y.; Wang, W.; Yuan, D.; Wang, Y.; Yang, T.; Li, L.; Sun, H.; Ren, S. Promotion of the Inactive Iron Sulfide to an Efficient Hydrodesulfurization Catalyst. *ACS Catal.* **2017**, *7*, 4805.
12. Habib, F. K.; Diner, C.; Stryker, J. M.; Semagina, N.; Gray, M.R. Suppression of Addition Reactions during Thermal Cracking Using Hydrogen and Sulfided Iron Catalyst. *Energy Fuels* **2013**, *27*, 6637.

13. Huffman, G. P.; Ganguly, B.; Zhao, J.; Rao, K. R. P. M.; Shah, N.; Feng, Z.; Huggins, F. E.; Taghiei, M. M.; Lu, F. Structure and Dispersion of Iron-Based Catalysts for Direct Coal Liquefaction. *Energy Fuels* **1993**, *7*, 285.
14. Herrick, D. E.; Tierney, J. W.; Wender, I.; Huffman, G. P.; Huggins, F. E. Activity and Characterization of Coprocessing Catalysts Produced from an Iron Pentacarbonyl Precursor. *Energy Fuels* **1990**, *4*, 231.
15. Tang, Y.; Curtis, C. W. Activity and Selectivity of Slurry-Phase Iron-Based Catalysts for Model Systems. *Energy Fuels* **1994**, *8*, 63.
16. Kelly, T. D.; Matos, G. R. *Historical Statistics for Mineral and Material Commodities in the United States, 2015*; U.S. Geological Survey Data Series 140; <https://www.usgs.gov/centers/nmic/historical-statistics-mineral-and-material-commodities-united-states>. Accessed on March 16, 2020.
17. Suzuki, T.; Yamada, H.; Sears, P. L.; Watanabe, Y. Hydrogenation and Hydrogenolysis of Coal Model Compounds by Using Finely Dispersed Catalysts. *Energy Fuels* **1989**, *3*, 707.
18. Gray, M. R. Fundamentals of Partial Upgrading of Bitumen. *Energy Fuels* **2019**, *33*, 6843.
19. Pradhan, V.; Herrick, D. E.; Tierney, J. W.; Wender, I. Finely Dispersed Iron, Iron-Molybdenum, and Sulfated Iron Oxides as Catalysts for Coprocessing Reactions. *Energy Fuels* **1991**, *5*, 712.
20. Quitian, A.; Ancheyta, J. Experimental Methods for Developing Kinetic Models for Hydrocracking Reactions with Slurry-Phase Catalyst Using Batch Reactors. *Energy Fuels* **2016**, *30*, 4419.
21. Del Bianco, A.; Panariti, N.; Di Carlo, S.; Elmouchnino, J.; Fixari, B.; Le Perchec, P. Thermocatalytic Hydroconversion of Heavy Petroleum Cuts with Dispersed Catalyst. *Appl. Catal.* **1993**, *94*, 1.
22. Gray, M. R. *Upgrading Oilsands Bitumen and Heavy Oil*; University of Alberta Press: Edmonton, Alberta, Canada, 2015.
23. Akbarzadeh, K.; Bressler, D.C.; Wang, J.; Gawrys, K. L.; Gray, M.R.; Kilpatrick, P.K.; Yarranton, H. W. Association Behavior of Pyrene Compounds as Models for Asphaltenes. *Energy Fuels* **2005**, *19*, 1268.
24. Alshareef, A. H. Asphaltenes: Definition, Properties, and Reactions of Model Compounds. *Energy Fuels* **2020**, *34*, 16.

25. Wei, C. H.; Dahl, L. F. The Molecular Structure of a Tricyclic Complex, $[\text{SFe}(\text{CO})_3]_2$. *Inorg. Chem.* **1965**, *4*, 1.
26. Brandt, P. F.; Lesch, D. A.; Stafford, P. R.; Rauchfuss, T. B.; Kolis, J. W.; Roof, L. C. $\text{Fe}_2(\text{S}_2)(\text{CO})_6$ and $\text{Fe}_3\text{Te}_2(\text{CO})_{9,10}$. *Inorg. Synth.* **1997**, *31*, 112.
27. Seyferth, D.; Henderson, R. S.; Song, L. -C. Chemistry of μ -Dithio-bis(tricarbonyliron), a Mimic of Inorganic Disulfides. 1. Formation of Di- μ -thiolato-bis(tricarbonyliron) Dianion. *Organometallics* **1982**, *1*, 125.
28. Di Giovanni, C.; Wang, W. A.; Nowak, S.; Grenèche, J.M.; Lecoq, H.; Mouton, L.; Giraud, M.; Tard, C. Bioinspired Iron Sulfide Nanoparticles for Cheap and Long-Lived Electrocatalytic Molecular Hydrogen Evolution in Neutral Water. *ACS Catal.* **2014**, *4*, 681.
29. Stanley, J. L.; Rauchfuss, T. B.; Wilson, S.R. Studies on the Condensation Pathway to and Properties of Diiron Azadithiolate Carbonyls. *Organometallics* **2007**, *26*, 1907.
30. Pratt, A. R.; Muir, I. J.; Nesbitt, H. W. X-ray Photoelectron and Auger Electron Spectroscopic Studies of Pyrrhotite and Mechanism of Air Oxidation. *Geochim. Cosmochim. Acta* **1994**, *58*, 827.
31. Jones, C. F.; LeCount, S.; Smart, R. S. C.; White, T. J. Compositional and Structural Alteration of Pyrrhotite Surfaces in Solution: XPS and XRD Studies. *Appl. Surf. Sci.* **1992**, *55*, 65.
32. Buckley, A. A.; Woods, R. X-ray Photoelectron Spectroscopy of Oxidized Pyrrhotite Surfaces: I. Exposure to Air. *Appl. Surf. Sci.* **1985**, *22*, 280.
33. Matamoros-Veloza, A.; Cespedes, O.; Johnson, B. R. G.; Stawski, T. M.; Terranova, U.; de Leeuw, N. H.; Benning, L. G. A Highly Reactive Precursor in the Iron Sulfide System. *Nat. Commun.* **2018**, *9*, 3125.
34. Smart, R. S. C.; Skinner, W. M.; Gerson, A. R. XPS of Sulphide Mineral Surfaces: Metal-Deficient, Polysulphides, Defects and Elemental Sulphur. *Surf. Interface Anal.* **1999**, *28*, 101.
35. Lin, Q.; Shimizu, K. I.; Satsuma, A. Hydrogenation of Pyrene Using Pd Catalysts Supported on Tungstated Metal Oxides. *Appl. Catal., A* **2010**, *387*, 166.
36. Tang, T.; Yin, C.; Wang, L.; Ji, Y.; Xiao, F. S. Good Sulfur Tolerance of a Mesoporous Beta Zeolite-Supported Palladium Catalyst in the Deep Hydrogenation of Aromatics. *J. Catal.* **2008**, *257*, 125.

37. Ting, P. S.; Curtis, C. W.; Cronauer, D. C. Reactions of Model Compounds in the Presence of Pyrene and MoS₂ to Simulate Coprocessing. *Energy Fuels* **1992**, *6*, 511.
38. Johnston, K. P. Hydrogenation-dehydrogenation of Pyrenes Catalysed by Sulphided Cobalt-Molybdate at Coal Liquefaction Conditions. *Fuel* **1984**, *63*, 463.
39. Korre, S. C.; Klein, M. T.; Quann, R. J. Polynuclear Aromatic Hydrocarbons Hydrogenation. 1. Experimental Reaction Pathways and Kinetics. *Ind. Eng. Chem. Res.* **1995**, *34*, 101.
40. Minabe, M.; Nakada, K. Hydrogenation of Pyrene and Catalytic Interconversion of Hydropyrenes. *Bull. Chem. Soc. Jpn.* **1985**, *58*, 1962.
41. Fu, P. P.; Lee, H. M.; Harvey, R. G. Regioselective Catalytic Hydrogenation of Polycyclic Aromatic Hydrocarbons under Mild Conditions. *J. Org. Chem.* **1980**, *45*, 2797.
42. Zhang, L.; Zhou, M.; Wang, A.; Zhang, T. Selective Hydrogenation over Supported Metal Catalysts: From Nanoparticles to Single Atoms. *Chem. Rev.* **2020**, *120*, 683.
43. Sun, L. B.; Zong, Z. M.; Kou, J. H.; Zhang, L. F.; Ni, Z. H.; Yu, G. Y.; Chen, H.; Wei, X. Y.; Lee, C. W. Activated Carbon-Catalyzed Hydrogenation of Polycyclic Arenes. *Energy Fuels* **2004**, *18*, 1500.
44. Sun, L. B.; Zong, Z. M.; Kou, J. H.; Liu, G. F.; Sun, X.; Wei, X. Y.; Zhou, G. J.; Lee, C. W. Activated Carbon-Catalyzed Hydrogen Transfer to α,ω -Diarylalkanes. *Energy Fuels* **2005**, *19*, 1.
45. Sun, L. B.; Wei, X. Y.; Liu, X. Q.; Zong, Z. M.; Li, W.; Kou, J. H. Selective Hydrogen Transfer to Anthracene and Its Derivatives over an Activated Carbon. *Energy Fuels* **2009**, *23*, 4877.
46. Olson, B. J. *The Role of Sulfur during the Cracking of n-Hexadecane and Cold Lake Bitumen with Alpha-Fe₂O₃ and Steam*; M.Sc. Thesis, University of Alberta, Edmonton, AB, CA, 2013.
47. Buchanan, R. H.; Jameson, G.; Oedjoe, D. Cyclic Migration of Bubbles in Vertically Vibrating Liquid Columns. *Ind. Eng. Chem. Fundam.* **1962**, *1*, 82.
48. Still, A. L.; Ghajar, A. J.; O'Hern, T.J. Effect of Amplitude on Mass Transport, Void Fraction and Bubble Size in a Vertically Vibrating Liquid-Gas Bubble Column Reactor. In *Proceedings of the ASME Fluids Engineering Summer Meeting, FEDSM2013*, Incline Village, NV, USA, July 7-11, 2013.

49. Elbing, B. R.; Still, A. L.; Ghajar, A. J. Review of bubble column reactors with vibration. *Ind. Eng. Chem. Res.* **2016**, *55*, 385.
50. Dutta, R. P.; Schobert, H. H. Hydrogenation/dehydrogenation of Polycyclic Aromatic Hydrocarbons Using Ammonium Tetrathiomolybdate as Catalyst Precursor. *Catal. Today* **1996**, *31*, 65.
51. Lemberon, J. L.; Guisnet, M. Phenanthrene Hydroconversion as a Potential Test Reaction for the Hydrogenating and Cracking Properties of Coal Hydroliquefaction Catalysts. *Appl. Catal.* **1984**, *13*, 181.
52. Girgis, M. J.; Gates, B. C. Reactivities, Reaction Networks, and Kinetics in High-Pressure Catalytic Hydroprocessing. *Ind. Eng. Chem. Res.* **1991**, *30*, 2021.
53. Girgis, M. J.; Gates, B. C. Catalytic Hydroprocessing of Simulated Heavy Coal Liquids. 2. Reaction Networks of Aromatic Hydrocarbons and Sulfur and Oxygen Heterocyclic Compounds. *Ind. Eng. Chem. Res.* **1994**, *33*, 2301.
54. Bhore, N. A.; Klein, M. T.; Bischoff, K. B. The Delplot Technique: A New Method for Reaction Pathway Analysis. *Ind. Eng. Chem. Res.* **1990**, *29*, 313.
55. Bhore, N. A.; Klein, M. T.; Bischoff, K. B. Species Rank in Reaction Pathways: Application of Delplot Analysis. *Chem. Eng. Sci.* **1990**, *45*, 2109.
56. Klein, M. T.; Hou, Z.; Bennett, C. Reaction Network Elucidation: Interpreting Delplots for Mixed Generation Products. *Energy Fuels* **2012**, *26*, 52.
57. Huang, T. C.; Kang, B. C. Hydrogenation of Naphthalene with Platinum-Aluminium Borate Catalysts. *Chem. Eng. J.* **1996**, *63*, 27.
58. Villasana, Y.; Ruscio-Vanalesti, F.; Pfaff, C.; Méndez, F. J.; Luis-Luis, M. Á.; Brito, J. L. Atomic Ratio Effect on Catalytic Performance of FeW-Based Carbides and Nitrides on Thiophene Hydrodesulfurization. *Fuel* **2013**, *110*, 259.
59. Curtis, C. W.; Chen, J. H.; Tang, Y. Hydrodesulfurization of Model Systems Using Slurry-Phase Catalysts. *Energy Fuels* **1995**, *9*, 195.
60. Srivastava, V. C. An Evaluation of Desulfurization Technologies for Sulfur Removal from Liquid Fuels. *RSC Adv.* **2012**, *2*, 759.
61. Huo, Z.; Jin, F.; Yao, G.; Enomoto, H.; Kishita, A. An in Situ Raman Spectroscopic Study of Benzothiophene and Its Desulfurization under Alkaline Hydrothermal Conditions. *Ind. Eng. Chem. Res.* **2015**, *54*, 1397.

62. Van Parijs, I. A.; Hosten, L. H.; Froment, G. F. Kinetics of Hydrodesulfurization on a CoMo/ γ -Al₂O₃ Catalyst. 2. Kinetics of the Hydrogenolysis of Benzothiophene. *Ind. Eng. Chem. Prod. Res. Dev.* **1986**, *25*, 437.
63. Wang, H.; Prins, R. HDS of Benzothiophene and Dihydrobenzothiophene over Sulfided Mo/ γ -Al₂O₃. *Appl. Catal., A* **2008**, *350*, 191.
64. Guin, J. A.; Lee, J. M.; Fan, C. W.; Curtis, C. W.; Lloyd, J. L.; Tarrer, A. R. Pyrite-Catalyzed Hydrogenolysis of Benzothiophene at Coal Liquefaction Conditions. *Ind. Eng. Chem. Process Des. Dev.* **1980**, *19*, 440.
65. Ogilvy, A. E.; Draganjac, M.; Rauchfuss, T. B.; Wilson, S. R. Activation and Desulfurization of Thiophene and Benzothiophene by Iron Carbonyls. *Organometallics* **1988**, *7*, 1171.

2.6. Associated content

Supporting information is provided in Appendix A

First- and second-rank Delplots (Figure A1); and possible reaction network for all substrates (Figure A2).

Chapter 3: Selective Hydrogenation and Defunctionalization of Heavy Oil Model Compounds Using an Unsupported Iron Catalyst

Published in Fuel

3.1. Introduction

The Canadian oil sands industry extracts, processes, and transports large volumes of highly viscous heavy crude oil. Because of this, research in bitumen and heavy oil upgrading is growing rapidly, with a keen focus on developing more economically viable and environmentally friendly processing technologies. One of the major challenges is the transportation of bitumen to refineries. This challenge is because the density and viscosity of extracted crude bitumen (7-10 °API) is insufficient to meet pipeline standards (≥ 19 °API). For transportation, the feedstock must be upgraded to pipeline-compatible synthetic crude oil (SCO) or blended with diluents prior to market delivery. Although SCO is more valuable than diluted bitumen, capital expenses, operating costs, and greenhouse gas (GHG) emissions associated with current bitumen upgraders make continued investments in such ventures unattractive.¹ The use of diluent for transporting bitumen is also undesirable, principally due to recovery and recycling costs, as well as the lower quality of the recovered bitumen, which retails at steep discounts relative to benchmark crude oils. More importantly, the diluent occupies 30-50% of pipeline volume, severely limiting the quantity of bitumen that can be transported over existing pipeline and rail networks.² Recent volatility in oil prices, coupled with ongoing limited pipeline capacity has driven the industry to explore emerging technologies for reducing or eliminating bitumen dilution, while avoiding the traditional upgrading process. Partial upgrading is an ideal term to apply to such objectives.

Partial upgrading encompasses any process that converts low-API gravity bitumen or heavy oil into a product that meets the density and viscosity specifications for transport by pipeline with limited or, more preferably, no use of diluents.³ This technology has gained momentum among academic researchers and commercial processors because it can produce refinery- and pipeline-grade feedstocks with lower capital and operating expenses compared to either full upgrading or dilution. The high-boiling components in heavy oil such as asphaltenes are mainly responsible for its high viscosity,⁴ therefore partial upgrading technologies focus on compositional modification of asphaltene fractions to reduce viscosity. Currently, most emerging partial upgrading technologies rely on high-temperature thermal conversion⁵ or partial deasphalting.^{1,6} Unfortunately, such thermal treatments produce reduced volumetric yields of unstable liquid products, which may require further processing in order to prevent pipeline fouling. Partial deasphalting produces a more stable and transportable product, but volume loss is even more severe.¹ Hydroprocessing under moderate conditions⁷ is a more desirable approach to bitumen partial upgrading because this process can, in principle, provide higher liquid yields of a more stable product with significant improvement in transport properties. These selective hydrogenation and limited defunctionalisation reactions of the polycyclic aromatic compounds in heavy oil can lead to the compositional changes that are known to significantly reduce viscosity.^{1,8}

Slurry-phase hydrogenation is among the most effective hydroprocessing methods for partial upgrading. In this process, highly-dispersed unsupported transition metal catalysts, typically Fe, Ni, Co, and Mo, are used to produce high quality distillates.⁹⁻¹² Colloidal catalysts are preferred over supported catalysts for partial upgrading, because the former is more easily dispersed in the

viscous feed. In addition, colloidal catalysts promote rapid uptake of hydrogen, making them more resistant to deactivation from coke formation.¹³⁻¹⁶ Because of their small size and dispersion in the reaction medium, colloidal catalysts used in slurry-phase hydrogenation are not usually recovered or recycled, but instead removed in waste streams. For this reason, inexpensive, earth-abundant and environmentally benign transition metals such as iron make ideal catalysts.¹⁷ While catalyst separation and recycling were outside the scope of this study, in an industrial process, the iron catalyst would likely be collected in any unconverted residue, recycled, and mixed with fresh feed and make-up catalyst.

Unsupported iron sulfide catalysts derived from precursors such as Fe_3O_4 ,¹⁸ $\text{Fe}(\text{CO})_5$,¹⁹ Fe_2O_3 ,²⁰ $\text{Fe}(\text{CO})_9$,²¹ and iron naphthenate²² have been used for hydroconversion of coal. The molecular similarities between coal and heavy crude oils²³⁻²⁶ suggest that comparable iron catalysts are likely to be well-suited for hydroprocessing bitumen into a partially upgraded product.

To model slurry-phase hydrogenation reactions in heavy oils, the investigation of representative model compounds is critical. Typically, the model compounds are small aromatic carbocycles and heterocycles, including pyrene, phenanthrene, naphthalene, anthracene, quinoline and benzothiophene, which are representative of key structural units, if not actual bitumen constituents, present in heavy crude oil (Figure 3.1).²⁷⁻²⁹ The behavior of these small molecules reveals structure-activity relationships pertinent to the optimization of catalyst design and reaction conditions. Model feeds containing both carbocyclic and heterocyclic aromatic hydrocarbons are particularly important because these mixtures better mimic the complex composition of heavy crude oil.

In chapter 2, it was demonstrated that colloidal and supported iron sulfide catalysts derived from a homogeneous presulfided single-component precursor, $\text{Fe}_2\text{S}_2(\text{CO})_6$, catalyzes partial hydrogenation of heavy oil model compounds, including pyrene, phenanthrene, and naphthalene, along with partial hydrodesulfurization of benzothiophene. For all these model compounds, the incorporation of a catalyst support was required to achieve high conversions, severely limiting potential applications of this methodology to partial upgrading. This led us to re-explore the hydrogenation of heavy oil model compounds using colloidal iron sulfide exclusively. Commonly studied polycyclic aromatic hydrocarbon heavy oil model compounds will be the principal targets in this work.

In this report, it was shown that unsupported iron sulfide particles also derived from $\text{Fe}_2\text{S}_2(\text{CO})_6$ can provide an active catalyst for partial hydrogenation of substituted anthracenes, as well as an extended range of nitrogen and sulfur heterocycles, including quinoline, acridine, benzothiophene and phenoxathiin. Yields of partially hydrogenated products are high while the reaction conditions are moderate. The effects of aromatic substituents at the 9- and 10- positions of anthracene are evaluated and model feeds containing mixtures of carbocyclic and heterocyclic aromatic compounds investigated for inhibition or synergy. Catalyst composition, including the use of cobalt as an adjunct metal, was also assessed in this slurry-phase strategy for partial upgrading.

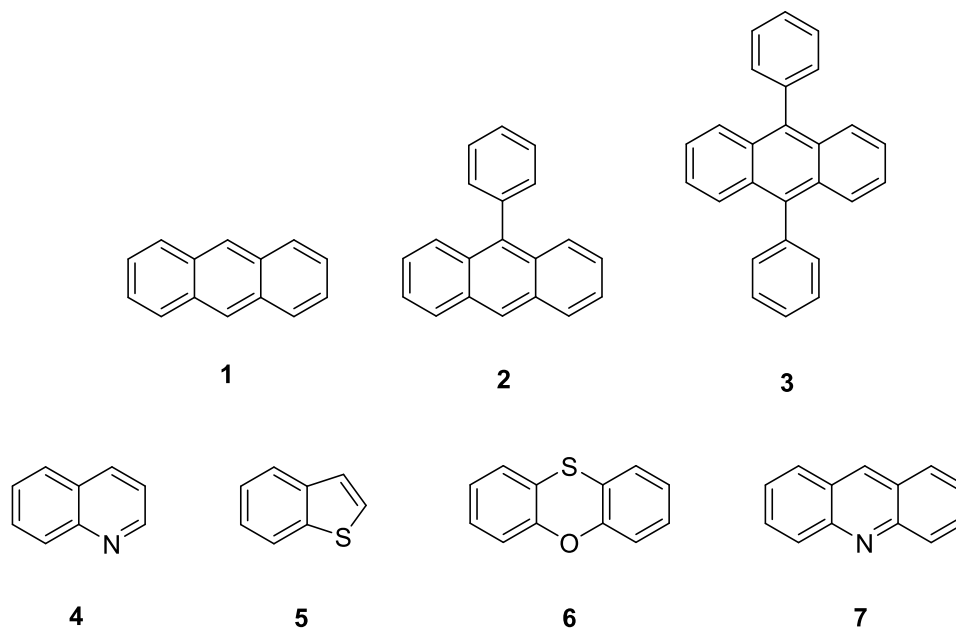


Figure 3.1. Heavy crude oil model compounds used to evaluate hydrogenation using unsupported catalyst from $\text{Fe}_2\text{S}_2(\text{CO})_6$.

3.2. Experimental section

3.2.1. Materials

Anthracene (99%), 1-methylnaphthalene (95%), 9,10-dihydroanthracene (97%), FeS (95%), benzothiophene (98%), quinoline (98%), 1,2,3,4-tetrahydroquinoline (98%), elemental sulfur ($\geq 99.5\%$), and iron (0) pentacarbonyl ($>99.99\%$) were purchased from Sigma-Aldrich and used as received. Reagent-grade toluene (Fisher Scientific), dicobalt octacarbonyl (95%, ACROS organics), 9,10-diphenylanthracene (99%, Alfa Aesar), and both phenoxathiine ($>98\%$ TCI) and 9-phenylanthracene (98%, TCI) were also used as received. Reagent-grade ammonium chloride, hexanes, magnesium sulphate, and methanol were obtained from Caledon Laboratory Chemicals.

3.2.2. Methods

A graphical representation of the experimental program is presented in Figure 3.2. The experimentation can be generalized as a catalyst preparation stage, followed by reactions with a variety of carbocycles and N- and S-heterocycles. After reactions, the products were separated from the catalyst phase, and each were analyzed.

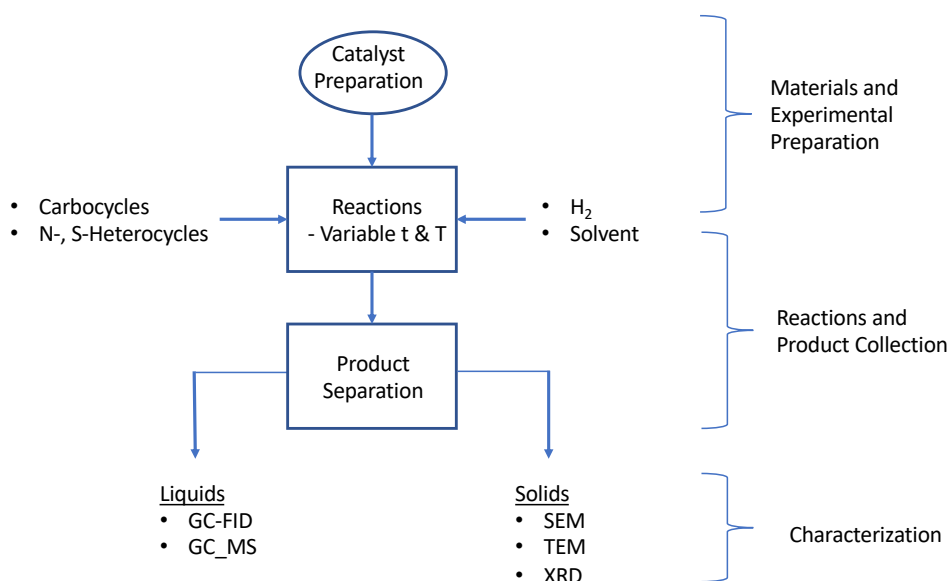


Figure 3.2. Graphical representation of the methods used for experimentation.

3.2.3. Precatalyst preparation

The procedure for the synthesis of $\text{Fe}_2\text{S}_2(\text{CO})_6$ is detailed in a previous report. The isolated yield of the purified red-brown, crystalline, and air-stable $\text{Fe}_2\text{S}_2(\text{CO})_6$ sublimate was 9.7 g (30% based on $\text{Fe}(\text{CO})_5$). The procedure for preparing $\text{Co}_2\text{FeS}(\text{CO})_9$ is found in Khattab et al.³⁰

3.2.4. Catalytic procedures, product, and catalyst recovery

Batch hydrogenation reactions were carried out in a 10 cm stainless-steel tubular microreactor attached to a high-temperature Swagelok severe service union/Bonnet needle valve. The volume of the microreactor was approximately 20 cm³ and its schematic is shown in Figure 3.3. For a typical experiment, the reactor was charged with a model compound (0.2 mmol), Fe₂S₂(CO)₆ (0.12 mmol Fe), and toluene solvent. Total solution volume was 5 mL. After sealing the vessel, the microreactor was purged six times using hydrogen gas, then pressurized with hydrogen (6 MPa cold) at ambient temperature and tested for gas leaks. The pressurized microreactor was then immersed in a preheated sand bath and agitated vertically at 850 rpm, to ensure thorough mixing. Reaction temperature inside the microreactor was attained within 5 min, as determined by a thermocouple. After the specified reaction time had elapsed, the reactor was rapidly cooled to room temperature using cold air.

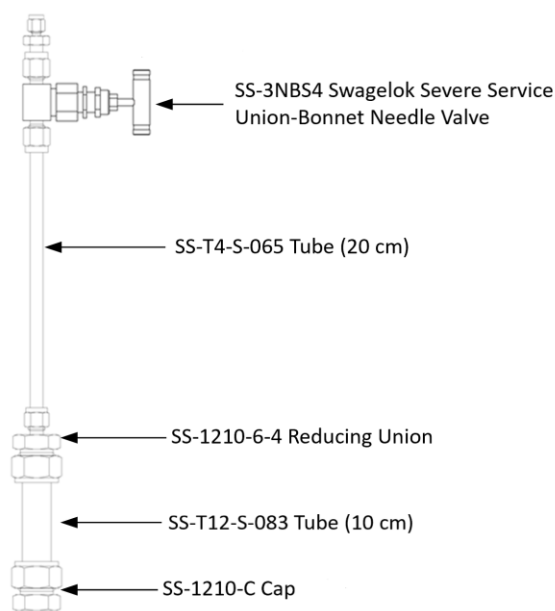


Figure 3.3. Schematic diagram of the batch microreactor.

The molar ratio of substrate to active metal (Fe) was kept constant in all experiments at 1.67 mol/mol. For reactions in the presence of quinoline, between 0.5 and 4 equivalents of quinoline per substrate was added to the reactor. For some reactions, elemental sulfur was used as a sulfiding agent, with between 1 to 10 equivalents of sulfur per $\text{Fe}_2\text{S}_2(\text{CO})_6$ added to the reactor. All reactions were performed in duplicate.

Liquid products from the reactor were separated via filtration using a 0.22 μm filter paper. The catalytic solids were retained on the 0.22 μm filter paper used to separate the products. The filter paper and supporting mesh were weighed prior to filtering the reaction products. The recovered catalyst together with the filter paper and the mesh were oven dried until constant mass, weighed and then the mass yield of filterable solids determined. Typically, the catalyst was recovered with only a 0.5 to 1% loss.

3.2.5. Liquid product characterization

Liquid reaction products were analyzed by gas chromatography with flame ionization detection (GC-FID) on an Agilent 6890N gas chromatograph equipped with HP-5 (5% phenyl)-methylpolysiloxane capillary column (30 m length \times 0.32 mm inner diameter \times 0.25 μm film thickness, helium as carrier gas) using 1-methylnaphthalene as an internal standard. The temperature program was 1 min at 100 $^\circ\text{C}$, 100 to 300 $^\circ\text{C}$ (20 $^\circ\text{C}/\text{min}$), and held at 300 $^\circ\text{C}$ for 2 min. The reaction products and unreacted substrate were identified by comparing GC retention times with those of pure commercially available standards. Compounds for which no pure standards were available, were instead identified by GC-mass spectrometry using an Agilent 6850 gas chromatograph equipped with HP-5 (5% phenyl)-methylpolysiloxane capillary column.

3.2.6. Catalytic solids characterization techniques

3.2.6.1. Scanning electron microscopy

The recovered catalyst was imaged by scanning electron microscopy (SEM) using a Hitachi S-2700 scanning electron microscope operating at 200 kV accelerating voltage. SEM equipped with a Princeton Gamma-Tech (PGT) IMIX digital imaging system and a PGT PRISM Intrinsic Germanium (IG) detector was employed to obtain EDX mapping images.

3.2.6.2. Transmission electron microscopy

A JEOL JEM-ARM200cF scanning transmission electron microscopy (STEM) and high-resolution TEM (HR-TEM) operating at an accelerating voltage of 200 kV was used to take images of the recovered in situ-generated catalyst. The HRTEM images were processed using Gatan Digital Micrograph software or ImageJ. TEM samples were prepared by depositing a droplet of a well-dispersed sample onto an ultra-thin carbon-coated copper grid obtained from Ted Pella. The grid was dried at least 24 h prior to data collection.

3.2.6.3. X-ray diffraction

A Rigaku Ultima IV diffractometer (38 kV, 38 mA) equipped with a Co K α radiation source ($\lambda = 1.78900 \text{ \AA}$) and 2θ ranging from 5° to 90° , D/Tex ultra-detector, operating at a scanning rate of 2° min^{-1} and a step size of 0.0200° was used to perform powder X-ray diffraction (XRD) analysis on the recovered iron sulfide catalyst. Phase identification was done using JADE 9.0 software coupled with the ICDD database.

3.3. Results and discussion

3.3.1. Catalyst characterization

As reported in chapter 2, thermogravimetric analysis (TGA) shows that the $\text{Fe}_2\text{S}_2(\text{CO})_6$ decomposes at 70 °C, releasing all CO ligands in a single-step, with the remaining FeS being stable at higher temperatures. Solvothermal decomposition of $\text{Fe}_2\text{S}_2(\text{CO})_6$ yields roughly spherical, polydisperse (55 to 182 nm) iron FeS nanoparticles, as revealed by SEM and TEM analysis (Figure 3.4a,e). High-resolution transmission electron microscopy (HR-TEM) imaging shows that the iron sulfide nanoparticles are crystalline (Figure 3.4f). These unsupported FeS nanoparticles are slightly larger than those obtained when $\text{Fe}_2\text{S}_2(\text{CO})_6$ is processed in the presence of activated carbon (45 to 110 nm) (chapter 2). SEM-EDX measurements (Figure 3.4b,c) confirm the presence and uniform dispersion of iron and sulfur in the nanoparticles. Powder X-ray diffraction indicates a crystalline pyrrhotite (Fe_{1-x}S) iron sulfide phase (Jade 9.0 PDF No. 04-011-1582) with the major reflections observed at 35.0, 39.7, 51.6, and 62.8° (Figure 3.5).³¹

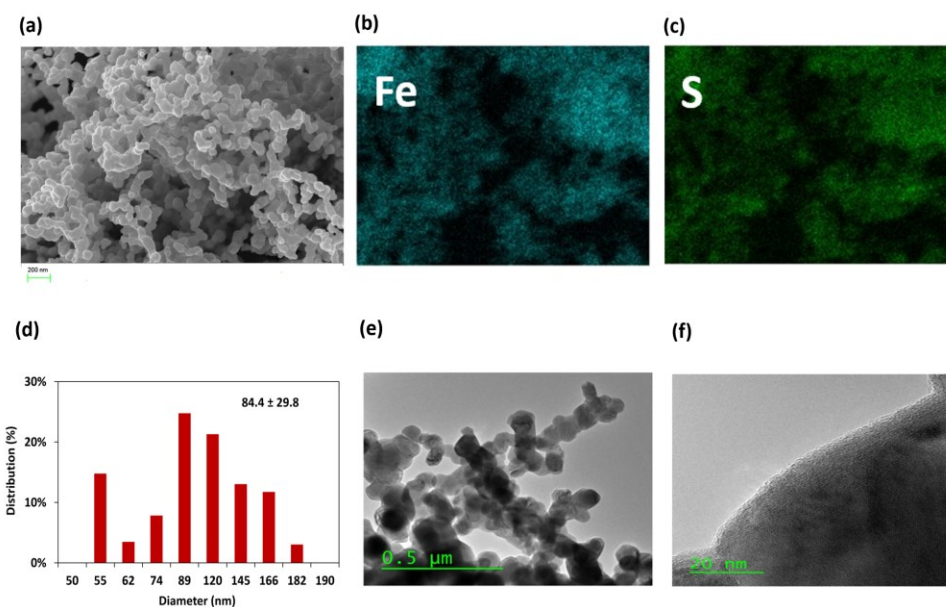


Figure 3.4. (a-d) SEM, EDX mapping images, and corresponding size distribution as well as (e) TEM and (f) HR-TEM images of the FeS nanocatalyst at 300 °C and 60 min.

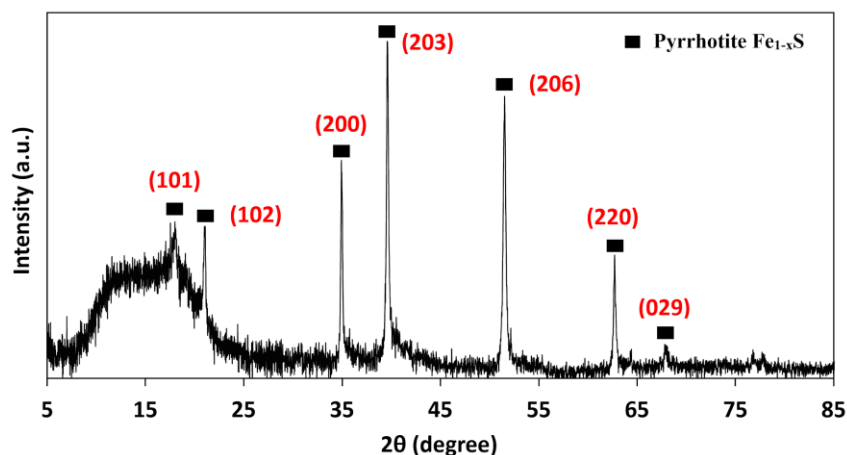


Figure 3.5. XRD pattern of unsupported FeS nanoparticles at 300 °C and 60 min.

3.3.2. Hydrogenation of anthracenes over unsupported $\text{Fe}_2\text{S}_2(\text{CO})_6$

Catalytic hydrogenations of anthracene (**1**), 9-phenylanthracene (**2**), and 9,10-diphenylanthracene (**3**) (Figure 3.1) were studied over the unsupported FeS catalyst. Under reaction conditions adopted from chapter 2 on supported catalysts (300 °C, 6 MPa cold H_2 pressure, and 1.67 mol/mol substrate to Fe ratio), anthracene is hydrogenated near-quantitatively (98.4%) to a mixture of 9,10-dihydroanthracene **8** (95.6%) and 1,2,3,4-tetrahydroanthracene **9** (2.4%) after one hour. The very small amount of tetrahydroanthracene **9** detected is likely formed by further hydrogenation and isomerization of 9,10-dihydroanthracene. The higher conversion obtained for anthracene using the unsupported FeS catalyst stands in contrast to the conversion obtained for pyrene (13%) and phenanthrene (4%) under identical conditions. This is explained by the intrinsically higher hydrogen acceptability of anthracene³² and its thermodynamically favourable adsorption to the catalyst surface compared to other polycyclic aromatic hydrocarbon molecules.^{33,34}

The concentrations of anthracene hydrogenation products **8** and **9** do not change significantly after 1h, suggesting that equilibrium conversion is attained or, equally likely, the catalyst is deactivated (Figure 3.6a,b). Compositional analysis of the spent catalyst reveals that an iron sulfide phase remains at the end of the reaction, while electron microscopic imaging did not reveal any extensive catalyst agglomeration. Furthermore, a control reaction using fresh catalyst and **8** results in minimal hydrogenation to tetrahydroanthracene **9** (2%), with the final equilibrium concentrations of **8** and **9** being nearly identical to that observed when hydrogenating anthracene. These data appear to rule out catalyst deactivation, and instead support competitive entropically-driven dehydrogenation of the reaction products as the reason for the halt in conversion of anthracene.^{35,36} Indeed, replacing hydrogen with an inert gas induces a dramatic shift in equilibrium in favor of dehydrogenation; under a nitrogen atmosphere, **8** is almost completely dehydrogenated to anthracene (91%). Such iron-catalyzed dehydrogenation reactions have been implicated in various catalytic reactions of hydrocarbons in the absence of exogenous hydrogen.^{37,38} Control reactions under these conditions show that in the absence of the iron source no conversion of any substrate is observed. Investigations of iron-catalyzed dehydrogenation and, in particular, hydrogen transfer continue.

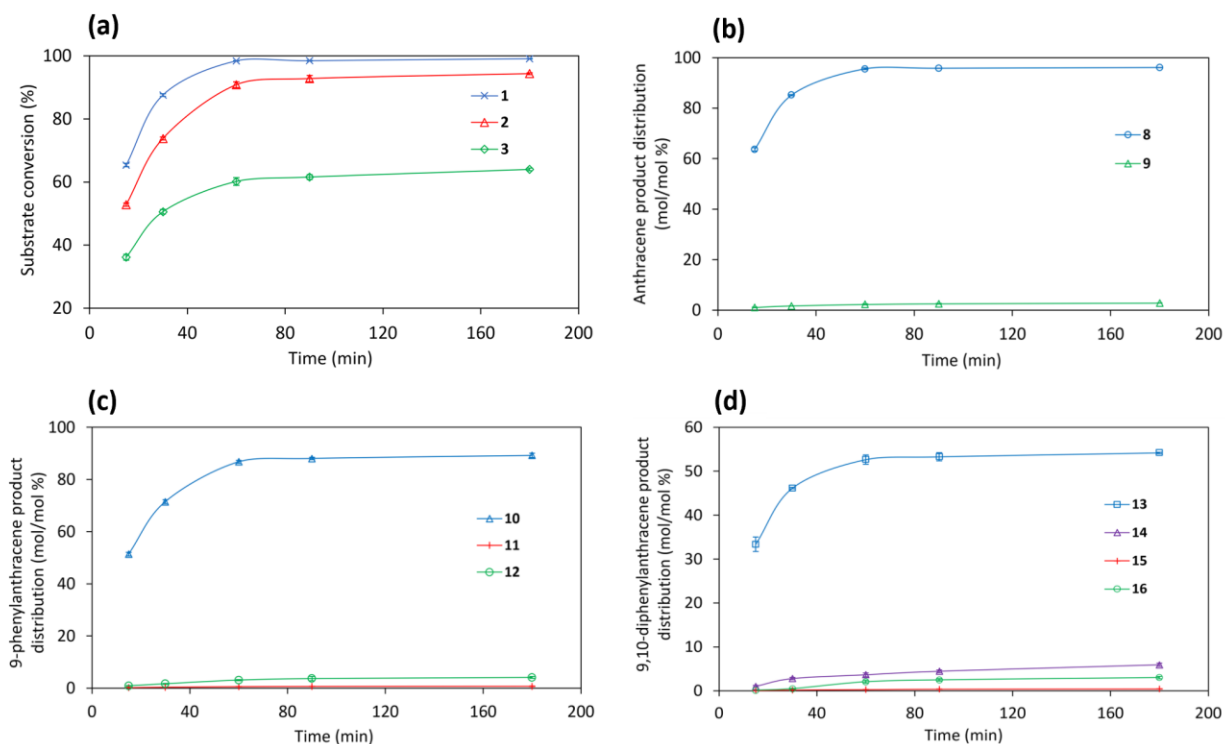
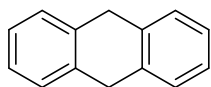


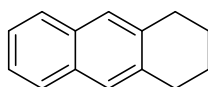
Figure 3.6. Conversion time profiles of (a) anthracene, 9-phenylanthracene, and 9,10-diphenylanthracene as well as their product distribution (b-d), respectively. Reaction conditions: temperature, 300 °C; cold H₂, 6 MPa; substrate to active metal (Fe) molar ratio, 1.67 mol/mol; time, 15-180 min.

The distribution of products from hydrogenating 9-phenylanthracene and 9,10-diphenylanthracene over the FeS nanoparticles largely mirrors that seen for anthracene, albeit with lower equilibrium concentrations of the partially hydrogenated products (Figure 3.6c, d). The major products remain 9,10-dihydroanthracenes (**10**, **13**, and **14**), with very small quantities of 1,4-dihydroanthracenes (**11** and **15**), and 1,2,3,4-tetrahydroanthracenes (**12** and **16**) are also detected (Figure 3.7). The 1,4-dihydroanthracenes are likely hydrogenated further to 1,2,3,4-tetrahydroanthracenes, independent of 9,10-dihydroanthracene formation (Figure B1 and B2, in Appendix B). For diphenylanthracene, both *cis* and *trans*-9,10-dihydro-9,10-diphenylanthracene (**13/14**) are obtained; the isomers were differentiated by the relative abundance of each of their molecular ions in mass spectra.^{39,40} The *trans* isomer is formed preferentially because of the lower torsional strain in the molecule relative

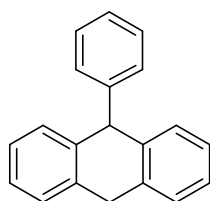
to the cis isomer.⁴¹ The lower overall conversions of the substituted anthracenes **2** and **3** relative to anthracene reflect the stereoelectronic influence of the phenyl substituent(s); adsorption of the sterically-encumbered anthracenes onto the catalyst surface is not favorable³⁹ – the phenyl substituents cannot attain a co-planar conformation without encountering severe torsional distress. The phenyl groups are thus strongly electron withdrawing, reducing the ‘hydrogen acceptability’ of these reactants.⁴⁰ The products from hydrogenating anthracenes show that the in situ-generated FeS catalyst is well-suited for the limited hydrogenation of polycyclic aromatic molecules. In contrast, catalytic hydrogenation of anthracene over precious metal catalysts typically affords highly hydrogenated tetra-, octa- and per-hydroanthracenes.⁴² Selective hydrogenation is desirable in many applications and is critical in potential partial upgrading schemes.⁴³



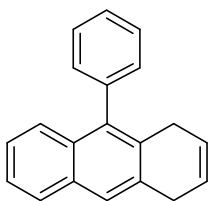
8



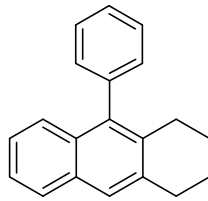
9



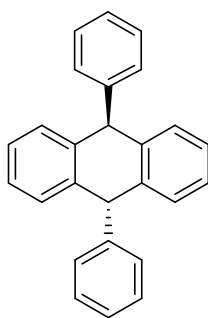
10



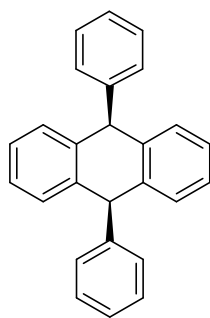
11



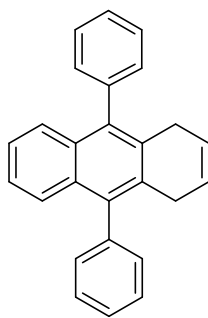
12



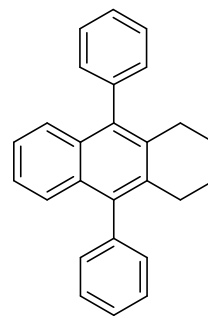
13



14



15



16

Figure 3.7. Structures of the products from the hydrogenation of anthracene, 9-phenylanthracene and 9,10-diphenylanthracene.

3.3.3. Mixed feeds: carbocyclic and N- and S-heterocyclic compounds

To better model complex petroleum streams, the FeS catalyst was used to hydrogenate mixtures of small polycyclic aromatic hydrocarbons, which are usually present in heavy crude oils. Iron based catalysts for the hydrogenation of N- and S-heterocyclic compounds are not well developed.⁴⁴ Feeds containing a sulfur or nitrogen heterocycle together with a carbocyclic substrate were evaluated. Conversions of anthracene and substituted derivatives **2** and **3** decreased when hydrogenated in the presence of either quinoline or benzothiophene, with the most dramatic effect observed at high heterocycle concentrations (Figure 3.8a,b). Inhibition of hydrogenation is more pronounced for the sterically hindered phenyl-substituted anthracene derivatives. Smaller, more basic, N- and S-heterocycles easily outcompete the aromatic hydrocarbons for binding to active metal active sites. The products of quinoline and benzothiophene partial hydrogenation are themselves significant inhibitors to conversion of the carbocycles.⁴⁵ In our case, 1,2,3,4-tetrahydroquinoline was the most effective inhibitor, causing a greater decrease in anthracene conversion than quinoline.^{41,46} Mixtures containing benzothiophene return even lower conversions of anthracene, likely due to strong binding of the sulfur atom with sulfur vacancies formed at the active sites. These results stand in contrast to the established literature, where N-heterocycles are usually the most effective catalyst inhibitors.^{47,48}

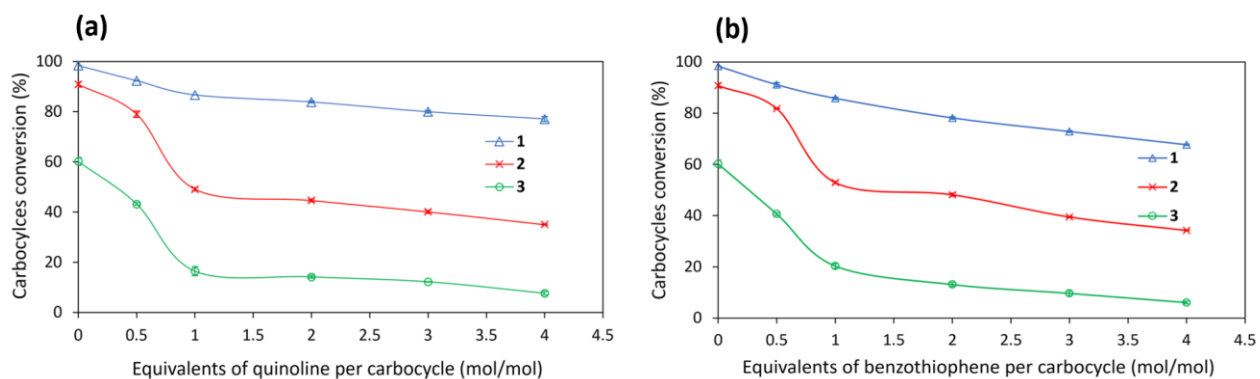


Figure 3.8. Effect of combining carbocycles with (a) quinoline and (b) benzothiophene on hydrogenation under unsupported $\text{Fe}_2\text{S}_2(\text{CO})_6$. Reaction conditions: temperature, 300 °C; cold H_2 , 6 MPa; substrate to Fe molar ratio, 1.67 mol/mol; time, 60 min.

Nitrogen and sulfur heterocycles are not simply catalyst poisons since heteroaromatics also undergo competitive hydrogenation, as well as some hydrodesulfurization of benzothiophene. Quinoline is converted to 1,2,3,4-tetrahydroquinoline (86%); benzothiophene is slowly converted to 2,3-dihydrobenzothiophene (**18**) (19 %), along with a trace of ethylbenzene (**19**) (Figure 3.9). No products from denitrogenation were isolated. Interestingly, when hydrogenating quinoline and benzothiophene in the presence of added anthracene, conversion of the heterocycles suffers from competitive binding of the carbocycle. As noted above, higher concentrations of the competitive inhibitors decrease overall conversion of the target substrate; the effect is more significant for benzothiophene than for quinoline. The extensive hydrogenation of quinoline and benzothiophene (Figure 3.10a, b) under such mild conditions over the colloidal FeS catalyst is remarkable. This result is in contrast to that from Curtis et al.⁴⁹ which showed that unsupported sulfided iron naphthenate- or acetylacetonate-derived heterogeneous catalysts do not promote hydrogenation or desulfurization of benzothiophene under comparable conditions. Iron catalysts are known to hydrogenate quinoline, but this methodology involves the use of homogeneous organometallic

precatalysts or supported iron.⁵⁰ Furthermore, reaction times are generally reported in days, incompatible with continuous processing.

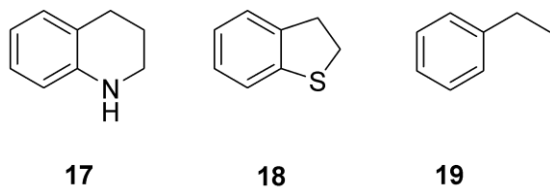


Figure 3.9. 1,2,3,4-tetrahydroquinoline, 2,3-dihydrobenzothiophene, and ethylbenzene.

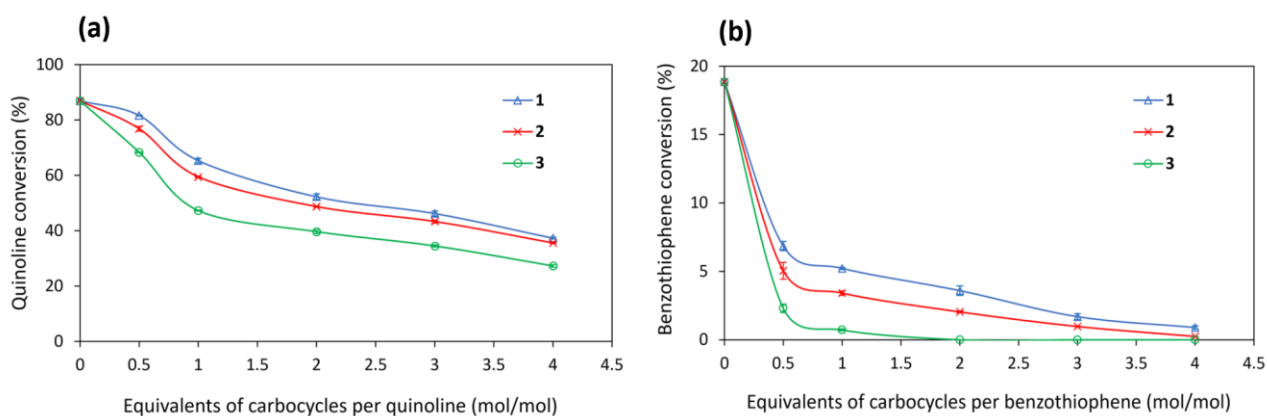


Figure 3.10. Conversion of (a) quinoline and (b) benzothiophene in the presence of either anthracene, 9-phenylanthracene, or 9,10-diphenylanthracene. Reaction conditions: temperature, 300 °C; cold H₂, 6 MPa; substrate to active metal (Fe) molar ratio, 1.67 mol/mol; time, 60 min.

3.3.4. Hydrotreating phenoxathiin and acridine

Hydrogenations of phenoxathiin **6** and acridine **7** are illuminating because the compounds are heteroatom-substituted structural analogues of anthracene, but bear enthalpically-distinct carbon–heteroatom bonds. Under standard reaction conditions (300 °C, 6 MPa cold H₂ pressure, 60 mins, 1.67 mol/mol substrate-to-Fe ratio), phenoxathiin is partially converted (10%) to diphenyl ether **20** (Figure 3.11) while acridine is converted nearly completely (96%) to 9,10-dihydroacridine **21**

along with minor amounts of 1,2,3,4-tetrahydroacridine (**22**), 1,2,3,4,4a,9,9a,10-octahydroacridine (**23**), and 1,2,3,4,5,6,7,8-octahydroacridine (**24**). For phenoxathiin, the weak C–S bond (65 kcal/mol) cleaves readily, while the much stronger C–O bond (86 kcal/mol) resists hydrogenolysis. No hydrogenation of the residual benzene-like aromatic rings was observed.⁴¹ Hydrogenation of a combination of anthracene and the two heterocycles maintains high conversions for anthracene (98%) and acridine (95%), but the conversion of phenoxathiin is significantly inhibited (3%).

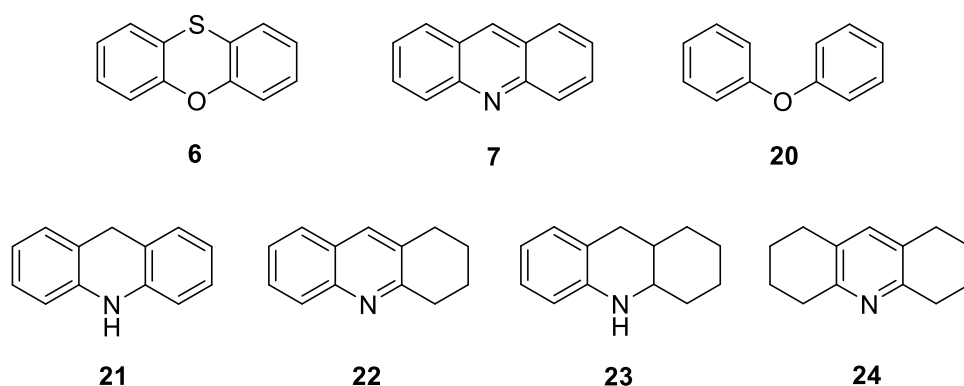


Figure 3.11. Phenoxathiin hydrodesulfurization and acridine hydrogenation products.

Taken together, these results demonstrate that this unsupported FeS catalyst is well-placed to challenge partial hydrogenation and hydrogenolysis of complex petroleum feeds, simultaneously processing an inestimable number of distinct carbocyclic and heterocyclic compounds. In such feeds, the data suggest that the relative activity of the catalyst increases in the order phenoxathiin < benzothiophene << diphenyl anthracene < phenyl anthracene < quinoline < acridine < anthracene. This trend is near-ideal for partial upgrading, where limited desulfurization combined with selective hydrogenation is desired, sufficient to convert viscous crude oils into pipeline grade liquids without overprocessing.¹ Further hydrogenation or hydrotreatment requires a return to traditional upgrading catalysts and thermal coking,⁵¹ or the use of expensive precious metals.⁵²

3.3.5. Effects of extraneous sulfur

The bulk structure of the nanoparticles remains unchanged during the reaction, but the chemical composition of the active sites is not indefinitely stable under hydrogen pressure. Exhaustive hydrogenolysis can eventually convert active surface sites to sulfur-free domains which are less effective for catalysis,^{53,54} requiring extraneous sulfur to maintain reactivity. To assess the impact of possible catalyst decomposition on conversion, the concentration of an external sulfiding agent, in this case elemental sulfur, was varied and the effects on the conversions of phenyl-substituted anthracenes determined. For both molecules, a 1: 5 molar ratio of precatalyst to sulfur was optimal; conversions increased by 6.7 % for **2** and 21.1 % for **3** compared to conversion in the absence of sulfur. These results confirm that a stable active FeS phase is maintained longer in the presence of the sulfiding agent (Figure 3.12). For typical heavy oils, continuous infusion of an external sulfiding agent is expected to become unnecessary; organosulfur molecules entrained in the feed can, in principle, provide sufficient elemental sulfur to maintain the nanoparticle active phase. As expected, higher loadings of sulfur (>5 S per $\text{Fe}_2\text{S}_2(\text{CO})_6$) is deleterious. At such high levels, sulfur outcompetes substrate(s) for adsorption onto the catalyst surface, effectively acting as a poison.

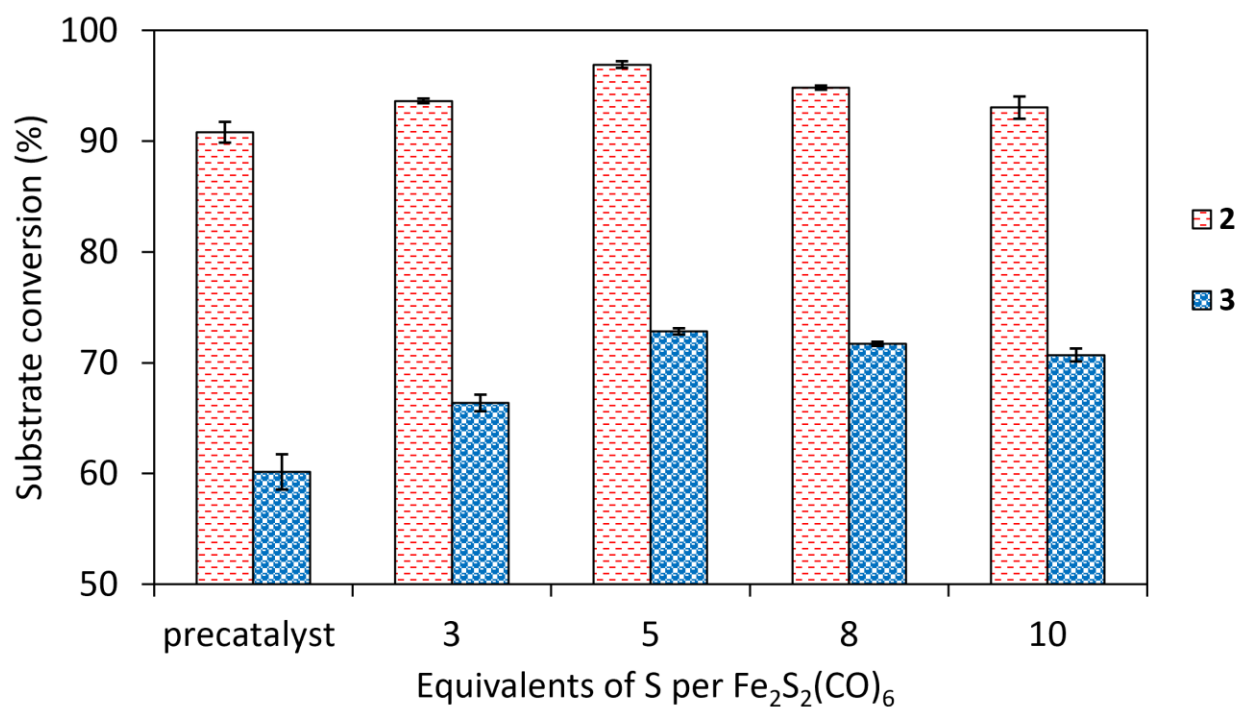


Figure 3.12. Effect of sulfur concentration on the catalytic hydrogenation of 9-phenylanthracene and 9,10-diphenylanthracene. Reaction conditions: temperature, 300 °C; cold H_2 , 6 MPa; time, 60 min. Standard error values are one standard deviation.

3.3.6. Effects of precatalyst on anthracene hydrogenation

Typical homogeneous iron precatalysts were compared to $\text{Fe}_2\text{S}_2(\text{CO})_6$ for anthracene hydrogenation. The composition of the precursor has a dramatic effect on both conversion and product distribution. The unsulfided catalyst derived from $\text{Fe}(\text{CO})_5$ mediates deep hydrogenation of anthracene, yielding tetra- and octa-hydroanthracenes as major products (Table 3.1, entry C, see Figure B4 for structures **25** and **26** in Appendix B). Highly reduced products are typically obtained from Mo, Ni, or precious metal catalysts^{42,51,55} Differences in active-site structures for sulfided and unsulfided pre-catalysts, as well as variations in binding mode(s), account for the divergent reactivity and longevity. In contrast, sulfidation of $\text{Fe}(\text{CO})_5$ (entries D, E) in situ leads to nearly identical product distributions as those obtained from $\text{Fe}_2\text{S}_2(\text{CO})_6$ (entries B, F). Although the iron active carbide phase (Figure B5 in Appendix B) obtained from $\text{Fe}(\text{CO})_5$ alone is highly active, the

active sites almost certainly revert to those of a sulfided iron under heavy crude oil processing conditions, but perhaps not of similar dimensions. The placement of cobalt as an adjunct metal in a trinuclear precatalyst³⁰ (entry G) has no effect on conversion or product distribution. Bulk FeS (entry H) was also ineffective, as were ball-milled FeS crystallites (entry I). It is important to note that the prepared Fe₂S₂(CO)₆ is a stable powder, and it can be stored indefinitely and handled without the use of special air-free techniques. By contrast, Fe(CO)₅ is pyrophoric and generates equilibrium concentrations of higher clusters and CO gas, rendering it unsuitable as a precatalyst for most industrial applications.

Table 3.1. Hydrogenation of anthracene over iron precatalysts.

| Entry | Catalyst precursor | Conversion (%) | Yield (%) | | | |
|-------|---|----------------|------------|------------|-----------|------------|
| | | | 8 | 9 | 25 | 26 |
| A | none | 0.0 | 0.0 | 0.0 | 0.0 | 0.0 |
| B | Fe ₂ S ₂ (CO) ₆ | 98.4 (0.1) | 95.6 (0.3) | 2.4 (0.2) | 0.0 | 0.0 |
| C | Fe(CO) ₅ | 100.0 | 20.9 (1.1) | 48.6 (0.3) | 0.8 (0.1) | 29.5 (1.1) |
| D | Fe(CO) ₅ -S ^a | 100.0 | 90.6 (0.6) | 9.1 (0.5) | 0.0 | 0.0 |
| E | Fe(CO) ₅ -S ^b | 99.2 (0.1) | 90.2 (0.8) | 8.8 (0.3) | 0.0 | 0.0 |
| F | Fe ₂ S ₂ (CO) ₆ ^a | 100.0 | 96.6 (0.4) | 3.2 (0.3) | 0.0 | 0.0 |
| G | Co ₂ FeS(CO) ₉ | 98.8 (0.3) | 95.3 (0.1) | 2.3 (0.2) | 0.0 | 0.0 |
| H | FeS | 5.0 (0.2) | 4.4 (0.3) | 0.0 | 0.0 | 0.0 |
| I | FeS ^c | 8.5 (0.3) | 8.3 (0.2) | 0.0 | 0.0 | 0.0 |

Reaction conditions: temperature, 300 °C; substrate to Fe molar ratio, 1.67 mol/mol; initial H₂, 6 MPa; total reactant solution, 5 mL; solvent, toluene; time, 60 min. ^aFe/S molar ratio, 0.333 mol/mol. ^bFe/S molar ratio, 1.0 mol/mol. ^cBall milled prior to use. Data are mean values for n = 2. Standard error values in parenthesis are one standard deviation.

3.4. Conclusions

Colloidal iron sulfide derived solely from a presulfided homogeneous iron complex, $\text{Fe}_2\text{S}_2(\text{CO})_6$ is active for partial hydrogenation of anthracene, 9-phenylanthracene, 9,10-diphenylanthracene, and N- and S-heterocyclic aromatic hydrocarbons. Anthracene hydrogenation proceeds nearly quantitatively, but lower conversions are obtained for phenyl-substituted analogues, showing that substrate steric and electronic profile plays a significant role in the susceptibility to hydrogen-transfer. Importantly, this nanoscale colloidal FeS catalyst simultaneously processes mixtures of carbocycles and heterocycles, making it suitable for further optimization and investigations of authentic feeds. The activity of the unsupported iron catalyst decreases in the order anthracene > acridine > quinoline > phenylanthracene > diphenylanthracene >> benzothiophene > phenoxathiin. Addition of extraneous sulfur leads to increase in conversion, but at high levels sulfur competes with the substrates for adsorption onto the catalyst surface, causing inhibition. We anticipate that this cost-effective catalyst derived from $\text{Fe}_2\text{S}_2(\text{CO})_6$ will disperse readily into viscous aromatic feeds introduced into a slurry-phase process for partial upgrading.

3.5. References

1. Gray, M. R. Fundamentals of Partial Upgrading of Bitumen. *Energy Fuels* **2019**, *33*, 6843.
2. Colyar, J. I. M. Has the Time for Partial Upgrading of Heavy Oil and Bitumen Arrived? *Pet. Technol. Q.* **2009**, *Q14*, 43.
3. Keesom, W.; Gieseman, J. *Bitumen Partial Upgrading 2018 Whitepaper AM0401A*; Alberta Innovates: Calgary, AB, **2018**; pp 152.
4. Zuo, P.; Qu, S.; Shen, W. Asphaltenes: Separations, Structural Analysis and Applications. *J. Energy Chem.* **2019**, *34*, 186.
5. Castaneda, L. C.; Munoz, J. A.; Ancheyta, J. Current Situation of Emerging Technologies for Upgrading of Heavy Oils. *Catal. Today* **2014**, *220*, 248.
6. Zachariah, A.; de Klerk, A. Partial Upgrading of Bitumen: Impact of Solvent Deasphalting and Visbreaking Sequence. *Energy Fuels* **2017**, *31*, 9374.
7. Xing, T.; Alvarez-Majmutov, A.; Chen, J. Bitumen Partial Upgrading by Mild Hydroprocessing in a Fixed-bed Reactor. *Fuel* **2019**, *235*, 696.
8. Hepler, L. G.; His, C. AOSTRA Technical Handbook on Oil Sands Bitumen and Heavy Oils. AOSTRA Technical Publication Series, vol. 6. Edmonton: Alberta Oil Sands Technology and Research Authority; 1989.
9. Li, C.; Li, J.; Yang, T.; Deng, W. Formation of Ni–MoS₃ Hollow Material with Enhanced Activity in Slurry-phase Hydrogenation of Heavy Oil. *Energy Fuels* **2019**, *33*, 10933.
10. Montanari, R.; Marchionna, M.; Rosi, S.; Panariti, N.; Delbianco, A.; SnamProgetti SpA; EniTecnologie SpA; ENI SpA, **2010**. Process for the Conversion of Heavy Charges Such as Heavy Crude Oils and Distillation Residues. U.S. Patent 7,691,256.
11. Bdwi, E. A.; Ali, S. A.; Quddus, M. R.; Al-Bogami, S. A.; Razzak, S. A.; Hossain, M. M. Kinetics of Promotional Effects of Oil-Soluble Dispersed Metal (Mo, Co, and Fe) Catalysts on Slurry Phase Hydrocracking of Vacuum Gas Oil. *Energy Fuels* **2017**, *31*, 3132.
12. Du, H.; Li, M.; Liu, D.; Ren, Y.; Duan, Y. Slurry-Phase Hydrocracking of Heavy Oil and Model Reactant: Effect of Dispersed Mo Catalyst. *Appl. Petrochem. Res.* **2015**, *5*, 89.
13. Nguyen, M. T.; Nguyen, N. T.; Cho, J.; Park, C.; Park, S.; Jung, J.; Lee, C. W. A Review on the Oil-soluble Dispersed Catalyst for Slurry-phase Hydrocracking of Heavy Oil. *J. Ind. Eng. Chem.* **2016**, *43*, 1.

14. Angeles, M. J.; Leyva, C.; Ancheyta, J.; Ramírez, S. A Review of Experimental Procedures for Heavy Oil Hydrocracking with Dispersed Catalyst. *Catal. Today* **2014**, *220*, 274.
15. Rana, M. S.; Samano, V.; Ancheyta, J.; Diaz, J. A. I. A Review of Recent Advances on Process Technologies for Upgrading of Heavy Oils and Residua. *Fuel* **2007**, *86*, 1216.
16. Zhang, S.; Liu, D.; Deng, W.; Que, G. A Review of Slurry-Phase Hydrocracking Heavy Oil Technology. *Energy Fuels* **2007**, *21*, 3057.
17. Quitian, A; Ancheyta, J. Experimental Methods for Developing Kinetic Models for Hydrocracking Reactions with Slurry-Phase Catalyst Using Batch Reactors. *Energy Fuels* **2016**, *30*, 4419.
18. Li, Y.; Ma, F., Su, X.; Shi, L.; Pan, B.; Sun, Z.; Hou, Y. Ultra-Large-Scale Synthesis of Fe₃O₄ Nanoparticles and Their Application for Direct Coal Liquefaction. *Ind. Eng. Chem. Res.* **2014**, *53*, 6718.
19. Suzuki, T.; Yamada, H.; Sears, P. L.; Watanabe, Y. Hydrogenation and hydrogenolysis of Coal Model Compounds by Using Finely Dispersed Catalysts. *Energy Fuels* **1989**, *3*, 707.
20. Kamiya, Y.; Nobusawa, T.; Futamura, S. Catalytic Effects of Iron Compounds and the Role of Sulfur in Coal Liquefaction and Hydrogenolysis of SRC. *Fuel Process. Technol.* **1988**, *18*, 1.
21. Suzuki, T.; Yamada, O.; Takahashi, Y.; Watanabe, Y. Hydroliquefaction of Low-Sulfur Coals Using Iron Carbonyl Complexes-Sulfur as Catalysts. *Fuel Process. Technol.* **1985**, *10*, 33.
22. Tang, Y.; Curtis, C.W. Activity and Selectivity of Slurry-Phase Iron-Based Catalysts for Model Systems. *Energy Fuels* **1994**, *8*, 63.
23. Hurt, M. R.; Borton, D. J.; Choi, H. J.; Kenttämaa, H. I. Comparison of the Structures of Molecules in Coal and Petroleum Asphaltenes by Using Mass Spectrometry. *Energy Fuels* **2013**, *27*, 3653.
24. Tang, W.; Hurt, M. R.; Sheng, H.; Riedeman, J. S.; Borton, D. J.; Slater, P.; Kenttämaa, H. I. Structural Comparison of Asphaltenes of Different Origins Using Multi-Stage Tandem Mass Spectrometry. *Energy Fuels* **2015**, *29*, 1309.
25. Hata, K.A.; Wada, K.; Mitsudo, T. A. Iron-Catalyzed Coprocessing of Coals and Vacuum Residues Using Syngas– Water as a Hydrogen Source. *Energy Fuels* **1998**, *12*, 1181.

26. Groenzin, H.; Mullins, O. C. Molecular Size and Structure of Asphaltenes from Various Sources. *Energy Fuels* **2000**, *14*, 677.
27. Gray, M. R. *Upgrading Oilsands Bitumen and Heavy Oil*; University of Alberta Press: Edmonton, Alberta, Canada, 2015.
28. Alshareef, A.H. Asphaltenes: Definition, Properties, and Reactions of Model Compounds. *Energy Fuels* **2020**, *34*, 16.
29. Akbarzadeh, K.; Bressler, D.C.; Wang, J.; Gawrys, K.L.; Gray, M.R.; Kilpatrick, P.K.; Yarranton, H.W. Association Behavior of Pyrene Compounds as Models for Asphaltenes. *Energy Fuels* **2005**, *19*, 1268.
30. Khattab, S. A.; Markó, L.; Bor, G.; Markó, B. Sulphur-Containing Metal Carbonyls VI. A Mixed Cobalt-Iron Carbonyl Sulphide. *J. Organomet. Chem.* **1964**, *1*, 373.
31. Di Giovanni, C.; Wang, W. A.; Nowak, S.; Grenèche, J. M.; Lecoq, H.; Mouton, L.; Giraud, M.; Tard, C. Bioinspired Iron Sulfide Nanoparticles for Cheap and Long-Lived Electrocatalytic Molecular Hydrogen Evolution in Neutral Water. *ACS Catal.* **2014**, *4*, 681.
32. Han, B.; Ma, P.; Cong, X.; Chen, H.; Zeng, X. Chromium- and Cobalt-Catalyzed, Regiocontrolled Hydrogenation of Polycyclic Aromatic Hydrocarbons: A Combined Experimental and Theoretical Study. *J. Am. Chem. Soc.* **2019**, *141*, 9018.
33. Tunega, D.; Zaoui, A. Adsorption of Polycyclic Aromatic Hydrocarbons on FeOOH Polymorphs: A Theoretical Study. *Surf. Sci.* **2021**, *706*, 121795.
34. Dang, Y.; Liu, Y.; Feng, X.; Chen, X.; Yang, C. Effect of Dispersion on the Adsorption of Polycyclic Aromatic Hydrocarbons over the γ -Al₂O₃ (110) Surface. *Appl. Surf. Sci.* **2019**, *486*, 137.
35. Cowley, S.; Wisler, W. The Thermodynamics of Anthracene Hydrocracking. *Fuel Process Technol.* **1979**, *2*, 317.
36. Girgis, M. J.; Gates, B. C. Reactivities, Reaction Networks, and Kinetics in High-Pressure Catalytic Hydroprocessing. *Ind. Eng. Chem. Res.* **1991**, *30*, 2021.
37. Li, L.; Yucui, H.; Weize, W.; Shisheng, L.; Shuhang, R. Behaviors of Tetralin and 9,10-dihydroanthracene as Hydrogen Donor Solvents in the Hydrogenolysis of Coal-Related Model Compounds. *Fuel Process. Technol.* **2019**, *191*, 202.

38. Chen, Z.; Xie, J.; Liu, Q.; Wang, H.; Gao, S.; Shi, L.; Liu, Z. Characterization of Direct Coal Liquefaction Catalysts by Their Sulfidation Behavior and Tetralin Dehydrogenation Activity. *J. Energy Inst.* **2019**, *92*, 1213.
39. Sun, L. B.; Wei, X. Y.; Liu, X. Q.; Zong, Z. M.; Li, W.; Kou, J. H. Selective Hydrogen Transfer to Anthracene and Its Derivatives over an Activated Carbon. *Energy Fuels* **2009**, *23*, 4877.
40. Yue, X. M.; Wei, X. Y.; Zhang, S. Q.; Liu, F. J.; Zong, Z. M. Yang, X. Q. Hydrogenation of Polycyclic Aromatic Hydrocarbons Over a Solid Superacid. *Fuel Process. Technol.* **2017**, *161*, 283.
41. Ting, P. S.; Curtis, C. W.; Cronauer, D. C. Reactions of Model Compounds in the Presence of Pyrene and Molybdenum Sulfide (MoS₂) to Simulate Coprocessing. *Energy Fuels* **1992**, *6*, 511.
42. Pinilla, J. L.; Garcia, A. B.; Philippot, K.; Lara, P.; Garcia-Suarez, E. J.; Millan, M. Carbon-Supported Pd Nanoparticles as Catalysts for Anthracene Hydrogenation. *Fuel* **2014**, *116*, 729.
43. Zhang, L.; Zhou, M.; Wang, A.; Zhang, T. Selective Hydrogenation over Supported Metal Catalysts: From Nanoparticles to Single Atoms. *Chem. Rev.* **2020**, *120*, 683.
44. Wei, Z.; Shao, F.; Wang, J. Recent Advances in Heterogeneous Catalytic Hydrogenation and Dehydrogenation of N-Heterocycles. *Chin. J. Catal.* **2019**, *40*, 980.
45. Shen, J.; Semagina, N. Inhibition of Diolefin Hydrogenation by Quinoline. *Energy Fuels* **2020**, *34*, 8769.
46. Nagai, M.; Sato, T.; Aiba, A. Poisoning Effect of Nitrogen Compounds on Dibenzothiophene Hydrodesulfurization on Sulfided NiMoAl₂O₃ Catalysts and Relation to Gas-Phase Basicity. *J. Catal.* **1986**, *97*, 52.
47. Curtis, C. W.; Chung, W. J. Effect of Coal and Residuum on Reactions Occurring in Coal-Petroleum Processing. *Energy Fuels* **1989**, *3*, 148.
48. Kim, H.; Curtis, C.W. Reaction Pathways of Model Coprocessing Systems Using Molybdenum Naphthenate and Excess Sulfur. *Energy Fuels* **1990**, *4*, 206.
49. Curtis, C. W.; Chen, J. H.; Tang, Y. Hydrodesulfurization of Model Systems Using Slurry-Phase Catalysts. *Energy Fuels* **1995**, *9*, 195.

50. Sahoo, B.; Kreyenschulte, C.; Agostini, G.; Lund, H.; Bachmann, S.; Scalone, M.; Junge, K.; Beller, M. A Robust Iron Catalyst for the Selective Hydrogenation of Substituted (iso) Quinolones. *Chem. Sci.* **2018**, *9*, 8134.
51. Pinilla, J. L.; Purón, H.; Torres, D.; Suelves, I.; Millan, M. Ni-MoS₂ Supported on Carbon Nanofibers as Hydrogenation Catalysts: Effect of Support Functionalization. *Carbon*, **2015**, *81*, 574.
52. Boudjahem, A. G.; Redjel, A.; Mokrane, T. Preparation, Characterization and Performance of Pd/SiO₂ Catalyst for Benzene Catalytic Hydrogenation. *J. Ind. Eng. Chem.* **2012**, *18*, 303.
53. Montano, P. A.; Stenberg, V. I.; Sweeny, P. In Situ Study of the Hydrogenation of Diphenyl Ether in the Presence of Pyrrhotite and Hydrogen Sulfide. *J. Phys. Chem.* **1986**, *90*, 156.
54. Herrick, D. E.; Tierney, J. W.; Wender, I.; Huffman, G. P.; Huggins, F. E. Activity and Characterization of Coprocessing Catalysts Produced from an Iron Pentacarbonyl Precursor. *Energy Fuels* **1990**, *4*, 231.
55. Zhang, Z. G.; Okada, K.; Yamamoto, M.; Yoshida, T. Hydrogenation of Anthracene over Active Carbon-Supported Nickel Catalyst. *Catal. Today* **1998**, *45*, 361.

3.6. Associated content

Supporting information is provided in Appendix B

Reaction networks proposed for all substrates (Figure B1-B3), structures of 1,2,3,4,4a,9,9a,10-octahydroanthracene (**25**) and 1,2,3,4,5,6,7,8-octahydroanthracene (**26**) (Figure B4), and XRD pattern of unsupported catalyst derived from Fe(CO)₅ (Figure B5).

Chapter 4: Efficient Unsupported Iron Catalyst for Transfer Hydrogenation of Carbocyclic and Heterocyclic Aromatic Compounds Using Mixed Hydrogen Donors

To be Submitted to Industrial & Engineering Chemistry Research

4.1 Introduction

Catalytic hydrogenation of unsaturated molecules is a ubiquitous chemical transformation with applications in diverse industrial processes such as crude oil refining, pharmaceutical synthesis, food processing, and plastics manufacturing.¹ One challenging subset of hydrogenation reactions is the conversion of energetically stable aromatic molecules into their saturated congeners, a transformation critical in petroleum refining.² Catalytic hydrogenation can be accomplished via two methods, direct hydrogenation using a low- or high-pressure of hydrogen gas or transfer hydrogenation, ideally using small organic molecules as hydrogen donors. Direct hydrogenation using H₂ is most widely used because of its superior atom economy and absence of undesired side products. Nevertheless, producing hydrogen via traditional methods is both energy- and carbon-intensive. Furthermore, handling hydrogen at the typical severe processing conditions required for hydrogenation presents serious safety and cost issues, although the former is less of an issue from an engineering perspective. In contrast, the hydrogen donor molecules used in transfer hydrogenation, such as alcohols, hydrazines, tetralin, tetrahydroquinoline, and decalin, are typically low cost, readily available, and easy-to-handle compared to molecular hydrogen. As a result, transfer hydrogenation is a convenient, powerful, and attractive method to access various saturated compounds and has been described as experiencing a “golden age”.³

Transfer hydrogenation reactions have been studied for over a century and continue to find wide application in industrial and academic processes. Transfer hydrogenation was first described in 1903 by Knoevenagel, who reported that a heterogeneous Pd catalyst promotes disproportionation of dimethyl 1,4-dihydroterephthalate to dimethyl terephthalate and cis-hexahydroterephthalate.⁴ Since then, the field of transition metal-catalyzed transfer hydrogenation has developed steadily, with catalysts based on precious metals such as Pd, Pt, Ru, and Rh demonstrating the greatest activity, versatility, and selectivity.^{5,6} The high costs of these metals, coupled with their low natural abundance and the severe environmental impact associated with refining metal ores, has led to a dramatic shift towards utilization of less-expensive earth-abundant metals in catalysis. This trend is reflected in the increasing reliance on three first-row transition metals, iron,⁷ cobalt,⁸ and nickel⁹ as catalysts for transfer hydrogenation. Of these, iron is the most attractive because of its high natural abundance, affordability, and negligible toxicity.

There are numerous reports of iron-catalyzed transfer hydrogenation reactions, the vast majority describing saturation of alkenes,⁷ alkynes,¹⁰ aldehydes,^{11,12} ketones,¹³ and imines.¹⁴ However, there are considerably fewer reports of iron-catalyzed transfer hydrogenation of more thermodynamically stable aromatic molecules. Complete or partial saturation of aromatic molecules is of great importance in numerous industries ranging from pharmaceutical and fine chemical synthesis to renewable and conventional crude oil refining. In particular, hydrogenation of polycyclic aromatic molecules under moderate to severe reaction conditions represents one of the most critical challenges for processing heavy petroleum feedstocks into readily transportable liquid products. Polycyclic aromatic hydrocarbons (PAHs) constitute an important class of compounds in heavy crude oil due to its limited transformative behavior during upgrading.¹⁵

There is significant precedent for transfer hydrogenation of polycyclic aromatic hydrocarbons using a base metal catalyst. Phillipov and coworkers¹⁶ reported that Raney Ni catalyst could smoothly convert selected arenes under mild hydrogen transfer conditions, but only after elongated treatment. Other catalytic transfer hydrogenation systems, including NiMo/ γ -Al₂O₃¹⁷ or BF₃/SiO₂-Al₂O₃¹⁸ have been investigated but produced lower yields of aromatic hydrogenation. Examples of transfer hydrogenation of aromatic hydrocarbons catalyzed by iron mostly involve homogeneous organometallic compounds supported by exotic ligand systems. These reactions often require rigorous exclusion of air and moisture and are incompatible with “dirty” industrial processes such as crude oil upgrading/refining.^{7,19} There are very few examples of iron-catalyzed transfer hydrogenation of polycyclic aromatic hydrocarbons. Li et al.²⁰ demonstrated that ferric oxide can be sulfided in situ to produce an active catalyst for partial hydrogenation of polycyclic arenes under relatively harsh reaction conditions. In chapter three of this thesis, a presulfided iron compound, Fe₂S₂(CO)₆, was described that catalyzes hydrogenation/dehydrogenation of polycyclic aromatic molecules such as 9,10-dihydroanthracene and anthracene under a nitrogen atmosphere, suggesting considerable potential as a transfer hydrogenation catalyst.

In this chapter, the use of the well-defined unsupported iron precatalyst, Fe₂S₂(CO)₆, is developed for efficient transfer hydrogenation of a range of polycyclic aromatic compounds. The yields of partially hydrogenated products are surprisingly high, and the process delivers an unprecedented distribution of products under moderate reaction conditions. This synthetic, single-source, presulfided precatalyst is straightforward to prepare at any scale and indefinitely stable to air and water, making the complex a good candidate for further development and use in petroleum processing. To the best of my knowledge, this is the first reported use of Fe₂S₂(CO)₆ for transfer hydrogenation of polycyclic arenes.

4.2. Experimental section

4.2.1. Materials

Tetralin (99%), quinoline (98%), quinoxaline ($\geq 98\%$), phenazine (98%), indane (95%), indoline (99%), anthracene (99%), 2-ethylanthracene (98%), 9,10-dihydroanthracene (97%), acridine (97%), 9-methylacridine (95%), 7,8-benzoquinoline (97%), 2-propanol ($\geq 99.5\%$), 3-methylquinoline (99%), 4-methylquinoline (98%), 1,2,3,4-tetrahydroquinoline (98%), 1,2,5,6-dibenzanthracene (97%), elemental sulfur ($\geq 99.5\%$), iron (0) pentacarbonyl ($> 99.99\%$), 6-methylquinoline ($\geq 98\%$), 8-methylquinoline (97%), isoquinoline (97%), 2,6-dimethylquinoline (98%), 2,7-dimethylquinoline (99%) were obtained from Sigma-Aldrich and used as received. Reagent-grade toluene (Fisher Scientific), 1,2,3,4-dibenzanthracene (97%, Fisher Scientific), 9,10-diphenylanthracene (99%, Alfa Aesar), and 9-phenylanthracene (98%, TCI) were also used without further purification. Magnesium sulphate, methanol, hexanes, and ammonium chloride (all reagent-grade) were purchased from Caledon Laboratory Chemicals.

4.2.2. Precatalyst preparation

Detailed procedure for preparing $\text{Fe}_2\text{S}_2(\text{CO})_6$ is reported in chapter 2. The purified iron complex was obtained as red-brown, crystalline, air- and moisture-stable sublimate [9.7 g; 30% based on $\text{Fe}(\text{CO})_5$].

4.2.3. Transfer hydrogenation reactions

Transfer hydrogenation reactions were carried out in a 10 cm stainless-steel tubular batch microreactor with approximate volume of 20 cm^3 , and equipped with a high-temperature Swagelok severe service union/Bonnet needle valve. For a typical experiment, the reactor was filled with a reaction solution containing 0.2 mmol substrate, 2.5 mL toluene, and 2.5 mL hydrogen donor (for

dual donor system this volume is varied between the two compounds), followed by addition of $\text{Fe}_2\text{S}_2(\text{CO})_6$ (0.12 mmol Fe). Each experiment had a constant substrate to active metal (Fe) molar ratio of 1.67 mol/mol. Following rigorous leak testing, the microreactor was purged five times with ultrahigh purity (99.999%) nitrogen gas purchased from Praxair Canada. The reactor was then pressurized (6 MPa cold) at room temperature with nitrogen, and immersed in a preheated sand bath equipped with vertical agitator (850 rpm) for thorough mixing. The reactions were performed in the 200 to 350°C temperature range under 30 min, with the inside of the microreactor reaching reaction temperature within 5 min, as determined by a thermocouple. After 30 min, the microreactor was quickly cooled to room temperature under a high-pressure cold air. Each transfer hydrogenation reaction was performed in duplicate.

The transfer hydrogenation liquid products and unreacted substrate were identified by gas chromatography (GC) using 1-methylnaphthalene as an internal standard, after separating it from the catalyst via filtration with a 0.22 μm filter paper. The GC was equipped with flame ionization detection (FID) on a calibrated Agilent 6890N gas chromatograph coupled with HP-5 (5% phenyl)-methylpolysiloxane capillary column (30 m length \times 0.32 mm inner diameter \times 0.25 μm film thickness, helium as carrier gas) for quantitative analyses. The oven temperature was initially maintained at 100°C for 1 min, and then increased to 300°C at a ramp rate of 20°C/min, and finally maintained at 300°C for 2 min. GC-mass spectrometry using an Agilent 6850 gas chromatograph equipped with HP-5 (5% phenyl)-methylpolysiloxane capillary column was used for qualitative analyses of compounds with no pure standards.

4.3. Results and discussion

Developing on the previous chapter, which showed equilibrium dehydrogenation/hydrogenation of 9,10-dihydroanthracene and anthracene by $\text{Fe}_2\text{S}_2(\text{CO})_6$ under nitrogen pressure, we initially investigated partial saturation of anthracene using an exogenous hydrogen donor molecule. The hydrothermal decomposition of $\text{Fe}_2\text{S}_2(\text{CO})_6$ and full characterization of the resulting active iron sulfide nanoparticles have been reported in chapters 2 and 3. Tetralin was initially studied as the hydrogen donor, because it is used ubiquitously in transfer hydrogenation reactions relevant to petroleum processing.²⁰⁻²⁵ All of the experiments in this chapter used a reaction time of 30 minutes. In chapter 3, using H_2 at 300°C , the experiments were in the kinetic regime at 30 min, as can be seen in Figure 3.6. By choosing a reaction time in the kinetic regime, differences between conditions and hydrogen donors will be observable.

The active colloidal catalyst derived from $\text{Fe}_2\text{S}_2(\text{CO})_6$, with no added sulfur promotes transfer hydrogenation of anthracene by tetralin, responding to temperature variations in typical fashion (Figure 4.1a). No conversion is observed at 200°C , while 45% conversion to 9,10-dihydroanthracene is obtained at 350°C . Only a trace of tetrahydroanthracene was detected by GC-MS. In contrast, we previously showed that the same catalyst leads to 98% conversion of anthracene to a mixture of partially saturated products at just 300°C using molecular hydrogen (6 MPa cold) as the reducing agent. For transfer hydrogenation, elevated reaction temperatures are required to drive the dehydrogenation of tetralin,^{18,26} ensuring a sufficient concentration of hydrogen on the catalyst to promote saturation of anthracene. As anticipated, dehydrogenation of tetralin and reduction of anthracene do not proceed to any appreciable level (1.3%) in the absence of the iron catalyst at 350°C . Toluene, a much more stable aromatic molecule, resists

hydrogenation even in the presence of the catalyst at elevated temperature and therefore acts as an inert solvent.

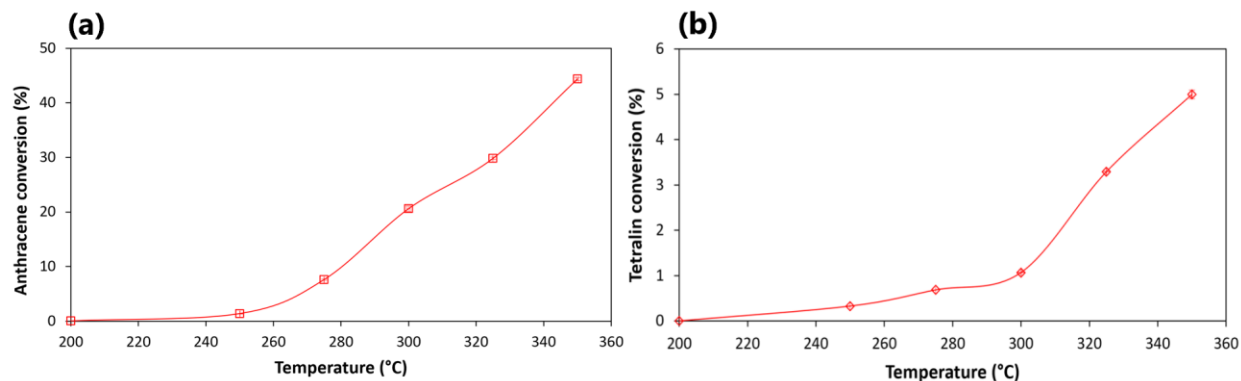


Figure 4.1. (a) Anthracene conversion as a function of temperature using tetralin as hydrogen donor and (b) tetralin conversion with temperature in the absence of a hydrogen acceptor. Reaction conditions: temperature, 200–350°C; cold N₂, 6 MPa; Fe₂S₂(CO)₆ (Fe, 0.12 mmol); Substrate to Fe molar ratio, 1.67 mol/mol; time, 30 min; anthracene, 0.2 mmol; toluene, 2.5 mL; tetralin, 2.5 mL in (a) and 0.20 mmol in (b).

To assess the effect of competitive dehydrogenation on the distribution of products at end of the reaction, control reactions starting with dihydroanthracene under the same conditions afforded 50% conversion to mostly anthracene. This result is similar to the that obtained when using anthracene as the substrate (56/44 anthracene to dihydroanthracene) suggesting that they are approaching an equilibrium conversion of anthracene. The similarity of these results reveals that catalytic hydrogenation and dehydrogenation are competitive processes in the presence of tetralin and the catalyst.

To assess catalyst inhibition, a potential catalyst poison was introduced to the system. Basic nitrogen donors such as quinoline were anticipated to bind to the most active sites on the catalyst surface,²⁷⁻²⁹ which if effective would limit catalyst activity. As expected, in this system quinoline effectively suppressed overall catalyst activity, reducing hydrogenation of anthracene to just 33%

| | | | | | |
|----|--|------------|-----|-----------------------|----------|
| 11 | Fe ₂ S ₂ (CO) ₆ | indoline | 2.5 | | 99 (0.2) |
| 12 | Fe ₂ S ₂ (CO) ₆ | indoline | 2.0 | | 98 (0.2) |
| 13 | Fe ₂ S ₂ (CO) ₆ | indoline | 1.5 | | 97 (0.1) |
| 14 | Fe ₂ S ₂ (CO) ₆ | indoline | 0.5 | | 58 (0.2) |
| 15 | Fe ₂ S ₂ (CO) ₆ | THQ | 0.5 | | 50 (0.4) |
| 16 | Fe ₂ S ₂ (CO) ₆ | 2-propanol | 2.0 | indoline ^b | 62 (0.7) |
| 17 | Fe ₂ S ₂ (CO) ₆ | tetralin | 2.0 | THQ ^b | 88 (0.3) |
| 18 | Fe ₂ S ₂ (CO) ₆ | tetralin | 2.0 | indoline ^b | 97 (0.3) |

Reaction conditions: temperature, 350 °C; cold N₂, 6 MPa; time, 30 min; anthracene, 0.2 mmol; toluene, 2.5 mL; hydrogen donor, 0.5-2.5 mL; additive, ^a0.03 mL and ^b0.5 mL; Fe₂S₂(CO)₆ (Fe, 0.12 mmol; Fe to substrate ratio, 0.6 mol/mol). Data are mean values for n = 2. Standard error values in parenthesis are one standard deviation. Structure: 1,2,3,4-tetrahydroquinoline (THQ).

These results reveal that strongly basic tetrahydroquinoline and indoline are the most effective hydrogen donors tested (Table 4.1, entries 10,11), smoothly converting anthracene to dihydroanthracene *nearly quantitatively*. Both 2-propanol and indane returned conversions similar to that obtained from tetralin (Table 4.1, entry 7-9). In the case of indoline or tetrahydroquinoline, greater than 50% anthracene hydrogenation was observed when the concentration of hydrogen donor molecule was reduced by 80% (Table 4.1, entries 14,15). It is noteworthy that the lower concentration of the N-heterocyclic donors still leads to greater anthracene conversion than when high concentrations of tetralin, indane or 2-propanol were used. This trend is consistent with that observed for other transfer hydrogenation systems³⁰ and is likely due to the high adsorption enthalpies of nitrogen heterocycles onto the iron surface, which in turn boosts the rate of dehydrogenation of these hydrogen donors and subsequent hydrogen atom transfer. We confirmed this by following the progress of dehydrogenation of low concentrations of each donor compound. As seen in Figure 4.2, the heterocycles were rapidly converted to the corresponding

dehydrogenated congeners (>80%) while no more than 7% conversion was observed for tetralin, indane or 2-propanol.

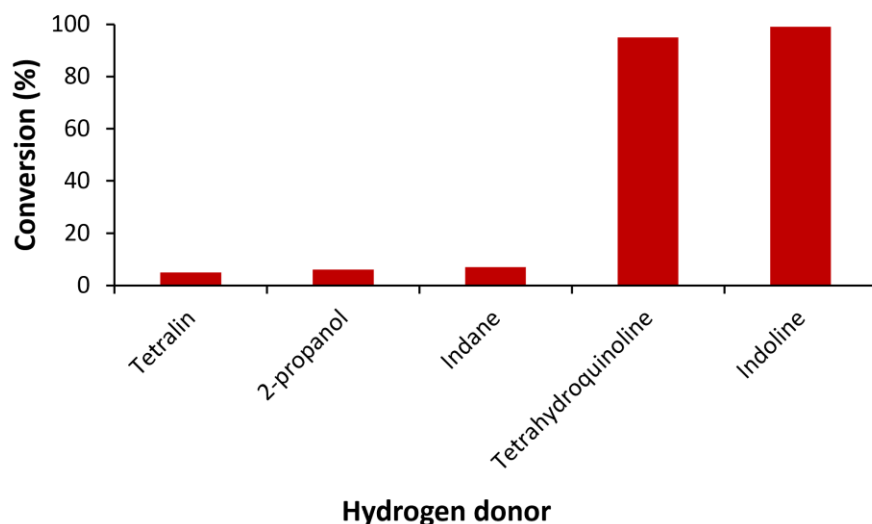


Figure 4.2. Iron-catalyzed dehydrogenation of various hydrogen donor compounds. Reaction conditions: temperature, 350 °C; cold N₂, 6 MPa; Fe₂S₂(CO)₆ (Fe, 0.12 mmol); Hydrogen donor to Fe molar ratio, 1.67 mol/mol; time, 30 min; hydrogen donor, 0.20 mmol; toluene, 2.5 mL.

Although indoline emerged as the most efficient hydrogen donor for the catalytic transfer hydrogenation, these donors are incompatible with authentic petroleum feeds. High concentrations of nitrogen heterocycles in petroleum lead to rapid deactivation of downstream refining catalysts.³³⁻³⁶ To address this problem, we sought to reduce concentration of indoline needed to promote transfer hydrogenation by addition of a high concentration of tetralin or 2-propanol, both less active hydrogen donors (Table 4.1, entries 16-18). A 4 : 1 mixture of tetralin and indoline was as effective as the use of indoline alone, producing nearly quantitative hydrogenation of anthracene (compare entry 18 with entries 11-13). In contrast, a mixture 2-propanol and indoline (4 : 1) returns a conversion of only 62% under these conditions (entry 16). These results stand in contrast to

Raney nickel-catalyzed transfer hydrogenation, wherein 2-propanol is generally a much superior hydrogen donor for the reduction of polycyclic aromatic compounds.¹⁶

The indoline-tetralin ratio in the dual hydrogen donor system was varied to determine the minimum amount of the nitrogen heterocycle necessary for efficient reduction of anthracene. As shown in Figure 4.3a, over 80% conversion is returned using a 40:1 tetralin-indoline mixture. As expected, conversion increases proportional to the indoline concentration with 97% anthracene hydrogenation using a 4:1 tetralin-indoline mixture.

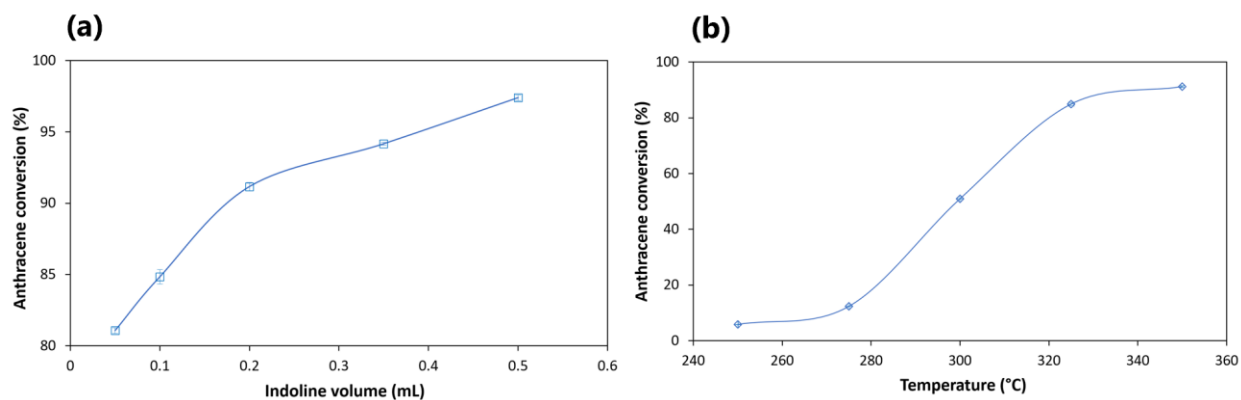


Figure 4.3. Anthracene conversion as a function of (a) indoline concentration at 350 °C and (b) temperature. Reaction conditions: temperature, 250-350 °C; cold N₂, 6 MPa; anthracene, 0.2 mmol; toluene, 2.5 mL; tetralin, 2.0 mL; indoline, 0.05-0.5 mL; Fe, 0.12 mmol; time, 30 min.

This tetralin-indoline mixed hydrogen donor system allows the transfer hydrogenation to proceed at lower reaction temperatures than seen for tetralin alone. At 250 °C, 6% of the anthracene is hydrogenated in the presence of a 10:1 tetralin-indoline mixture (Figure 4.3b), compared to no conversion for tetralin alone (see Figure 4.1a,b). As the temperature was increased in this mixed donor system, anthracene conversion responded in typical fashion;^{37,38} increasing from 6% at 250°C, to 90% at 325°C. Above 325°C, the conversion of anthracene plateaus (Figure 4.3b). This result suggests a transition from the kinetic regime to one of equilibrium conversion at the higher

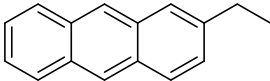
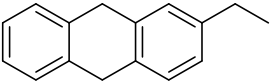
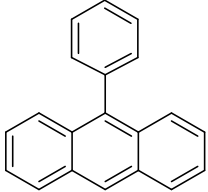
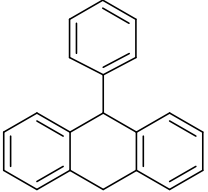
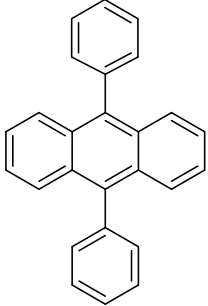
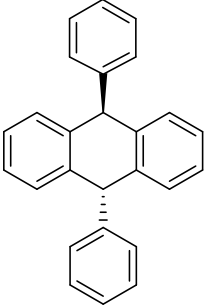
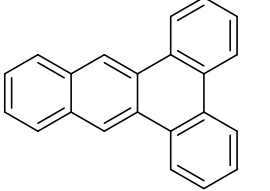
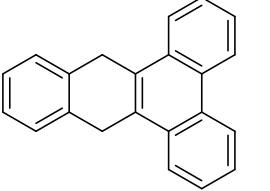
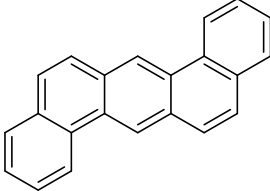
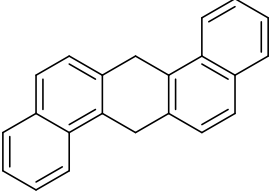
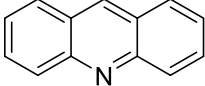
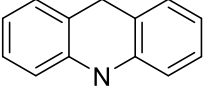
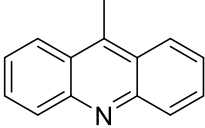
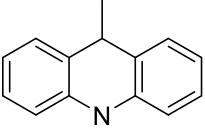
rates associated with elevated temperatures, in this regime there is likely greater desorption of anthracene, tetralin, and/or indoline at the higher temperature.^{39,40}

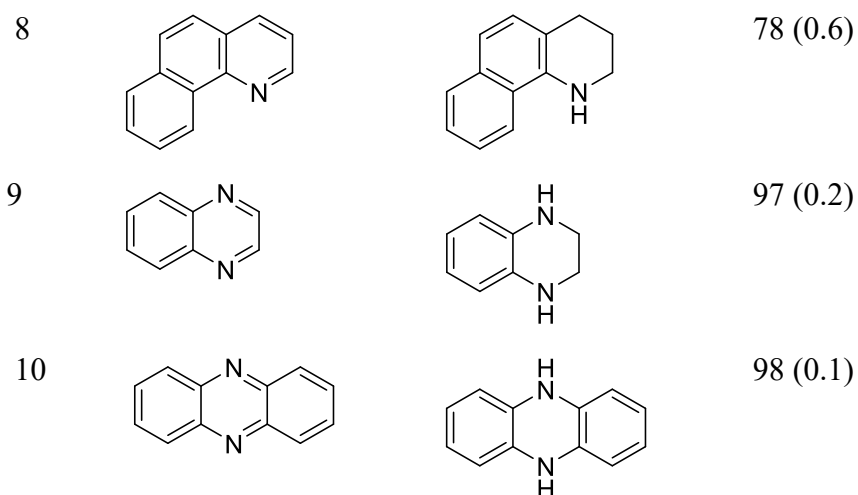
4.3.1. Scope of catalytic transfer arene hydrogenations

With optimized conditions in hand, I explored the scope of iron-catalyzed transfer hydrogenation of polycyclic aromatic compounds related to those found in heavy crude oil. Alkyl-substituted anthracene was smoothly converted (Table 4.2, entry 1). Limited conversions were obtained for phenyl substituted and fused benzene ring anthracene derivatives (Table 4.2, entry 2-5). This is generally due to the electron-withdrawing bulky arene substituents, which do not favor facile adsorption of substrate onto the catalyst surface,⁴¹ leading to slower hydrogenation of 9-phenylanthracene (72%), 9,10-diphenylanthracene (46%), 1,2,3,4-dibenzanthracene (26%), and 1,2,5,6-dibenzanthracene (21%).

Larger fused nitrogen polycyclic aromatic compounds are efficiently hydrogenated using the iron sulfide/indoline-tetralin system. Both acridine and 9-methyl acridine were converted to the corresponding tetrahydro acridine in greater than 90% conversion (Table 4.2, entry 6,7). The hydrogenation of 7,8-benzoquinoline is less facile, converting 78% to the partially hydrogenated product (Table 4.2, entry 8). Finally, the pyrazine-based molecules quinoxaline and phenazine are readily converted to partially hydrogenated products (Table 4.2, entry 9,10).

Table 4.2. Substrate scope of carbocyclic and heterocyclic aromatic compounds under unsupported iron-catalyzed transfer hydrogenation using mixed hydrogen donors.

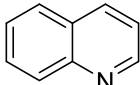
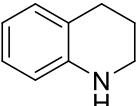
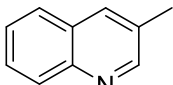
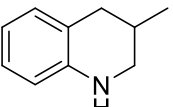
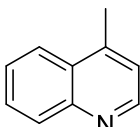
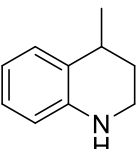
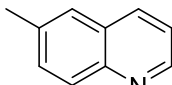
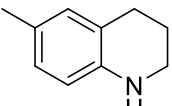
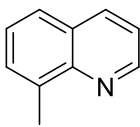
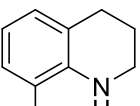
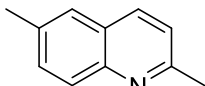
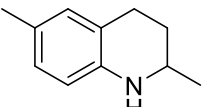
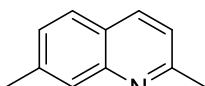
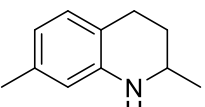
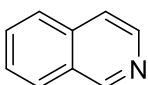
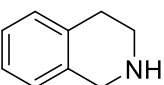
| entry | substrate | product | conversion (%) |
|-------|---|---|----------------|
| 1 |  |  | 96 (0.2) |
| 2 |  |  | 72 (0.8) |
| 3 |  |  | 46 (0.6) |
| 4 |  |  | 26 (0.4) |
| 5 |  |  | 21 (0.8) |
| 6 |  |  | 96 (0.2) |
| 7 |  |  | 93 (0.4) |



Reaction conditions: substrate, 0.2 mmol; temperature, 325 °C; cold N₂, 6 MPa; toluene, 2.5 mL; tetralin, 2.0 mL; indoline, 0.2 mL; Fe₂S₂(CO)₆ (Fe, 0.12 mmol); time, 30 min. Data are mean values for n = 2. Standard error values in parenthesis are one standard deviation.

Gratifyingly, this catalytic transfer hydrogenation is readily applicable to a much more challenging class of polycyclic aromatic compounds: quinoline-based heterocycles. Quinolines are ubiquitous in heavy oils and hydrogenation of quinolines is believed to be a key reaction for petroleum processing. All of the quinoline compounds were transformed to their corresponding 1,2,3,4-tetrahydroquinolines in good to excellent conversion (Table 4.3). Quinoline itself was hydrogenated to tetrahydroquinoline in 99% conversion at 325°C using the indoline-tetralin donor system (Table 4.3, entry 1). Both mono- and dimethylquinolines were also smoothly transformed, irrespective of the substitution pattern on the quinoline core (Table 4.3, entry 2-7). Surprisingly, each of the substrates returned a single product. For instance, 4-methylquinoline is hydrogenated to only 4-methyl-1,2,3,4-tetrahydroquinoline. This is interesting because the formation of 4-methyl-5,6,7,8-tetrahydroquinoline product is also highly feasible and has been reported in literature.⁴² Reduction of isoquinoline also produced remarkable conversion, 95% (Table 4.3, entry 8).

Table 4.3. Unsupported iron-catalyzed transfer hydrogenation of quinoline derived substrates using mixed hydrogen donors.

| entry | substrate | product | conversion (%) |
|-------|---|---|----------------|
| 1 |  |  | 99 (0.4) |
| 2 |  |  | 97 (0.2) |
| 3 |  |  | 98 (0.3) |
| 4 |  |  | 96 (0.2) |
| 5 |  |  | 98 (0.3) |
| 6 |  |  | 94 (0.4) |
| 7 |  |  | 95 (0.5) |
| 8 |  |  | 95 (0.7) |

Reaction conditions: substrate, 0.2 mmol; temperature, 325°C; cold N₂, 6 MPa; toluene, 2.5 mL; tetralin, 2.0 mL; indoline, 0.2 mL; Fe₂S₂(CO)₆ (Fe, 0.12 mmol); time, 30 min. Data are mean values for n = 2. Standard error values in parenthesis are one standard deviation.

The highly efficient reduction of the quinoline- and pyrazine-based heterocycles renders this iron sulfide transfer hydrogenation system highly attractive beyond the realm of petroleum processing. Tetrahydroquinolines and tetrahydropyrazines are critical substructures in active pharmaceutical molecules and agrochemicals.⁴³ With further optimization, this method for selective hydrogenation of nitrogen heterocycles has potential to be applied in the manufacture of fine chemicals.

4.3.2 Catalyst recycling

The heterogeneous iron sulfide transfer hydrogenation catalyst was evaluated for deactivation and reuse. As shown in Figure 4.4, the unsupported, in situ-generated iron catalyst was reused up to four times for quinoline hydrogenation with only modest decrease (25%) in activity. The catalysts were isolated and recycled using simple filtration, with no efforts made to exclude air or moisture, and without further sulfidation. Notably, the iron-based catalyst does not display the usual steep loss in activity between the first and second cycles that is often observed with conventional NiMoS or CoMoS catalysts. The sustained activity reflects the chemical and structural robustness of the iron sulfide phase, key requirements for deployment in any large-scale industrial process. This robustness is particularly important for potential use of this catalyst in the partial upgrading of heavy crude oil, where a cheap, reusable, and relatively active catalyst is required.¹⁵

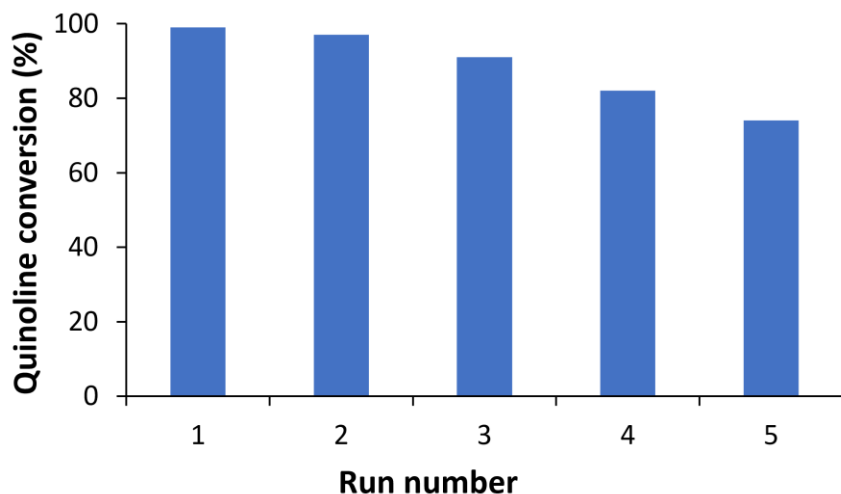


Figure 4.4. Catalyst recycling for the transfer hydrogenation of quinoline to tetrahydroquinoline. Reaction conditions: substrate, 0.2 mmol; temperature, 325 °C; cold N₂, 6 MPa; toluene, 2.5 mL; tetralin, 2.0 mL; indoline, 0.2 mL; Fe₂S₂(CO)₆ (Fe, 0.12 mmol); time, 30 min.

4.4. Conclusions

In summary, we have developed an efficient single-source unsupported iron catalyst for selective transfer hydrogenation of carbocyclic and heterocyclic aromatic compounds using mixed hydrogen donors modeling key structures and functionality found in petroleum. The data suggest that this and related iron sulfur complexes may be suitable for deployment in partial upgrading processes, where selective hydrogenation with limited heteroatom removal is the objective. Under moderate reaction conditions, a dual hydrogen donor system outperforms single donor systems with good tolerance for alkyl and aryl substituents. Tetrahydroquinolines have a range of important applications for both pharmaceutical and agrochemical industries. Broad substrate scope, inexpensive and nontoxic catalyst, good reproducibility and repeatability, moderate reaction conditions, cost-effective hydrogen donors, and simple operations make this protocol potentially scalable and competitive alternative to existing transfer hydrogenation methods.

4.5. References

1. Zhang, L.; Zhou, M.; Wang, A.; Zhang, T. Selective Hydrogenation Over Supported Metal Catalysts: From Nanoparticles to Single Atoms. *Chem. Rev.* **2020**, *120*, 683.
2. Wiesenfeldt, M. P.; Nairoukh, Z.; Dalton, T.; Glorius, F. Selective Arene Hydrogenation for Direct Access to Saturated Carbo- and Heterocycles. *Angew. Chem. Int. Ed.* **2019**, *58*, 10460.
3. Wang, D.; Astruc, D. The Golden Age of Transfer Hydrogenation. *Chem. Rev.* **2015**, *115*, 6621.
4. Knoevenagel, E.; Bergdolt, B. Ueber das Verhalten Des Δ 2.5-Dihydroterephthalsäuredimethylesters Bei Höheren Temperaturen und in Gegenwart Von Palladiummohr. *Ber. Dtsch. Chem. Ges.* **1903**, *36*, 2857.
5. Gelis, C.; Heusler, A.; Nairoukh, Z.; Glorius, F. Catalytic Transfer Hydrogenation of Arenes and Heteroarenes. *Chem. - Eur. J.* **2020**, *26*, 14090.
6. Wang, Y.; Cao, X.; Zhao, L.; Pi, C.; Ji, J.; Cui, X.; Wu, Y. Generalized Chemoselective Transfer Hydrogenation/Hydrodeuteration. *Adv. Synth. Catal.* **2020**, *362*, 4119.
7. Espinal-Viguri, M.; Neale, S. E.; Coles, N. T.; Macgregor, S. A.; Webster, R. L. Room Temperature Iron-Catalyzed Transfer Hydrogenation and Regioselective Deuteration of Carbon–Carbon Double Bonds. *J. Am. Chem. Soc.* **2019**, *141*, 572.
8. Chen, F.; Sahoo, B.; Kreyenschulte, C.; Lund, H.; Zeng, M.; He, L.; Junge, K.; Beller, M. Selective Cobalt Nanoparticles for Catalytic Transfer Hydrogenation of N-Heteroarenes. *Chem. Sci.* **2017**, *8*, 6239.
9. Vermaak, V.; Vosloo, H. C.; Swarts, A. J. Fast and Efficient Nickel (II)-Catalysed Transfer Hydrogenation of Quinolines with Ammonia Borane. *Adv. Synth. Catal.* **2020**, *362*, 5788.
10. Wienhöfer, G.; Westerhaus, F. A.; Jagadeesh, R. V.; Junge, K.; Junge, H.; Beller, M. Selective Iron-Catalyzed Transfer Hydrogenation of Terminal Alkynes. *Chem. Commun.* **2012**, *48*, 4827.
11. Zhang, P.; Li, X.; Qi, X.; Sun, H.; Fuhr, O.; Fenske, D. Transfer Hydrogenation of Aldehydes Catalyzed by Silyl Hydrido Iron Complexes Bearing a [PSiP] Pincer Ligand. *RSC Adv.* **2018**, *8*, 14092.

12. Wienhöfer, G.; Westerhaus, F. A.; Junge, K.; Beller, M. Fast and Selective Iron-Catalyzed Transfer Hydrogenations of Aldehydes. *J. Organomet. Chem.* **2013**, *744*, 156.
13. Magubane, M. N.; Nyamato, G. S.; Ojwach, S. O.; Munro, O. Q. Structural, Kinetic, and DFT Studies of the Transfer Hydrogenation of Ketones Mediated by (Pyrazole)pyridine Iron(II) and Nickel(II) Complexes. *RSC Adv.* **2016**, *6*, 65205.
14. Pan, H. -J.; Ng, T. W.; Zhao, Y. Iron-Catalyzed Transfer Hydrogenation of Imines Assisted by an Iron-Based Lewis Acid. *Org. Biomol. Chem.* **2016**, *14*, 5490.
15. Gray, M. R. Fundamentals of Partial Upgrading of Bitumen. *Energy Fuels* **2019**, *33*, 6843.
16. Philippov, A. A.; Chibiryayev, A. M.; Martyanov, O. N. Catalyzed Transfer Hydrogenation by 2-propanol for Highly Selective PAHs Reduction. *Catal. Today.* **2021**, *379*, 15.
17. Zhao, Y.; Gray, M. R.; Wei, F. Rejuvenation of Residue Hydroconversion Catalysts by H-Donor Solvents. *Catal. Lett.* **2008**, *125*, 69.
18. Winiarek, P.; Fedoryńska, E.; Cholewiński, P. Transfer Hydrogenation of Phenanthrene in the Presence of Boron Modified Alumina or Silica-alumina. *React. Kinet. Catal. Lett.* **1995**, *55*, 191.
19. Linford-Wood, T. G.; Coles, N. T.; Webster, R. L. Room Temperature Iron Catalyzed Transfer Hydrogenation Using n-Butanol and Poly(methylhydrosiloxane). *Green Chem.* **2021**, *23*, 2703.
20. Li, L.; Hou, Y.; Wu, W.; Liang, S.; Ren, S. Behaviors of Tetralin and 9,10-dihydroanthracene as Hydrogen Donor Solvents in the Hydrogenolysis of Coal-Related Model Compounds. *Fuel Process. Technol.* **2019**, *191*, 202.
21. Alemán-Vázquez, L. O.; Torres-Mancera, P.; Ancheyta, J.; Ramírez-Salgado, J. Use of Hydrogen Donors for Partial Upgrading of Heavy Petroleum. *Energy Fuels* **2016**, *30*, 9050.
22. Kim, D. W.; Jeon, P. R.; Moon, S.; Lee, C. H. Upgrading of Petroleum Vacuum Residue Using a Hydrogen-donor Solvent with Acid-Treated Carbon. *Energy Convers. Manage.* **2018**, *161*, 234.
23. Alemán-Vázquez, L. O.; Cano-Domínguez, J. L.; García-Gutiérrez, J. L. Effect of Tetralin, Decalin and Naphthalene as Hydrogen Donors in the Upgrading of Heavy Oils. *Procedia Eng.* **2012**, *42*, 532.

24. Ovalles, C.; Rodriguez, H. Extra Heavy Crude Oil Downhole Upgrading Using Hydrogen Donors Under Cyclic Steam Injection Conditions: Physical and Numerical Simulation Studies. *J. Can. Pet. Technol.* **2008**, 4701.
25. Park, H. -B.; Kim, K. -D.; Lee, Y. -K. Promoting Asphaltene Conversion by Tetralin for Hydrocracking of Petroleum Pitch. *Fuel* **2018**, 222, 105.
26. Zhang, Z. G.; Yoshida, T. Behavior of Hydrogen Transfer in the Hydrogenation of Anthracene Over Activated Carbon. *Energy Fuels* **2001**, 15, 708.
27. Salazar, N.; Schmidt, S. B.; Lauritsen, J. V. Adsorption of Nitrogenous Inhibitor Molecules on MoS₂ and CoMoS Hydrodesulfurization Catalysts Particles Investigated by Scanning Tunneling Microscopy. *J. Catal.* **2019**, 370, 232.
28. Nagai, M.; Kabe, T. Selectivity of Molybdenum Catalyst in Hydrodesulfurization, Hydrodenitrogenation, and Hydrodeoxygenation: Effect of Additives on Dibenzothiophene Hydrodesulfurization. *J. Catal.* **1983**, 81, 440.
29. Lavopa, V.; Satterfield, C. N. Poisoning of Thiophene Hydrodesulfurization by Nitrogen-Compounds. *J. Catal.* **1988**, 110, 375.
30. Gould, K. A.; Wiehe, I. A. Natural Hydrogen Donors in Petroleum Resids. *Energy Fuels* **2007**, 21, 1199.
31. Guin, J. A.; Curtis, C. W.; Kwon, K. C. Pyrite-Catalysed Coal Liquefaction Using Quinoline/Tetrahydroquinoline as an H-Donor System. *Fuel* **1983**, 62, 1412.
32. Chen, X.; Yang, Z.; Chen, X.; Liang, W.; Zhu, Z.; Xie, F.; Li, Y. Hydrogen-Transfer-Mediated N-Arylation of Naphthols Using Indolines as Hydrogen Donors. *J. Org. Chem.* **2020**, 85, 508.
33. Fu, C. M.; Schaffer, A. M. Effect of Nitrogen Compounds on Cracking Catalysts. *Ind. Eng. Chem. Prod. Res. Dev.* **1985**, 24, 68.
34. Ho, T. C.; Katritzky, A. R.; Cato, S. J. Effect of Nitrogen Compounds on Cracking Catalysts. *Ind. Eng. Chem. Res.* **1992**, 31, 1589.
35. Shen, J.; Semagina, N. Inhibition of Diolefin Hydrogenation by Quinoline. *Energy Fuels* **2020**, 34, 8769.
36. Hegedűs, L.; Szőke-Molnár, K.; Sajó, I. E.; Sranko, D. F.; Schay, Z. Poisoning and Reuse of Supported Precious Metal Catalysts in the Hydrogenation of N-Heterocycles Part I: Ruthenium-Catalysed Hydrogenation of 1-methylpyrrole. *Catal. Lett.* **2018**, 148, 1939.

37. Zhang, Z. G.; Okada, K.; Yamamoto, M.; Yoshida, T. Hydrogenation of Anthracene Over Active Carbon-Supported Nickel Catalyst. *Catal. Today*, **1998**, *45*, 361.
38. Pinilla, J. L.; Arcelus-Arrillaga, P.; Puron, H.; Millan, M. Reaction Pathways of Anthracene Selective Catalytic Steam Cracking Using a NiK/Al₂O₃ Catalyst. *Fuel* **2013**, *109*, 303.
39. Girgis, M. J.; Gates, B. C. Reactivities, Reaction Networks, and Kinetics in High-Pressure Catalytic Hydroprocessing. *Ind. Eng. Chem. Res.* **1991**, *30*, 2021.
40. Cowley, S.; Wiser, W. The Thermodynamics of Anthracene Hydrocracking. *Fuel Process. Technol.* **1979**, *2*, 317.
41. Sun, L. B.; Wei, X. Y.; Liu, X. Q.; Zong, Z. M.; Li, W.; Kou, J. H. Selective Hydrogen Transfer to Anthracene and Its Derivatives over an Activated Carbon. *Energy Fuels* **2009**, *23*, 4877.
42. Chen, F.; Surkus, A. E.; He, L.; Pohl, M. M.; Radnik, J.; Topf, C.; Junge, K.; Beller, M. Selective Catalytic Hydrogenation of Heteroarenes with N-Graphene-Modified Cobalt Nanoparticles (Co₃O₄-Co/NGr@ α -Al₂O₃). *J. Am. Chem. Soc.* **2015**, *137*, 11718.
43. Sridharan, V.; Suryavanshi, P. A.; Menendez, J. C. Advances in the Chemistry of Tetrahydroquinolines. *Chem. Rev.* **2011**, *111*, 7157.

Chapter 5: Conclusions and Recommendations for Future Work

5.1. Conclusions

This thesis focused primarily on iron-catalyzed partial hydrogenation and limited defunctionalization of key polycyclic and heteroaromatic substructures readily present in heavy crude oil, which are important reaction requirements in partial upgrading processes. The iron catalyst discussed build on work by Habib and coworkers from Professor Emeritus Murray R. Gray's research group (University of Alberta). Both supported and unsupported sulfided iron catalysts were reported to significantly suppress addition reactions during thermal cracking under hydrogenation conditions using a model compound. Importantly, the group showed the significance of utilizing a low-cost iron-based catalyst, relative to nickel- or molybdenum-based catalyst for coke reduction in thermal cracking processes under hydrogen. In this thesis, the hypothesis was that nanosized iron catalysts can significantly promote partial hydrogenation and limited desulfurization and denitrogenation of several key polycyclic aromatic and heteroaromatic compounds during partial upgrading of heavy crude oil, potentially resulting in pipeline-compatible product.

In chapter 2, I have described the synthesis and characterization of a presulfided iron precatalyst $\text{Fe}_2\text{S}_2(\text{CO})_6$, which is the backbone of all catalytic reactions in this thesis. The iron sulfide complex is formed from the reaction of elemental sulfur and $\text{Fe}(\text{CO})_5$, and isolated as red-brown air-stable crystals with high solubility in hydrocarbon media. The active phase, consisting of iron sulfide nanoparticles, was in situ-generated from $\text{Fe}_2\text{S}_2(\text{CO})_6$ in toluene, with no added sulfur. This chapter established the dramatic importance of a support for catalyzed partial hydrogenation and

desulfurization of pyrene, phenanthrene, naphthalene, and benzothiophene under $\text{Fe}_2\text{S}_2(\text{CO})_6$. Activated carbon, γ -alumina, and activated silica were all effective dispersants for the Fe precatalyst in obtaining high conversions of the polycondensed aromatics under moderate conditions. In contrast, unsupported $\text{Fe}_2\text{S}_2(\text{CO})_6$ produced relatively low partially reduced products. The reactivity depicted self-consistent substrate dependence, varying with the resonance energy stabilization of the starting compounds and partially saturated intermediates coupled with the surface adsorption enthalpy of the aromatic ring system. Generally, the Fe precursor demonstrated high selectivity for partial hydrogenation and limited desulfurization, making it desirable in potential partial upgrading schemes. However, further optimization and applications of the catalyst system to the hydroprocessing of authentic petroleum feeds in future is essential.

Chapter 3 describes a facile procedure which utilizes unsupported $\text{Fe}_2\text{S}_2(\text{CO})_6$ exclusively to explore the selective hydrogenation and defunctionalization of carbocyclic and heterocyclic aromatic heavy oil model compounds. The active catalyst derived from $\text{Fe}_2\text{S}_2(\text{CO})_6$ were highly effective for the partial hydrogenation of substituted anthracenes and aromatic nitrogen and sulfur heterocycles. The phenyl substituents significantly influenced the reactivity of the anthracene series primarily via stereoelectronic effects, with conversions decreasing with size of substituents. Several polyaromatic heterocycles were partially hydrogenated as well as mixed feeds, comprising of combinations of model compounds, with limited desulfurization or denitrogenation, increasing in the order phenoxathiine < benzothiophene << diphenylanthracene < phenylanthracene < quinoline < acridine < anthracene. The results showed that the in situ-generated unsupported iron sulfide nanoparticles are well-suited for selective partial saturation and limited defunctionalization, which are key requirements for catalytic partial upgrading of heavy crude. Introduction of extraneous sulfur must be well controlled to prevent inhibition since it easily competes with the

substrates for adsorption onto the catalyst surface. Future work on this unsupported catalytic system should be focused on enhancing its activity by introducing a second inexpensive metal and then using that to evaluate a variety of complex model compounds readily available in heavy crude oil. Also, applications of this protocol to the partial upgrading of various heavy crudes are important to authenticate this catalytic system.

In chapter 4, the background of transfer hydrogenation was introduced. The recent advances of iron-catalyzed transfer hydrogenation were reviewed. Readily available hydrogen donor solvents, including tetralin, 2-propanol, indane, indoline, and tetrahydroquinoline were substituted for hydrogen gas to partially hydrogenate carbocyclic- and N-heterocyclic aromatic compounds. Basic nitrogen compounds resulted in near quantitative conversions of anthracene, while the two carbocyclic donor compounds (tetralin and indane) and 2-propanol produced limited conversions. The results demonstrated that a dual hydrogen donor system outperforms single donor systems to permit efficient transfer hydrogenation of the various polycyclic aromatic substrates under moderate reaction conditions with good tolerance for alkyl and aryl substituents. The reactivity of the catalyst is governed by the thermodynamically favorable adsorption of N-heterocycles to the catalyst surface, which in turn allows for facile dehydrogenation, followed by rapid hydrogen atoms transfer to the substrate. This protocol presents an inexpensive and viable catalytic system for partial reduction and limited defunctionalization of key polycyclic aromatic hydrocarbon units dominant in heavy crude oil.

Bibliography

1. IEA, 2021 World Energy Outlook. <https://iea.blob.core.windows.net/assets/4ed140c1-c3f3-4fd9-acae-789a4e14a23c/WorldEnergyOutlook2021.pdf> (accessed on March 16, 2022).
2. Demirbas, A.; Bafail, A.; Nizami, A. S. Heavy oil upgrading: Unlocking the Future Fuel Supply. *Pet. Sci. Technol.* **2016**, *34*, 303-308.
3. Hein, F. J. Geology of Bitumen and Heavy oil: An Overview. *J. Pet. Sci. Eng.* **2017**, *154*, 551-563.
4. Hills, D. J.; Hooks, C. H.; McIntyre-Redden, M. R.; Crooke, L. A.; Tew Jr, B. H.; Parks, K. Oil Sands in Alabama, USA: A Fresh Look at an Emerging Potential Resource. *Bull. Can. Petrol. Geol.* **2016**, *64*, 278-290.
5. AER, 2021. ST98:2021. Alberta Energy Outlook. <https://static.aer.ca/prd/documents/sts/ST98/2021/st98-2021-executivesummary.pdf> (accessed on March 15, 2022).
6. Meyer, R. F.; Attanasi, E. D.; Freeman, P. A. Heavy Oil and Natural Bitumen Resources in Geological Basins of the World. U.S. Geological Survey Open-File Report 2007, 1084, 1-42, <http://pubs.usgs.gov/of/2007/1084/> (accessed on March 16, 2022).
7. Greene, D. L.; Hopson, J. L.; Li, J. Running Out of and Into Oil: Analyzing Global Oil Depletion and Transition Through 2050. *Transp. Res. Rec.* **2004**, *1880*, 1-9.
8. Canadian Association of Petroleum Producers CAPP. *Crude Oil Forecast, Markets and Transportation 2021*. <https://www.capp.ca/publications-and-statistics/publications/320292> (accessed on March 16, 2022).
9. de Klerk, A.; Gray, M. R.; Zerpa, N. Unconventional oil and gas: Oilsands. *In Future Energy. Improved, Sustainable and Clean Options for Our Planet*, 2nd Edition; Letcher, T. M., Ed.; Elsevier: Amsterdam, 2014; pp 95-116.
10. Gray, M. R. *Upgrading Oilsands Bitumen and Heavy Oil*; University of Alberta Press: Edmonton, Alberta, Canada, 2015.
11. Hart, A. A Review of Technologies for Transporting Heavy Crude Oil and Bitumen via Pipelines. *J. Pet. Explor. Prod. Technol.* **2014**, *4*, 327-336.

12. de Klerk, A. Processing Unconventional Oil: Partial Upgrading of Oilsands Bitumen. *Energy Fuels* **2021**, *35*, 14343-14360.
13. Gray, M. R. Fundamentals of Partial Upgrading of Bitumen. *Energy Fuels* **2019**, *33*, 6843.
14. Oil Sands Magazine. <https://www.oilsandsmagazine.com/technical/bitumen-upgrading> (accessed on September 20, 2022).
15. Alshareef, A. H. Asphaltenes: Definition, Properties, and Reactions of Model Compounds. *Energy Fuels* **2020**, *34*, 16.
16. Kamkar, M.; Natale, G. A Review on Novel Applications of Asphaltenes: A Valuable Waste. *Fuel* **2021**, *285*, 119272.
17. Zuo, P.; Qu, S.; Shen, W. Asphaltenes: Separations, Structural Analysis and Applications. *J. Energy Chem.* **2019**, *34*, 186–207.
18. Mitchell, D. L.; Speight, J. G. The solubility of asphaltenes in hydrocarbon solvents. *Fuel* **1973**, *52*, 149–152.
19. Speight, J. G. Petroleum Asphaltenes-Part 1: Asphaltenes, resins and the structure of petroleum. *Oil Gas Sci. Technol.* **2004**, *59*, 467–477.
20. Castaneda, L. C.; Munoz, J. A.; Ancheyta, J. Current Situation of Emerging Technologies for Upgrading of Heavy Oils. *Catal. Today* **2014**, *220*, 248.
21. Gray, M. R.; McCaffrey, W. C. Role of Chain Reactions and Olefin Formation in Cracking, Hydroconversion, and Coking of Petroleum and Bitumen Fractions. *Energy Fuels* **2002**, *16*, 756–766.
22. McMillen, D. F.; Golden, D. M. Hydrocarbon Bond Dissociation Energies. *Annu. Rev. Phys. Chem.* **1982**, *33*, 493-532.
23. Rana, M. S.; Samano, V.; Ancheyta, J.; Diaz, J. A. I. A Review of Recent Advances on Process Technologies for Upgrading of Heavy Oils and Residua. *Fuel* **2007**, *86*, 1216.
24. Speight, J. G. New Approaches to Hydroprocessing. *Catal. Today* **2004**, *98*, 55-60.
25. Joshi, J. B.; Pandit, A. B.; Kataria, K. L.; Kulkarni, R. P.; Sawarkar, A. N.; Tandon, D.; Ram, Y.; Kumar, M. M. Petroleum Residue Upgradation via Visbreaking: A Review. *Ind. Eng. Chem. Res.* **2008**, *47*, 8960-8988.
26. Speight, J. G. Visbreaking: A Technology of the Past and the Future. *Sci. Iran.* **2012**, *19*, 569–573.

27. Marafi, A.; Albazzaz, H.; Rana, M. S. Hydroprocessing of Heavy Residual Oil: Opportunities and Challenges. *Catal. Today* **2019**, *329*, 125-134.
28. Prado, G. H.; Rao, Y.; de Klerk, A. Nitrogen Removal from Oil: A Review. *Energy Fuels* **2017**, *31*, 14-36.
29. Bello, S. S.; Wang, C.; Zhang, M.; Gao, H.; Han, Z.; Shi, L.; Su, F.; Xu, G. A Review on the Reaction Mechanism of Hydrodesulfurization and Hydrodenitrogenation in Heavy Oil Upgrading. *Energy Fuels* **2021**, *35*, 10998-11016.
30. Furimsky, E. Selection of catalysts and reactors for hydroprocessing. *Appl. Catal., A* **1998**, *171*, 177-206.
31. Ancheyta, J.; Rana, M. S.; Furimsky, E. Hydroprocessing of Heavy Petroleum Feeds: Tutorial. *Catal. Today* **2005**, *109*, 3-15.
32. Fellows, G. K.; Mansell, R.; Schlenker, R.; Winter, J. *Public-Interest Benefit Evaluation of Partial-Upgrading Technology*, SPP Research Papers AB; University of Calgary, The School of Public Policy: Calgary, 2017; Vol. 10.
33. AER, 2018. ST98:2018. Alberta's Energy Reserves & Supply/Demand Outlook. <https://www.aer.ca/providing-information/data-and-reports/statistical-reports/st98/archives> (accessed on April 2, 2022).
34. Keesom, W.; Gieseeman, J. *Bitumen Partial Upgrading 2018 Whitepaper AM0401A*; Alberta Innovates: Calgary, AB, **2018**; pp 152.
35. Eagle Ford Condensate Price Index. <https://www.barchart.com/cmdty/indexes/us-crude-oil/explore/CLPAUS133.CM> (accessed on November 17, 2022).
36. Colyar, J. I. M. Has the Time for Partial Upgrading of Heavy Oil and Bitumen Arrived? *Pet. Technol. Q.* **2009**, *Q14*, 43.
37. Ng, S. H.; Heshka, N. E.; Zheng, Y.; Ling, H.; Wang, J.; Liu, Q.; Little, E.; Wang, H.; Ding, F. Preliminary Assessment of a Strategy for Processing Oil Sands Bitumen to Reduce Carbon Footprint. *Energy Fuels* **2021**, *35*, 9489-9496.
38. Enbridge Quality Pooling. *Enbridge: Quality Pooling Specification Package*; Edmonton, 2022. https://www.enbridge.com/~/_media/Enb/Documents/Shippers/Quality_Pooling_Specification_Package.pdf?la=en (accessed April 28, 2022).

39. Winter, J.; Goodday, V.; Fellows, G. K. Enabling Partial Upgrading in Alberta: A Review of the Regulatory Framework and Opportunities for Improvement. *School Public Policy Publ.* 2019; 12: 0-47.
40. Yañez Jaramillo, L. M.; de Klerk, A. Partial Upgrading of Bitumen by Thermal Conversion at 150–300°C. *Energy Fuels* **2018**, 32, 3299-3311.
41. Kaminski, T.; Husein, M. M. Partial Upgrading of Athabasca Bitumen using Thermal Cracking. *Catalysts* **2019**, 9, 431.
42. Alvarez-Majmutov, A.; Gieleciak, R.; Chen, J. Enhanced Representation of Thermal Cracking Chemistry in the Context of Bitumen Partial Upgrading. *Energy Fuels* **2021**, 35, 12005-12018.
43. Salehzadeh, M.; Kaminski, T.; Husein, M. M. An Optimized Thermal Cracking Approach for Onsite Upgrading of Bitumen. *Fuel* **2022**, 307, 121885.
44. Díaz-Boffelli, G.; Ancheyta, J.; Muñoz, J. A. D.; Centeno, G. Experimental Study and Economic Analysis of Heavy Oil Partial Upgrading by Solvent Deasphalting–Hydrotreating. *Energy Fuels* **2018**, 32, 55–59.
45. Zachariah, A.; de Klerk, A. Partial Upgrading of Bitumen: Impact of Solvent Deasphalting and Visbreaking Sequence. *Energy Fuels* **2017**, 31, 9374.
46. Gholami, R.; Alvarez-Majmutov, A.; Chen, J. Process Modelling and Simulation of Bitumen Partial Upgrading: Analysis of Solvent Deasphalting-Thermal Cracking Configuration. *Can. J. Chem. Eng.* **2021**, 1-14.
47. Xing, T.; Alvarez-Majmutov, A.; Chen, J. Bitumen Partial Upgrading by Mild Hydroprocessing in a Fixed-bed Reactor. *Fuel* **2019**, 235, 696.
48. Gholami, R.; Alvarez-Majmutov, A.; Xing, T.; Chen, J. Bitumen Partial Upgrading Through Fixed-Bed Hydroprocessing: Examining Catalyst Stability. *Fuel* **2021**, 287, 119830.
49. Djimasbe, R.; Varfolomeev, M. A.; Al-Muntaser, A. A.; Yuan, C.; Feoktistov, D. A.; Suwaid, M. A.; Kirgizov, A. J.; Davletshin, R. R.; Zinnatullin, A. L.; Fatou, S. D.; Galeev, R. I. Oil Dispersed Nickel-Based Catalyst for Catalytic Upgrading of Heavy Oil Using Supercritical Water. *Fuel* **2022**, 313, 122702.

50. Schacht-Hernández, P.; Portales-Martínez, B.; Laredo, G. C.; Pérez-Romo, P.; Domínguez-Esquivel, J. M. Homogeneous Catalyst for In-Situ Hydrotreating of Heavy Oils. *Appl. Catal., A* **2019**, *577*, 99-106.
51. Kim, S. H.; Kim, K. D.; Lee, Y. K. Effects of Dispersed MoS₂ Catalysts and Reaction Conditions on Slurry Phase Hydrocracking of Vacuum Residue. *J. Catal.* **2017**, *347*, 127-137.
52. Nguyen, T. S.; Tayakout-Fayolle, M.; Lacroix, M.; Gotteland, D.; Aouine, M.; Bacaud, R.; Afanasiev, P.; Geantet, C. Promotion Effects with Dispersed Catalysts for Residue Slurry Hydroconversion. *Fuel* **2015**, *160*, 50-56.
53. Kang, K. H.; Nguyen, N. T.; Seo, P. W.; Seo, H.; Kim, G. T.; Kang, N.; Lee, C. W.; Han, S. J.; Chung, M. C.; Park, S. Slurry-Phase Hydrocracking of Heavy Oil over Mo Precursors: Effect of Triphenylphosphine Ligands. *J. Catal.* **2020**, *384*, 106-121.
54. Schacht, P.; Díaz-García, L.; Aguilar, J.; Ramírez, S. Upgrading of Heavy Crude Oil with W-Zr Catalyst. *Adv. Chem. Eng. Sci.* **2014**, *4*, 250-257.
55. Jeong, H. R.; Lee, Y. K. Comparison of Unsupported WS₂ and MoS₂ Catalysts for Slurry Phase Hydrocracking of Vacuum Residue. *Appl. Catal., A* **2019**, *572*, 90-96.
56. Morelos-Santos, O.; de la Torre, A. R.; Melo-Banda, J. A.; Schacht-Hernández, P.; Portales-Martínez, B.; Soto-Escalante, I.; José-Yacamán, M. A Novel Direct Method in One-Step for Catalytic Heavy Crude Oil Upgrading using Iron Oxide Nanoparticles. *Catal. Today* **2022**, *392*, 60-71.
57. Luo, H.; Sun, J.; Deng, W.; Li, C.; Du, F. Preparation of Oil-Soluble Fe-Ni Sulfide Nanoparticles for Slurry-Phase Hydrocracking of Residue. *Fuel* **2022**, *321*, 124029.
58. Bdwi, E. A.; Ali, S. A.; Quddus, M. R.; Al-Bogami, S. A.; Razzak, S. A.; Hossain, M. M. Kinetics of Promotional Effects of Oil-Soluble Dispersed Metal (Mo, Co, and Fe) Catalysts on Slurry Phase Hydrocracking of Vacuum Gas Oil. *Energy Fuels* **2017**, *31*, 3132.
59. Suwaid, M. A.; Varfolomeev, M. A.; Al-Muntaser, A. A.; Yuan, C.; Starshinova, V. L.; Zinnatullin, A.; Vagizov, F. G.; Rakhmatullin, I. Z.; Emelianov, D. A.; Chemodanov, A. E. In-Situ Catalytic Upgrading of Heavy Oil using Oil-Soluble Transition Metal-Based Catalysts. *Fuel* **2020**, *281*, 118753.
60. Quitian, A.; Fernández, Y.; Ancheyta, J. Viscosity Reduction of Heavy Oil during Slurry-Phase Hydrocracking. *Chem. Eng. Technol.* **2019**, *42*, 148-155.

61. Kim, S. H.; Kim, K. D.; Lee, D.; Lee, Y. K. Structure and Activity of Dispersed Co, Ni, or Mo Sulfides for Slurry Phase Hydrocracking of Vacuum Residue. *Journal of Catalysis* **2018**, *364*, 131-140.
62. Al-Attas, T. A.; Zahir, M. H.; Ali, S. A.; Al-Bogami, S. A.; Malaibari, Z.; Razzak, S. A. Hossain, M. M. Novel (Co-, Ni)-p-tert-Butylcalix [4] Arenes as Dispersed Catalysts for Heavy Oil Upgrading: Synthesis, Characterization, and Performance Evaluation. *Energy Fuels* **2018**, *33*, 561-573.
63. Murray, A.; Omajali J.; Del Mastio, Y.; Hart A, Wood J.; Macaskie L. Potential for conversion of Waste Platinum Group Metals in Road Dust into Biocatalysts for Cracking Heavy Oil. *Adv. Mater. Res.* **2015**, *11306*, 623-626. Trans Tech Publ.
64. Hart, A.; Omajali, J. B.; Murray, A. J.; Macaskie, L. E.; Greaves, M.; Wood, J. Comparison of the Effects of Dispersed Noble Metal (Pd) Biomass Supported Catalysts with Typical Hydrogenation (Pd/C, Pd/Al₂O₃) and Hydrotreatment Catalysts (CoMo/Al₂O₃) for In-Situ Heavy Oil Upgrading with Toe-to-Heel Air Injection (THAI). *Fuel* **2016**, *180*, 367-376.
65. Hossain, M. M.; Al-Saleh, M. A.; Shalabi, M. A.; Kimura, T.; Inui, T. Pd–Rh Promoted Co/HPS Catalysts for Heavy Oil Upgrading. *Appl. Catal., A* **2004**, *278*, 65-71.
66. Panariti, N.; Del Bianco, A.; Del Piero, G.; Marchionna, M. Petroleum Residue Upgrading with Dispersed Catalysts: Part 1. Catalysts Activity and Selectivity. *Appl. Catal., A* **2000**, *204*, 203-213.
67. Fürstner, A. Iron Catalysis in Organic Synthesis: A Critical Assessment of What it Takes to Make This Base Metal a Multitasking Champion. *ACS Cent. Sci.* **2016**, *2*, 778-789.
68. Chakraborty, S.; Brennessel, W. W.; Jones, W. D. A Molecular Iron Catalyst for the Acceptorless Dehydrogenation and Hydrogenation of N-heterocycles. *J. Am. Chem. Soc.* **2014**, *136*, 8564-8567.
69. Kelly, T. D.; Matos, G. R. *Historical Statistics for Mineral and Material Commodities in the United States, 2015*; U.S. Geological Survey Data Series 140; <https://www.usgs.gov/centers/nmic/historical-statistics-mineral-and-material-commodities-united-states> (accessed on March 25, 2022).
70. Yuan, Y.; Wang, L.; Gao, L. Nano-Sized Iron Sulfide: Structure, Synthesis, Properties, and Biomedical Applications. *Front. Chem.* **2020**, *8*, 818.

71. Man, Z.; Li, P.; Zhou, D.; Wang, Y.; Liang, X.; Zang, R.; Li, P.; Zuo, Y.; Lam, Y. M.; Wang, G. Two Birds with One Stone: FeS₂@C Yolk–Shell Composite for High-Performance Sodium-Ion Energy Storage and Electromagnetic Wave Absorption. *Nano Lett.* **2020**, *20*, 3769-3777.
72. Chen, H.; Zhu, L.; Liu, H.; Li, W. Efficient Iron Sulfide Counter Electrode for Quantum Dots-Sensitized Solar Cells. *J. Power Sources* **2014**, *245*, 406-410.
73. Yang, Y.; Chen, T.; Sumona, M.; Gupta, B. S.; Sun, Y.; Hu, Z.; Zhan, X. Utilization of Iron Sulfides for Wastewater Treatment: A Critical Review. *Rev. Environ. Sci. Biotechnol.* **2017**, *16*, 289-308.
74. Rickard, D.; Luther, G. W. Chemistry of Iron Sulfides. *Chem. Rev.* **2007**, *107*, 514-562.
75. Ning, J.; Zheng, Y. G.; Young, D.; Brown, B.; Nesic, S. Thermodynamic Study of Hydrogen Sulfide Corrosion of Mild Steel. *Corrosion* **2014**, *70*, 375–389.
76. Bai, P.; Zheng, S.; Chen, C.; Zhao, H. Investigation of the Iron–Sulfide Phase Transformation in Nanoscale. *Cryst. Growth Des.* **2014**, *14*, 4295-4302.
77. Bhargava, S. K.; Garg, A.; Subasinghe, N. D. In Situ High-Temperature Phase Transformation Studies on Pyrite. *Fuel* **2009**, *88*, 988-993.
78. Gao, S.; Brown, B.; Young, D.; Singer, M. Formation of Iron Oxide and Iron Sulfide at High Temperature and Their Effects on Corrosion. *Corros. Sci.* **2018**, *135*, 167-176.
79. Anderson, R. R.; Bockrath, B. C. Effect of Sulphur on Coal Liquefaction in the Presence of Dispersed Iron or Molybdenum Catalysts. *Fuel* **1984**, *63*, 329-333.
80. Herrick, D. E.; Tierney, J. W.; Wender, I.; Huffman, G. P.; Huggins, F. E. Activity and Characterization of Coprocessing Catalysts Produced from an Iron Pentacarbonyl Precursor. *Energy Fuels* **1990**, *4*, 231.
81. Pradhan, V.; Herrick, D. E.; Tierney, J. W.; Wender, I. Finely Dispersed Iron, Iron-Molybdenum, and Sulfated Iron Oxides as Catalysts for Coprocessing Reactions. *Energy Fuels* **1991**, *5*, 712.
82. Huffman, G. P.; Ganguly, B.; Zhao, J.; Rao, K. R. P. M.; Shah, N.; Feng, Z.; Huggins, F. E.; Taghiei, M. M.; Lu, F. Structure and Dispersion of Iron-Based Catalysts for Direct Coal Liquefaction. *Energy Fuels* **1993**, *7*, 285.
83. Ogata, E.; Wei, X. Y.; Horie, K.; Nishijima, A.; Saito, I.; Ukegawa, K. Catalysis of Iron Sulfates on Hydroconversion of 1-methylnaphthalene. *Catal. Today* **1998**, *43*, 161-169.

84. Yang, L.; Sheng, J. J. Pyrite Effects on the Oxidation of In Situ Crude Oil. *J. Pet. Sci. Eng.* **2022**, *209*, 109812.
85. Murphy, R.; Strongin, D. R. Surface Reactivity of Pyrite and Related Sulfides. *Surf. Sci. Rep.* **2009**, *64*, 1–45.
86. Wang, H.; Salveson, I. A review on the Mineral Chemistry of the Non-stoichiometric Iron Sulfide, Fe_{1-x}S ($0 \leq x \leq 0.125$): Polymorphs, Phase Relations and Transitions, Electronic and Magnetic Structures. *Phase Transitions* **2005**, *78*, 547-567.
87. Belzile, N.; Chen, Y. W.; Cai, M. F.; Li, Y. A Review on Pyrrhotite Oxidation. *J. Geochem. Explor.* **2004**, *84*, 65-76.
88. Herbert, F. W. Mechanisms Governing the Growth, Reactivity and Stability of Iron Sulfides. Ph.D. Dissertation, Massachusetts Institute of Technology: Cambridge, Massachusetts, 2015.
89. Ramselaar, W. L. T. M.; Craje, M. W. J.; Hadders, R. H.; Gerkema, E.; de Beer, V. H. J.; van der Kraan, A. M. Sulfidation of Carbon-Supported Iron Oxide Catalysts. *Appl. Catal.* **1990**, *65*, 69-84.
90. Brandt, P. F.; Lesch, D. A.; Stafford, P. R.; Rauchfuss, T. B.; Kolis, J. W.; Roof, L. C. $\text{Fe}_2(\text{S}_2)(\text{CO})_6$ and $\text{Fe}_3\text{Te}_2(\text{CO})_{9,10}$. *Inorg. Synth.* **1997**, *31*, 112.
91. Seyferth, D.; Henderson, R. S.; Song, L. -C. Chemistry of μ -Dithio-bis(tricarbonyliron), a Mimic of Inorganic Disulfides. 1. Formation of Di- μ -thiolato-bis(tricarbonyliron) Dianion. *Organometallics* **1982**, *1*, 125.
92. Di Giovanni, C.; Wang, W. A.; Nowak, S.; Grenèche, J. M.; Lecoq, H.; Mouton, L.; Giraud, M.; Tard, C. Bioinspired Iron Sulfide Nanoparticles for Cheap and Long-Lived Electrocatalytic Molecular Hydrogen Evolution in Neutral Water. *ACS Catal.* **2014**, *4*, 681.
93. Ranganathan, R.; Denis, J. D.; Pruden, B. B. Hydrocracking of Heavy Oils Using Iron Coal Catalyst. U.S. Patent 4,214,977, 1980.
94. Bhattacharyya, A.; Mezza, B. J. Process for Using Catalyst with Rapid Formation of Iron Sulfide in Slurry Hydrocracking. Patent No. US 8,277,638 B2, 2012.
95. Habib, F. K.; Diner, C.; Stryker, J. M.; Semagina, N.; Gray, M. R. Suppression of Addition Reactions during Thermal Cracking Using Hydrogen and Sulfided Iron Catalyst. *Energy Fuels* **2013**, *27*, 6637.

96. Al-Marshed, A.; Hart, A.; Leeke, G.; Greaves, M.; Wood, J. Optimization of Heavy Oil Upgrading Using Dispersed Nanoparticulate Iron Oxide as a Catalyst. *Energy Fuels* **2015**, *29*, 6306-6316.
97. Dawood, F.; Anda, M.; Shafiullah, G. M. Hydrogen Production for Energy: An Overview. *Int. J. Hydrogen Energy* **2020**, *45*, 3847-3869.
98. Animation of Explosion at Tesoro's Anacortes Refinery 2010.
<https://www.youtube.com/watch?v=8vPaQYM-tWs> (accessed on November 17, 2022).
99. de Vries, J. G.; Elsevier, C. J. *The Handbook of Homogeneous Hydrogenation*; Wiley-VCH: Weinheim, 2007.
100. Wang, D.; Astruc, D. The Golden Age of Transfer Hydrogenation. *Chem. Rev.* **2015**, *115*, 6621-6686.
101. Alemán-Vázquez, L. O.; Torres-Mancera, P.; Ancheyta, J.; Ramírez-Salgado, J. Use of Hydrogen Donors for Partial Upgrading of Heavy Petroleum. *Energy Fuels* **2016**, *30*, 9050-9060.
102. Zhao, F.; Xu, T.; Zhu, G.; Wang, K.; Xu, X.; Liu, L. A Review on the Role of Hydrogen Donors in Upgrading Heavy Oil and Bitumen. *Sustainable Energy Fuels* **2022**, *6*, 1866-1890.
103. Carlson, C. S.; Langer, A. W.; Stewart, J.; Hill, R. M. Thermal hydrogenation. Transfer of Hydrogen from Tetralin to Cracked Residua. *Ind. Eng. Chem.* **1958**, *50*, 1067-1070.
104. Ignasiak, T. M.; Strausz, O. P. Reaction of Athabasca Asphaltene with Tetralin. *Fuel* **1978**, *57*, 617-621.
105. Sanford, E. C.; Xu, C. M. Relationship Between Solids Formation, Residuum Conversion, Liquid Yields and Losses During Athabasca Bitumen Processing in the Presence of a Variety of Chemicals. *Can. J. Chem. Eng.* **1996**, *74*, 347-352.
106. Alemán-Vázquez, L. O.; Cano-Domínguez, J. L.; García-Gutiérrez, J. L. Effect of Tetralin, Decalin and Naphthalene as Hydrogen Donors in the Upgrading of Heavy Oils. *Procedia Eng.* **2012**, *42*, 532-539.
107. Li, L.; Hou, Y.; Wu, W.; Liang, S.; Ren, S. Behaviors of Tetralin and 9,10-dihydroanthracene as Hydrogen Donor Solvents in the Hydrogenolysis of Coal-Related Model Compounds. *Fuel Process. Technol.* **2019**, *191*, 202-210.

108. de Vries, J. G.; Elsevier, C. J. *The Handbook of Homogeneous Hydrogenation*; Wiley-VCH: Weinheim, 2007.
109. Han, B.; Ma, P.; Cong, X.; Chen, H.; Zeng, X. Chromium- and Cobalt-Catalyzed, Regiocontrolled Hydrogenation of Polycyclic Aromatic Hydrocarbons: A Combined Experimental and Theoretical Study. *J. Am. Chem. Soc.* **2019**, *141*, 9018.
110. Liu, Z. Q.; Wei, X. Y.; Liu, F. J.; Wang, B. J.; Zong, Z.M. Temperature-Controlled Hydrogenation of Anthracene over Nickel Nanoparticles Supported on Attapulgite Powder. *Fuel* **2018**, *223*, 222.
111. Hagen, J. *Industrial Catalysis: A Practical Approach*; Wiley-VCH: Weinheim, 2015.
112. Sánchez, J.; Moreno, A.; Mondragón, F.; Smith, K. J. Morphological and Structural Properties of MoS₂ and MoS₂-Amorphous Silica-Alumina Dispersed Catalysts for Slurry-Phase Hydroconversion. *Energy Fuels* **2018**, *32*, 7066.
113. Li, Y.; Ma, F.; Su, X.; Shi, L.; Pan, B.; Sun, Z.; Hou, Y. Ultra-Large-Scale Synthesis of Fe₃O₄ Nanoparticles and Their Application for Direct Coal Liquefaction. *Ind. Eng. Chem. Res.* **2014**, *53*, 6718.
114. Stanislaus, A.; Cooper, B. H. Aromatic Hydrogenation Catalysis: A review. *Catal. Rev. Sci. Eng.* **1994**, *36*, 75.
115. Deng, W.; Lu, J.; Li, C. Hydrogenation Behavior of Bicyclic Aromatic Hydrocarbons in the Presence of a Dispersed Catalyst. *Energy Fuels* **2015**, *29*, 5600.
116. Tanimu, A.; Alhooshani, K. Advanced Hydrodesulfurization Catalysts: A Review of Design and Synthesis. *Energy Fuels* **2019**, *33*, 2810.
117. Giustra, Z. X.; Ishibashi, J. S.; Liu, S. Y. Homogeneous Metal Catalysis for Conversion between Aromatic and Saturated Compounds. *Coord. Chem. Rev.* **2016**, *314*, 134.
118. Li, H.; Liu, J.; Li, J.; Hu, Y.; Wang, W.; Yuan, D.; Wang, Y.; Yang, T.; Li, L.; Sun, H.; Ren, S. Promotion of the Inactive Iron Sulfide to an Efficient Hydrodesulfurization Catalyst. *ACS Catal.* **2017**, *7*, 4805.
119. Habib, F. K.; Diner, C.; Stryker, J. M.; Semagina, N.; Gray, M.R. Suppression of Addition Reactions during Thermal Cracking Using Hydrogen and Sulfided Iron Catalyst. *Energy Fuels* **2013**, *27*, 6637.

120. Huffman, G. P.; Ganguly, B.; Zhao, J.; Rao, K. R. P. M.; Shah, N.; Feng, Z.; Huggins, F. E.; Taghiei, M. M.; Lu, F. Structure and Dispersion of Iron-Based Catalysts for Direct Coal Liquefaction. *Energy Fuels* **1993**, *7*, 285.
121. Herrick, D. E.; Tierney, J. W.; Wender, I.; Huffman, G. P.; Huggins, F. E. Activity and Characterization of Coprocessing Catalysts Produced from an Iron Pentacarbonyl Precursor. *Energy Fuels* **1990**, *4*, 231.
122. Tang, Y.; Curtis, C. W. Activity and Selectivity of Slurry-Phase Iron-Based Catalysts for Model Systems. *Energy Fuels* **1994**, *8*, 63.
123. Kelly, T. D.; Matos, G. R. *Historical Statistics for Mineral and Material Commodities in the United States, 2015*; U.S. Geological Survey Data Series 140; <https://www.usgs.gov/centers/nmic/historical-statistics-mineral-and-material-commodities-united-states>. Accessed on March 16, 2020.
124. Suzuki, T.; Yamada, H.; Sears, P. L.; Watanabe, Y. Hydrogenation and Hydrogenolysis of Coal Model Compounds by Using Finely Dispersed Catalysts. *Energy Fuels* **1989**, *3*, 707.
125. Gray, M. R. Fundamentals of Partial Upgrading of Bitumen. *Energy Fuels* **2019**, *33*, 6843.
126. Pradhan, V.; Herrick, D. E.; Tierney, J. W.; Wender, I. Finely Dispersed Iron, Iron-Molybdenum, and Sulfated Iron Oxides as Catalysts for Coprocessing Reactions. *Energy Fuels* **1991**, *5*, 712.
127. Quitian, A.; Ancheyta, J. Experimental Methods for Developing Kinetic Models for Hydrocracking Reactions with Slurry-Phase Catalyst Using Batch Reactors. *Energy Fuels* **2016**, *30*, 4419.
128. Del Bianco, A.; Panariti, N.; Di Carlo, S.; Elmouchnino, J.; Fixari, B.; Le Perchec, P. Thermocatalytic Hydroconversion of Heavy Petroleum Cuts with Dispersed Catalyst. *Appl. Catal.* **1993**, *94*, 1.
129. Gray, M. R. *Upgrading Oilsands Bitumen and Heavy Oil*; University of Alberta Press: Edmonton, Alberta, Canada, 2015.
130. Akbarzadeh, K.; Bressler, D.C.; Wang, J.; Gawrys, K. L.; Gray, M.R.; Kilpatrick, P.K.; Yarranton, H. W. Association Behavior of Pyrene Compounds as Models for Asphaltene. *Energy Fuels* **2005**, *19*, 1268.
131. Alshareef, A. H. Asphaltene: Definition, Properties, and Reactions of Model Compounds. *Energy Fuels* **2020**, *34*, 16.

132. Wei, C. H.; Dahl, L. F. The Molecular Structure of a Tricyclic Complex, $[\text{SFe}(\text{CO})_3]_2$. *Inorg. Chem.* **1965**, *4*, 1.
133. Brandt, P. F.; Lesch, D. A.; Stafford, P. R.; Rauchfuss, T. B.; Kolis, J. W.; Roof, L. C. $\text{Fe}_2(\text{S}_2)(\text{CO})_6$ and $\text{Fe}_3\text{Te}_2(\text{CO})_{9,10}$. *Inorg. Synth.* **1997**, *31*, 112.
134. Seyferth, D.; Henderson, R. S.; Song, L. -C. Chemistry of μ -Dithio-bis(tricarbonyliron), a Mimic of Inorganic Disulfides. 1. Formation of Di- μ -thiolato-bis(tricarbonyliron) Dianion. *Organometallics* **1982**, *1*, 125.
135. Di Giovanni, C.; Wang, W. A.; Nowak, S.; Grenèche, J.M.; Lecoq, H.; Mouton, L.; Giraud, M.; Tard, C. Bioinspired Iron Sulfide Nanoparticles for Cheap and Long-Lived Electrocatalytic Molecular Hydrogen Evolution in Neutral Water. *ACS Catal.* **2014**, *4*, 681.
136. Stanley, J. L.; Rauchfuss, T. B.; Wilson, S.R. Studies on the Condensation Pathway to and Properties of Diiron Azadithiolate Carbonyls. *Organometallics* **2007**, *26*, 1907.
137. Pratt, A. R.; Muir, I. J.; Nesbitt, H. W. X-ray Photoelectron and Auger Electron Spectroscopic Studies of Pyrrhotite and Mechanism of Air Oxidation. *Geochim. Cosmochim. Acta* **1994**, *58*, 827.
138. Jones, C. F.; LeCount, S.; Smart, R. S. C.; White, T. J. Compositional and Structural Alteration of Pyrrhotite Surfaces in Solution: XPS and XRD Studies. *Appl. Surf. Sci.* **1992**, *55*, 65.
139. Buckley, A. A.; Woods, R. X-ray Photoelectron Spectroscopy of Oxidized Pyrrhotite Surfaces: I. Exposure to Air. *Appl. Surf. Sci.* **1985**, *22*, 280.
140. Matamoros-Veloza, A.; Cespedes, O.; Johnson, B. R. G.; Stawski, T. M.; Terranova, U.; de Leeuw, N. H.; Benning, L. G. A Highly Reactive Precursor in the Iron Sulfide System. *Nat. Commun.* **2018**, *9*, 3125.
141. Smart, R. S. C.; Skinner, W. M.; Gerson, A. R. XPS of Sulphide Mineral Surfaces: Metal-Deficient, Polysulphides, Defects and Elemental Sulphur. *Surf. Interface Anal.* **1999**, *28*, 101.
142. Lin, Q.; Shimizu, K. I.; Satsuma, A. Hydrogenation of Pyrene Using Pd Catalysts Supported on Tungstated Metal Oxides. *Appl. Catal., A* **2010**, *387*, 166.
143. Tang, T.; Yin, C.; Wang, L.; Ji, Y.; Xiao, F. S. Good Sulfur Tolerance of a Mesoporous Beta Zeolite-Supported Palladium Catalyst in the Deep Hydrogenation of Aromatics. *J. Catal.* **2008**, *257*, 125.

144. Ting, P. S.; Curtis, C. W.; Cronauer, D. C. Reactions of Model Compounds in the Presence of Pyrene and MoS₂ to Simulate Coprocessing. *Energy Fuels* **1992**, *6*, 511.
145. Johnston, K. P. Hydrogenation-dehydrogenation of Pyrenes Catalysed by Sulphided Cobalt-Molybdate at Coal Liquefaction Conditions. *Fuel* **1984**, *63*, 463.
146. Korre, S. C.; Klein, M. T.; Quann, R. J. Polynuclear Aromatic Hydrocarbons Hydrogenation. 1. Experimental Reaction Pathways and Kinetics. *Ind. Eng. Chem. Res.* **1995**, *34*, 101.
147. Minabe, M.; Nakada, K. Hydrogenation of Pyrene and Catalytic Interconversion of Hydropyrenes. *Bull. Chem. Soc. Jpn.* **1985**, *58*, 1962.
148. Fu, P. P.; Lee, H. M.; Harvey, R. G. Regioselective Catalytic Hydrogenation of Polycyclic Aromatic Hydrocarbons under Mild Conditions. *J. Org. Chem.* **1980**, *45*, 2797.
149. Zhang, L.; Zhou, M.; Wang, A.; Zhang, T. Selective Hydrogenation over Supported Metal Catalysts: From Nanoparticles to Single Atoms. *Chem. Rev.* **2020**, *120*, 683.
150. Sun, L. B.; Zong, Z. M.; Kou, J. H.; Zhang, L. F.; Ni, Z. H.; Yu, G. Y.; Chen, H.; Wei, X. Y.; Lee, C. W. Activated Carbon-Catalyzed Hydrogenation of Polycyclic Arenes. *Energy Fuels* **2004**, *18*, 1500.
151. Sun, L. B.; Zong, Z. M.; Kou, J. H.; Liu, G. F.; Sun, X.; Wei, X. Y.; Zhou, G. J.; Lee, C. W. Activated Carbon-Catalyzed Hydrogen Transfer to α,ω -Diarylalkanes. *Energy Fuels* **2005**, *19*, 1.
152. Sun, L. B.; Wei, X. Y.; Liu, X. Q.; Zong, Z. M.; Li, W.; Kou, J. H. Selective Hydrogen Transfer to Anthracene and Its Derivatives over an Activated Carbon. *Energy Fuels* **2009**, *23*, 4877.
153. Olson, B. J. *The Role of Sulfur during the Cracking of n-Hexadecane and Cold Lake Bitumen with Alpha-Fe₂O₃ and Steam*; M.Sc. Thesis, University of Alberta, Edmonton, AB, CA, 2013.
154. Buchanan, R. H.; Jameson, G.; Oedjoe, D. Cyclic Migration of Bubbles in Vertically Vibrating Liquid Columns. *Ind. Eng. Chem. Fundam.* **1962**, *1*, 82.
155. Still, A. L.; Ghajar, A. J.; O'Hern, T.J. Effect of Amplitude on Mass Transport, Void Fraction and Bubble Size in a Vertically Vibrating Liquid-Gas Bubble Column Reactor. In *Proceedings of the ASME Fluids Engineering Summer Meeting, FEDSM2013*, Incline Village, NV, USA, July 7-11, 2013.

156. Elbing, B. R.; Still, A. L.; Ghajar, A. J. Review of bubble column reactors with vibration. *Ind. Eng. Chem. Res.* **2016**, *55*, 385.
157. Dutta, R. P.; Schobert, H. H. Hydrogenation/dehydrogenation of Polycyclic Aromatic Hydrocarbons Using Ammonium Tetrathiomolybdate as Catalyst Precursor. *Catal. Today* **1996**, *31*, 65.
158. Lemberon, J. L.; Guisnet, M. Phenanthrene Hydroconversion as a Potential Test Reaction for the Hydrogenating and Cracking Properties of Coal Hydroliquefaction Catalysts. *Appl. Catal.* **1984**, *13*, 181.
159. Girgis, M. J.; Gates, B. C. Reactivities, Reaction Networks, and Kinetics in High-Pressure Catalytic Hydroprocessing. *Ind. Eng. Chem. Res.* **1991**, *30*, 2021.
160. Girgis, M. J.; Gates, B. C. Catalytic Hydroprocessing of Simulated Heavy Coal Liquids. 2. Reaction Networks of Aromatic Hydrocarbons and Sulfur and Oxygen Heterocyclic Compounds. *Ind. Eng. Chem. Res.* **1994**, *33*, 2301.
161. Bhore, N. A.; Klein, M. T.; Bischoff, K. B. The Delplot Technique: A New Method for Reaction Pathway Analysis. *Ind. Eng. Chem. Res.* **1990**, *29*, 313.
162. Bhore, N. A.; Klein, M. T.; Bischoff, K. B. Species Rank in Reaction Pathways: Application of Delplot Analysis. *Chem. Eng. Sci.* **1990**, *45*, 2109.
163. Klein, M. T.; Hou, Z.; Bennett, C. Reaction Network Elucidation: Interpreting Delplots for Mixed Generation Products. *Energy Fuels* **2012**, *26*, 52.
164. Huang, T. C.; Kang, B. C. Hydrogenation of Naphthalene with Platinum-Aluminium Borate Catalysts. *Chem. Eng. J.* **1996**, *63*, 27.
165. Villasana, Y.; Ruscio-Vanalesti, F.; Pfaff, C.; Méndez, F. J.; Luis-Luis, M. Á.; Brito, J. L. Atomic Ratio Effect on Catalytic Performance of FeW-Based Carbides and Nitrides on Thiophene Hydrodesulfurization. *Fuel* **2013**, *110*, 259.
166. Curtis, C. W.; Chen, J. H.; Tang, Y. Hydrodesulfurization of Model Systems Using Slurry-Phase Catalysts. *Energy Fuels* **1995**, *9*, 195.
167. Srivastava, V. C. An Evaluation of Desulfurization Technologies for Sulfur Removal from Liquid Fuels. *RSC Adv.* **2012**, *2*, 759.
168. Huo, Z.; Jin, F.; Yao, G.; Enomoto, H.; Kishita, A. An in Situ Raman Spectroscopic Study of Benzothiophene and Its Desulfurization under Alkaline Hydrothermal Conditions. *Ind. Eng. Chem. Res.* **2015**, *54*, 1397.

169. Van Parijs, I. A.; Hosten, L. H.; Froment, G. F. Kinetics of Hydrodesulfurization on a CoMo/ γ -Al₂O₃ Catalyst. 2. Kinetics of the Hydrogenolysis of Benzothiophene. *Ind. Eng. Chem. Prod. Res. Dev.* **1986**, *25*, 437.
170. Wang, H.; Prins, R. HDS of Benzothiophene and Dihydrobenzothiophene over Sulfided Mo/ γ -Al₂O₃. *Appl. Catal., A* **2008**, *350*, 191.
171. Guin, J. A.; Lee, J. M.; Fan, C. W.; Curtis, C. W.; Lloyd, J. L.; Tarrer, A. R. Pyrite-Catalyzed Hydrogenolysis of Benzothiophene at Coal Liquefaction Conditions. *Ind. Eng. Chem. Process Des. Dev.* **1980**, *19*, 440.
172. Ogilvy, A. E.; Draganjac, M.; Rauchfuss, T. B.; Wilson, S. R. Activation and Desulfurization of Thiophene and Benzothiophene by Iron Carbonyls. *Organometallics* **1988**, *7*, 1171.
173. Gray, M. R. Fundamentals of Partial Upgrading of Bitumen. *Energy Fuels* **2019**, *33*, 6843.
174. Colyar, J. I. M. Has the Time for Partial Upgrading of Heavy Oil and Bitumen Arrived? *Pet. Technol. Q.* **2009**, Q14, 43.
175. Keesom, W.; Gieseman, J. *Bitumen Partial Upgrading 2018 Whitepaper AM0401A*; Alberta Innovates: Calgary, AB, **2018**; pp 152.
176. Zuo, P.; Qu, S.; Shen, W. Asphaltenes: Separations, Structural Analysis and Applications. *J. Energy Chem.* **2019**, *34*, 186.
177. Castaneda, L. C.; Munoz, J. A.; Ancheyta, J. Current Situation of Emerging Technologies for Upgrading of Heavy Oils. *Catal. Today* **2014**, *220*, 248.
178. Zachariah, A.; de Klerk, A. Partial Upgrading of Bitumen: Impact of Solvent Deasphalting and Visbreaking Sequence. *Energy Fuels* **2017**, *31*, 9374.
179. Xing, T.; Alvarez-Majmutov, A.; Chen, J. Bitumen Partial Upgrading by Mild Hydroprocessing in a Fixed-bed Reactor. *Fuel* **2019**, *235*, 696.
180. Hepler, L. G.; His, C. AOSTRA Technical Handbook on Oil Sands Bitumen and Heavy Oils. AOSTRA Technical Publication Series, vol. 6. Edmonton: Alberta Oil Sands Technology and Research Authority; 1989.
181. Li, C.; Li, J.; Yang, T.; Deng, W. Formation of Ni–MoS₃ Hollow Material with Enhanced Activity in Slurry-phase Hydrogenation of Heavy Oil. *Energy Fuels* **2019**, *33*, 10933.

182. Montanari, R.; Marchionna, M.; Rosi, S.; Panariti, N.; Delbianco, A.; SnamProgetti SpA; EniTecnologie SpA; ENI SpA, **2010**. Process for the Conversion of Heavy Charges Such as Heavy Crude Oils and Distillation Residues. U.S. Patent 7,691,256.
183. Bdwi, E. A.; Ali, S. A.; Quddus, M. R.; Al-Bogami, S. A.; Razzak, S. A.; Hossain, M. M. Kinetics of Promotional Effects of Oil-Soluble Dispersed Metal (Mo, Co, and Fe) Catalysts on Slurry Phase Hydrocracking of Vacuum Gas Oil. *Energy Fuels* **2017**, *31*, 3132.
184. Du, H.; Li, M.; Liu, D.; Ren, Y.; Duan, Y. Slurry-Phase Hydrocracking of Heavy Oil and Model Reactant: Effect of Dispersed Mo Catalyst. *Appl. Petrochem. Res.* **2015**, *5*, 89.
185. Nguyen, M. T.; Nguyen, N. T.; Cho, J.; Park, C.; Park, S.; Jung, J.; Lee, C. W. A Review on the Oil-soluble Dispersed Catalyst for Slurry-phase Hydrocracking of Heavy Oil. *J. Ind. Eng. Chem.* **2016**, *43*, 1.
186. Angeles, M. J.; Leyva, C.; Ancheyta, J.; Ramírez, S. A Review of Experimental Procedures for Heavy Oil Hydrocracking with Dispersed Catalyst. *Catal. Today* **2014**, *220*, 274.
187. Rana, M. S.; Samano, V.; Ancheyta, J.; Diaz, J. A. I. A Review of Recent Advances on Process Technologies for Upgrading of Heavy Oils and Residua. *Fuel* **2007**, *86*, 1216.
188. Zhang, S.; Liu, D.; Deng, W.; Que, G. A Review of Slurry-Phase Hydrocracking Heavy Oil Technology. *Energy Fuels* **2007**, *21*, 3057.
189. Quitian, A.; Ancheyta, J. Experimental Methods for Developing Kinetic Models for Hydrocracking Reactions with Slurry-Phase Catalyst Using Batch Reactors. *Energy Fuels* **2016**, *30*, 4419.
190. Li, Y.; Ma, F.; Su, X.; Shi, L.; Pan, B.; Sun, Z.; Hou, Y. Ultra-Large-Scale Synthesis of Fe₃O₄ Nanoparticles and Their Application for Direct Coal Liquefaction. *Ind. Eng. Chem. Res.* **2014**, *53*, 6718.
191. Suzuki, T.; Yamada, H.; Sears, P. L.; Watanabe, Y. Hydrogenation and hydrogenolysis of Coal Model Compounds by Using Finely Dispersed Catalysts. *Energy Fuels* **1989**, *3*, 707.
192. Kamiya, Y.; Nobusawa, T.; Futamura, S. Catalytic Effects of Iron Compounds and the Role of Sulfur in Coal Liquefaction and Hydrogenolysis of SRC. *Fuel Process. Technol.* **1988**, *18*, 1.
193. Suzuki, T.; Yamada, O.; Takahashi, Y.; Watanabe, Y. Hydroliquefaction of Low-Sulfur Coals Using Iron Carbonyl Complexes-Sulfur as Catalysts. *Fuel Process. Technol.* **1985**, *10*, 33.

194. Tang, Y.; Curtis, C.W. Activity and Selectivity of Slurry-Phase Iron-Based Catalysts for Model Systems. *Energy Fuels* **1994**, *8*, 63.
195. Hurt, M. R.; Borton, D. J.; Choi, H. J.; Kenttämaa, H. I. Comparison of the Structures of Molecules in Coal and Petroleum Asphaltenes by Using Mass Spectrometry. *Energy Fuels* **2013**, *27*, 3653.
196. Tang, W.; Hurt, M. R.; Sheng, H.; Riedeman, J. S.; Borton, D. J.; Slater, P.; Kenttämaa, H. I. Structural Comparison of Asphaltenes of Different Origins Using Multi-Stage Tandem Mass Spectrometry. *Energy Fuels* **2015**, *29*, 1309.
197. Hata, K.A.; Wada, K.; Mitsudo, T. A. Iron-Catalyzed Coprocessing of Coals and Vacuum Residues Using Syngas– Water as a Hydrogen Source. *Energy Fuels* **1998**, *12*, 1181.
198. Groenzin, H.; Mullins, O. C. Molecular Size and Structure of Asphaltenes from Various Sources. *Energy Fuels* **2000**, *14*, 677.
199. Gray, M. R. *Upgrading Oilsands Bitumen and Heavy Oil*; University of Alberta Press: Edmonton, Alberta, Canada, 2015.
200. Alshareef, A.H. Asphaltenes: Definition, Properties, and Reactions of Model Compounds. *Energy Fuels* **2020**, *34*, 16.
201. Akbarzadeh, K.; Bressler, D.C.; Wang, J.; Gawrys, K.L.; Gray, M.R.; Kilpatrick, P.K.; Yarranton, H.W. Association Behavior of Pyrene Compounds as Models for Asphaltenes. *Energy Fuels* **2005**, *19*, 1268.
202. Khattab, S. A.; Markó, L.; Bor, G.; Markó, B. Sulphur-Containing Metal Carbonyls VI. A Mixed Cobalt-Iron Carbonyl Sulphide. *J. Organomet. Chem.* **1964**, *1*, 373.
203. Di Giovanni, C.; Wang, W. A.; Nowak, S.; Grenèche, J. M.; Lecoq, H.; Mouton, L.; Giraud, M.; Tard, C. Bioinspired Iron Sulfide Nanoparticles for Cheap and Long-Lived Electrocatalytic Molecular Hydrogen Evolution in Neutral Water. *ACS Catal.* **2014**, *4*, 681.
204. Han, B.; Ma, P.; Cong, X.; Chen, H.; Zeng, X. Chromium- and Cobalt-Catalyzed, Regiocontrolled Hydrogenation of Polycyclic Aromatic Hydrocarbons: A Combined Experimental and Theoretical Study. *J. Am. Chem. Soc.* **2019**, *141*, 9018.
205. Tunega, D.; Zaoui, A. Adsorption of Polycyclic Aromatic Hydrocarbons on FeOOH Polymorphs: A Theoretical Study. *Surf. Sci.* **2021**, *706*, 121795.

206. Dang, Y.; Liu, Y.; Feng, X.; Chen, X.; Yang, C. Effect of Dispersion on the Adsorption of Polycyclic Aromatic Hydrocarbons over the γ -Al₂O₃ (110) Surface. *Appl. Surf. Sci.* **2019**, *486*, 137.
207. Cowley, S.; Wisler, W. The Thermodynamics of Anthracene Hydrocracking. *Fuel Process Technol.* **1979**, *2*, 317.
208. Girgis, M. J.; Gates, B. C. Reactivities, Reaction Networks, and Kinetics in High-Pressure Catalytic Hydroprocessing. *Ind. Eng. Chem. Res.* **1991**, *30*, 2021.
209. Li, L.; Yucui, H.; Weize, W.; Shisheng, L.; Shuhang, R. Behaviors of Tetralin and 9,10-dihydroanthracene as Hydrogen Donor Solvents in the Hydrogenolysis of Coal-Related Model Compounds. *Fuel Process. Technol.* **2019**, *191*, 202.
210. Chen, Z.; Xie, J.; Liu, Q.; Wang, H.; Gao, S.; Shi, L.; Liu, Z. Characterization of Direct Coal Liquefaction Catalysts by Their Sulfidation Behavior and Tetralin Dehydrogenation Activity. *J. Energy Inst.* **2019**, *92*, 1213.
211. Sun, L. B.; Wei, X. Y.; Liu, X. Q.; Zong, Z. M.; Li, W.; Kou, J. H. Selective Hydrogen Transfer to Anthracene and Its Derivatives over an Activated Carbon. *Energy Fuels* **2009**, *23*, 4877.
212. Yue, X. M.; Wei, X. Y.; Zhang, S. Q.; Liu, F. J.; Zong, Z. M. Yang, X. Q. Hydrogenation of Polycyclic Aromatic Hydrocarbons Over a Solid Superacid. *Fuel Process. Technol.* **2017**, *161*, 283.
213. Ting, P. S.; Curtis, C. W.; Cronauer, D. C. Reactions of Model Compounds in the Presence of Pyrene and Molybdenum Sulfide (MoS₂) to Simulate Coprocessing. *Energy Fuels* **1992**, *6*, 511.
214. Pinilla, J. L.; Garcia, A. B.; Philippot, K.; Lara, P.; Garcia-Suarez, E. J.; Millan, M. Carbon-Supported Pd Nanoparticles as Catalysts for Anthracene Hydrogenation. *Fuel* **2014**, *116*, 729.
215. Zhang, L.; Zhou, M.; Wang, A.; Zhang, T. Selective Hydrogenation over Supported Metal Catalysts: From Nanoparticles to Single Atoms. *Chem. Rev.* **2020**, *120*, 683.
216. Wei, Z.; Shao, F.; Wang, J. Recent Advances in Heterogeneous Catalytic Hydrogenation and Dehydrogenation of N-Heterocycles. *Chin. J. Catal.* **2019**, *40*, 980.
217. Shen, J.; Semagina, N. Inhibition of Diolefin Hydrogenation by Quinoline. *Energy Fuels* **2020**, *34*, 8769.

218. Nagai, M.; Sato, T.; Aiba, A. Poisoning Effect of Nitrogen Compounds on Dibenzothiophene Hydrodesulfurization on Sulfided NiMoAl₂O₃ Catalysts and Relation to Gas-Phase Basicity. *J. Catal.* **1986**, *97*, 52.
219. Curtis, C. W.; Chung, W. J. Effect of Coal and Residuum on Reactions Occurring in Coal-Petroleum Processing. *Energy Fuels* **1989**, *3*, 148.
220. Kim, H.; Curtis, C.W. Reaction Pathways of Model Coprocessing Systems Using Molybdenum Naphthenate and Excess Sulfur. *Energy Fuels* **1990**, *4*, 206.
221. Curtis, C. W.; Chen, J. H.; Tang, Y. Hydrodesulfurization of Model Systems Using Slurry-Phase Catalysts. *Energy Fuels* **1995**, *9*, 195.
222. Sahoo, B.; Kreyenschulte, C.; Agostini, G.; Lund, H.; Bachmann, S.; Scalone, M.; Junge, K.; Beller, M. A Robust Iron Catalyst for the Selective Hydrogenation of Substituted (iso) Quinolones. *Chem. Sci.* **2018**, *9*, 8134.
223. Pinilla, J. L.; Purón, H., Torres, D.; Suelves, I.; Millan, M. Ni-MoS₂ Supported on Carbon Nanofibers as Hydrogenation Catalysts: Effect of Support Functionalization. *Carbon*, **2015**, *81*, 574.
224. Boudjahem, A. G.; Redjel, A.; Mokrane, T. Preparation, Characterization and Performance of Pd/SiO₂ Catalyst for Benzene Catalytic Hydrogenation. *J. Ind. Eng. Chem.* **2012**, *18*, 303.
225. Montano, P. A.; Stenberg, V. I.; Sweeny, P. In Situ Study of the Hydrogenation of Diphenyl Ether in the Presence of Pyrrhotite and Hydrogen Sulfide. *J. Phys. Chem.* **1986**, *90*, 156.
226. Herrick, D. E.; Tierney, J. W.; Wender, I.; Huffman, G. P.; Huggins, F. E. Activity and Characterization of Coprocessing Catalysts Produced from an Iron Pentacarbonyl Precursor. *Energy Fuels* **1990**, *4*, 231.
227. Zhang, Z. G.; Okada, K.; Yamamoto, M.; Yoshida, T. Hydrogenation of Anthracene over Active Carbon-Supported Nickel Catalyst. *Catal. Today* **1998**, *45*, 361.
228. Zhang, L.; Zhou, M.; Wang, A.; Zhang, T. Selective Hydrogenation Over Supported Metal Catalysts: From Nanoparticles to Single Atoms. *Chem. Rev.* **2020**, *120*, 683.
229. Wiesenfeldt, M. P.; Nairoukh, Z.; Dalton, T.; Glorius, F. Selective Arene Hydrogenation for Direct Access to Saturated Carbo- and Heterocycles. *Angew. Chem. Int. Ed.* **2019**, *58*, 10460.

230. Wang, D.; Astruc, D. The Golden Age of Transfer Hydrogenation. *Chem. Rev.* **2015**, *115*, 6621.
231. Knoevenagel, E.; Bergdolt, B. Ueber das Verhalten Des Δ 2.5-Dihydroterephthalsäuredimethylesters Bei Höheren Temperaturen und in Gegenwart Von Palladiummohr. *Ber. Dtsch. Chem. Ges.* **1903**, *36*, 2857.
232. Gelis, C.; Heusler, A.; Nairoukh, Z.; Glorius, F. Catalytic Transfer Hydrogenation of Arenes and Heteroarenes. *Chem. - Eur. J.* **2020**, *26*, 14090.
233. Wang, Y.; Cao, X.; Zhao, L.; Pi, C.; Ji, J.; Cui, X.; Wu, Y. Generalized Chemoselective Transfer Hydrogenation/Hydrodeuteration. *Adv. Synth. Catal.* **2020**, *362*, 4119.
234. Espinal-Viguri, M.; Neale, S. E.; Coles, N. T.; Macgregor, S. A.; Webster, R. L. Room Temperature Iron-Catalyzed Transfer Hydrogenation and Regioselective Deuteration of Carbon–Carbon Double Bonds. *J. Am. Chem. Soc.* **2019**, *141*, 572.
235. Chen, F.; Sahoo, B.; Kreyenschulte, C.; Lund, H.; Zeng, M.; He, L.; Junge, K.; Beller, M. Selective Cobalt Nanoparticles for Catalytic Transfer Hydrogenation of N-Heteroarenes. *Chem. Sci.* **2017**, *8*, 6239.
236. Vermaak, V.; Vosloo, H. C.; Swarts, A. J. Fast and Efficient Nickel (II)-Catalysed Transfer Hydrogenation of Quinolines with Ammonia Borane. *Adv. Synth. Catal.* **2020**, *362*, 5788.
237. Wienhöfer, G.; Westerhaus, F. A.; Jagadeesh, R. V.; Junge, K.; Junge, H.; Beller, M. Selective Iron-Catalyzed Transfer Hydrogenation of Terminal Alkynes. *Chem. Commun.* **2012**, *48*, 4827.
238. Zhang, P.; Li, X.; Qi, X.; Sun, H.; Fuhr, O.; Fenske, D. Transfer Hydrogenation of Aldehydes Catalyzed by Silyl Hydrido Iron Complexes Bearing a [PSiP] Pincer Ligand. *RSC Adv.* **2018**, *8*, 14092.
239. Wienhöfer, G.; Westerhaus, F. A.; Junge, K.; Beller, M. Fast and Selective Iron-Catalyzed Transfer Hydrogenations of Aldehydes. *J. Organomet. Chem.* **2013**, *744*, 156.
240. Magubane, M. N.; Nyamato, G. S.; Ojwach, S. O.; Munro, O. Q. Structural, Kinetic, and DFT Studies of the Transfer Hydrogenation of Ketones Mediated by (Pyrazole)pyridine Iron(II) and Nickel(II) Complexes. *RSC Adv.* **2016**, *6*, 65205.
241. Pan, H. -J.; Ng, T. W.; Zhao, Y. Iron-Catalyzed Transfer Hydrogenation of Imines Assisted by an Iron-Based Lewis Acid. *Org. Biomol. Chem.* **2016**, *14*, 5490.
242. Gray, M. R. Fundamentals of Partial Upgrading of Bitumen. *Energy Fuels* **2019**, *33*, 6843.

243. Philippov, A. A.; Chibiryaev, A. M.; Martyanov, O. N. Catalyzed Transfer Hydrogenation by 2-propanol for Highly Selective PAHs Reduction. *Catal. Today*. **2021**, *379*, 15.
244. Zhao, Y.; Gray, M. R.; Wei, F. Rejuvenation of Residue Hydroconversion Catalysts by H-Donor Solvents. *Catal. Lett.* **2008**, *125*, 69.
245. Winiarek, P.; Fedoryńska, E.; Cholewiński, P. Transfer Hydrogenation of Phenanthrene in the Presence of Boron Modified Alumina or Silica-alumina. *React. Kinet. Catal. Lett.* **1995**, *55*, 191.
246. Linford-Wood, T. G.; Coles, N. T.; Webster, R. L. Room Temperature Iron Catalyzed Transfer Hydrogenation Using n-Butanol and Poly(methylhydrosiloxane). *Green Chem.* **2021**, *23*, 2703.
247. Li, L.; Hou, Y.; Wu, W.; Liang, S.; Ren, S. Behaviors of Tetralin and 9,10-dihydroanthracene as Hydrogen Donor Solvents in the Hydrogenolysis of Coal-Related Model Compounds. *Fuel Process. Technol.* **2019**, *191*, 202.
248. Alemán-Vázquez, L. O.; Torres-Mancera, P.; Ancheyta, J.; Ramírez-Salgado, J. Use of Hydrogen Donors for Partial Upgrading of Heavy Petroleum. *Energy Fuels* **2016**, *30*, 9050.
249. Kim, D. W.; Jeon, P. R.; Moon, S.; Lee, C. H. Upgrading of Petroleum Vacuum Residue Using a Hydrogen-donor Solvent with Acid-Treated Carbon. *Energy Convers. Manage.* **2018**, *161*, 234.
250. Alemán-Vázquez, L. O.; Cano-Domínguez, J. L.; García-Gutiérrez, J. L. Effect of Tetralin, Decalin and Naphthalene as Hydrogen Donors in the Upgrading of Heavy Oils. *Procedia Eng.* **2012**, *42*, 532.
251. Ovalles, C.; Rodriguez, H. Extra Heavy Crude Oil Downhole Upgrading Using Hydrogen Donors Under Cyclic Steam Injection Conditions: Physical and Numerical Simulation Studies. *J. Can. Pet. Technol.* **2008**, 4701.
252. Park, H. -B.; Kim, K. -D.; Lee, Y. -K. Promoting Asphaltene Conversion by Tetralin for Hydrocracking of Petroleum Pitch. *Fuel* **2018**, *222*, 105.
253. Zhang, Z. G.; Yoshida, T. Behavior of Hydrogen Transfer in the Hydrogenation of Anthracene Over Activated Carbon. *Energy Fuels* **2001**, *15*, 708.
254. Salazar, N.; Schmidt, S. B.; Lauritsen, J. V. Adsorption of Nitrogenous Inhibitor Molecules on MoS₂ and CoMoS Hydrodesulfurization Catalysts Particles Investigated by Scanning Tunneling Microscopy. *J. Catal.* **2019**, *370*, 232.

255. Nagai, M.; Kabe, T. Selectivity of Molybdenum Catalyst in Hydrodesulfurization, Hydrodenitrogenation, and Hydrodeoxygenation: Effect of Additives on Dibenzothiophene Hydrodesulfurization. *J. Catal.* **1983**, *81*, 440.
256. Lavopa, V.; Satterfield, C. N. Poisoning of Thiophene Hydrodesulfurization by Nitrogen-Compounds. *J. Catal.* **1988**, *110*, 375.
257. Gould, K. A.; Wiehe, I. A. Natural Hydrogen Donors in Petroleum Resids. *Energy Fuels* **2007**, *21*, 1199.
258. Guin, J. A.; Curtis, C. W.; Kwon, K. C. Pyrite-Catalysed Coal Liquefaction Using Quinoline/Tetrahydroquinoline as an H-Donor System. *Fuel* **1983**, *62*, 1412.
259. Chen, X.; Yang, Z.; Chen, X.; Liang, W.; Zhu, Z.; Xie, F.; Li, Y. Hydrogen-Transfer-Mediated N-Arylation of Naphthols Using Indolines as Hydrogen Donors. *J. Org. Chem.* **2020**, *85*, 508.
260. Fu, C. M.; Schaffer, A. M. Effect of Nitrogen Compounds on Cracking Catalysts. *Ind. Eng. Chem. Prod. Res. Dev.* **1985**, *24*, 68.
261. Ho, T. C.; Katritzky, A. R.; Cato, S. J. Effect of Nitrogen Compounds on Cracking Catalysts. *Ind. Eng. Chem. Res.* **1992**, *31*, 1589.
262. Shen, J.; Semagina, N. Inhibition of Diolefin Hydrogenation by Quinoline. *Energy Fuels* **2020**, *34*, 8769.
263. Hegedűs, L.; Szőke-Molnár, K.; Sajó, I. E.; Sranko, D. F.; Schay, Z. Poisoning and Reuse of Supported Precious Metal Catalysts in the Hydrogenation of N-Heterocycles Part I: Ruthenium-Catalysed Hydrogenation of 1-methylpyrrole. *Catal. Lett.* **2018**, *148*, 1939.
264. Zhang, Z. G.; Okada, K.; Yamamoto, M.; Yoshida, T. Hydrogenation of Anthracene Over Active Carbon-Supported Nickel Catalyst. *Catal. Today*, **1998**, *45*, 361.
265. Pinilla, J. L.; Arcelus-Arrillaga, P.; Puro, H.; Millan, M. Reaction Pathways of Anthracene Selective Catalytic Steam Cracking Using a NiK/Al₂O₃ Catalyst. *Fuel* **2013**, *109*, 303.
266. Girgis, M. J.; Gates, B. C. Reactivities, Reaction Networks, and Kinetics in High-Pressure Catalytic Hydroprocessing. *Ind. Eng. Chem. Res.* **1991**, *30*, 2021.
267. Cowley, S.; Wiser, W. The Thermodynamics of Anthracene Hydrocracking. *Fuel Process. Technol.* **1979**, *2*, 317.

268. Sun, L. B.; Wei, X. Y.; Liu, X. Q.; Zong, Z. M.; Li, W.; Kou, J. H. Selective Hydrogen Transfer to Anthracene and Its Derivatives over an Activated Carbon. *Energy Fuels* **2009**, *23*, 4877.
269. Chen, F.; Surkus, A. E.; He, L.; Pohl, M. M.; Radnik, J.; Topf, C.; Junge, K.; Beller, M. Selective Catalytic Hydrogenation of Heteroarenes with N-Graphene-Modified Cobalt Nanoparticles (Co₃O₄-Co/NGr@ α -Al₂O₃). *J. Am. Chem. Soc.* **2015**, *137*, 11718.
270. Sridharan, V.; Suryavanshi, P. A.; Menendez, J. C. Advances in the Chemistry of Tetrahydroquinolines. *Chem. Rev.* **2011**, *111*, 7157.

Appendix A: Chapter 2 Supporting Information

A.1. Product ranks and reaction network schemes

While no attempts have been made to establish mechanistic pathways for these arene hydrogenations, close inspection of the available data using the Delplot technique¹⁻³ reveals some information about the order of appearance of each reaction product in the catalytic reactions. First-rank Delplots display product selectivity (product yield/ conversion) as a function of reactant conversion, with primary products possessing a positive intercept, whereas nonprimary ones have intercepts equal to zero. This technique has been used to classify products of hydrocracked asphaltene over NiMo/ γ -Al₂O₃,⁴ and is being adopted by a number of catalysis researchers.⁵⁻⁹ In the present study, examination of the first-rank Delplot intercepts (Figure A1a-c) provide discrimination between products, suggesting that dihydropyrene (**5**), dihydrophenanthrene (**9**), tetrahydrophenanthrene (**10**), and dihydrobenzothiophene (**12**) were primary products while tetrahydropyrene (**6**) and ethylbenzene (**13**) were secondary products, as reported in previous studies.¹⁰⁻¹³ The data for the hexahydropyrenes (**7** and **8**) were inconclusive; therefore, second-rank Delplots, which displays product yield/conversion² ratio, were plotted against reactant conversion. In this plot, secondary products are identified by a curve with a finite non-zero y-intercept, while primary products are identified by the divergent behavior of the representative line.³ As seen in Figure A1d-f, divergent behavior of the curves representing the dihydropyrene, dihydrophenanthrene, tetrahydrophenanthrene, and dihydrobenzothiophene confirms that these are primary products. Conversely, the line for hexahydropyrenes has a positive intercept (Figure A1d) indicating secondary product status. These identifications are preliminary and based on the limited data currently available; further experiments are necessary to establish conclusively the product rankings. Naphthalene hydrogenation produced a single product; hence its reaction

network was straightforward. The proposed reaction networks for all substrates are presented in Figure A2.

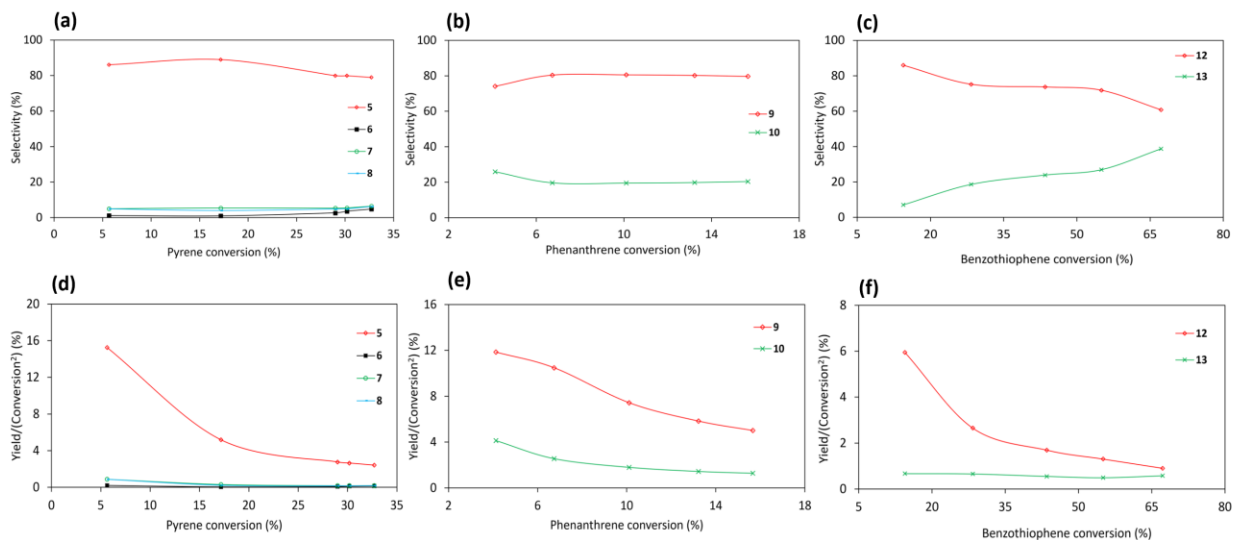


Figure A1. First-rank Delplots of (a) pyrene and (b) phenanthrene, and (c) benzothiophene. Second-rank Delplots of (d) pyrene, (e) phenanthrene, and (f) benzothiophene. Reaction conditions: temperature; 250-350 °C; cold H₂, 6 MPa; activated carbon, 0.1 g; time, 60 min.

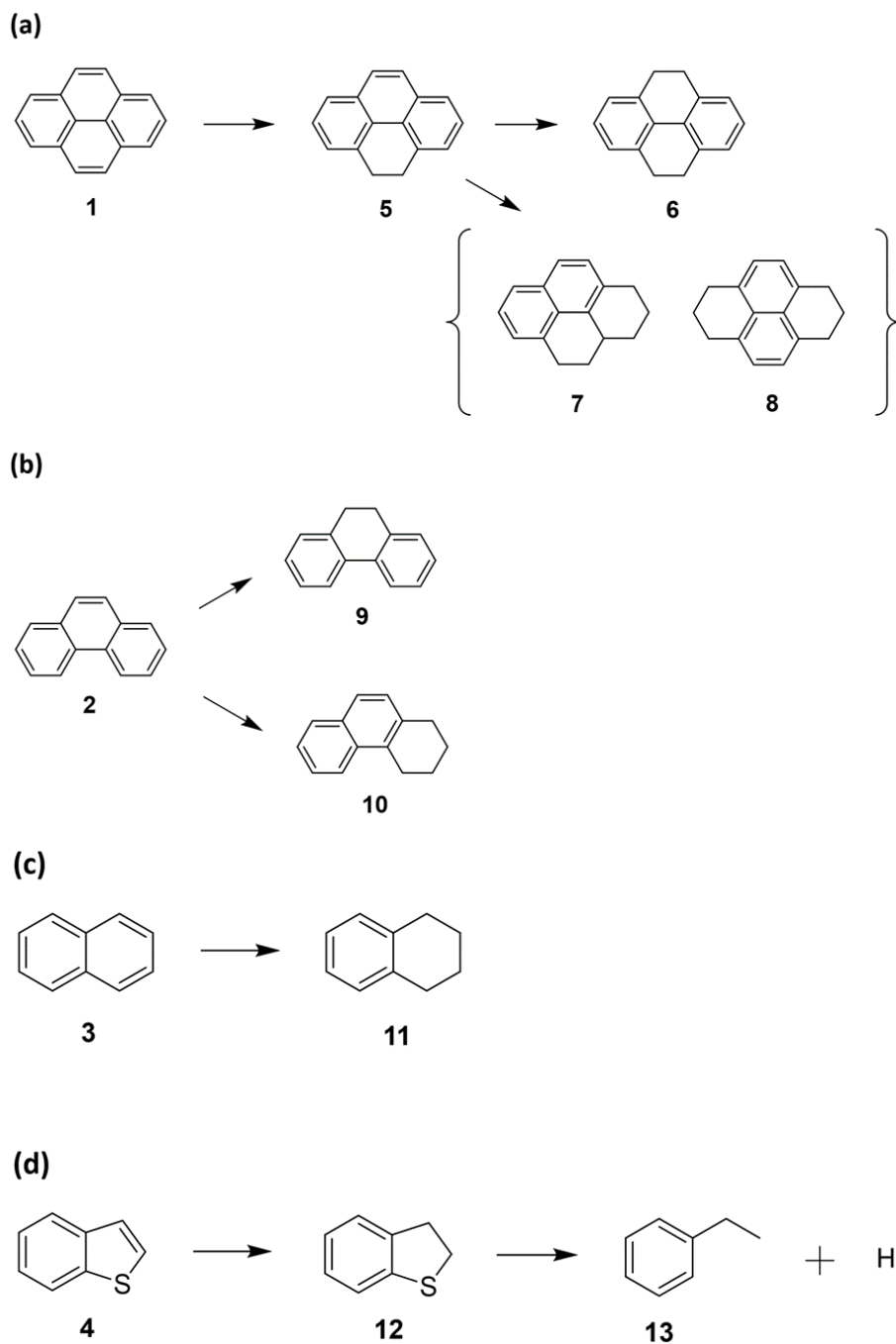


Figure A2. Reaction networks proposed for (a) pyrene, (b) phenanthrene, and (c) naphthalene, hydrogenation, and (d) benzothiophene hydrodesulfurization over $\text{Fe}_2\text{S}_2(\text{CO})_6$. Structures: 4,5-dihydropyrene (**5**), 4,5,9,10-tetrahydropyrene (**6**), 1,2,3,3a,4,5-hexahydropyrene (**7**), 1,2,3,6,7,8-hexahydropyrene (**8**), 9,10-dihydrophenanthrene (**9**), 1,2,3,4-tetrahydrophenanthrene (**10**), 1,2,3,4-tetrahydronaphthalene (**11**), 2,3-dihydrobenzothiophene (**12**), and ethylbenzene (**13**).

References to Appendix A

1. Bhore, N. A.; Klein, M. T.; Bischoff, K. B. The Delplot Technique: A New Method for Reaction Pathway Analysis. *Ind. Eng. Chem. Res.* **1990**, *29*, 313.
2. Bhore, N. A.; Klein, M. T.; Bischoff, K. B. Species Rank in Reaction Pathways: Application of Delplot Analysis. *Chem. Eng. Sci.* **1990**, *45*, 2109.
3. Klein, M. T.; Hou, Z.; Bennett, C. Reaction Network Elucidation: Interpreting Delplots for Mixed Generation Products. *Energy Fuels* **2012**, *26*, 52.
4. Zhao, Y.; Yu, Y. Kinetics of Asphaltene Thermal Cracking and Catalytic Hydrocracking. *Fuel Process. Technol.* **2011**, *92*, 977.
5. Miller, J. H.; Bui, L.; Bhan, A. Pathways, Mechanisms, and Kinetics: A Strategy to Examine Byproduct Selectivity in Partial Oxidation Catalytic Transformations on Reducible Oxides. *React. Chem. Eng.* **2019**, *4*, 784.
6. Sheehan, J. D.; Savage, P. E. Reaction Pathways and Kinetics of Tryptophan in Hot, Compressed Water. *Chem. Eng. J.* **2020**, *390*, 124600.
7. Smith, C. M.; Savage, P. E. Reactions of Polycyclic Alkylaromatics: 5. Pyrolysis of Methylantracenes. *AIChE J.* **1993**, *39*, 1355.
8. Yun, G. N.; Ghampson, I. T.; Movick, W. J.; Vargheese, V.; Kobayashi, Y.; Oyama, S. T. Applicability of the Delplot Method for the Determination of Catalytic Reaction Sequences: Hydrodeoxygenation of γ -valerolactone on Ni₂P/MCM-41. *Chem. Eng. Sci.* **2020**, *223*, 115697.
9. Schachtl, E.; Zhong, L.; Kondratieva, E.; Hein, J.; Gutiérrez, O. Y.; Jentys, A.; Lercher, J. A. Understanding Ni Promotion of MoS₂/ γ -Al₂O₃ and Its Implications for the Hydrogenation of Phenanthrene. *ChemCatChem* **2015**, *7*, 4118.
10. Schachtl, E.; Yoo, J. S.; Gutiérrez, O. Y.; Studt, F.; Lercher, J. A. Impact of Ni Promotion on the Hydrogenation Pathways of Phenanthrene on MoS₂/ γ -Al₂O₃. *J. Catal.* **2017**, *352*, 171.
11. Lin, Q.; Shimizu, K. I.; Satsuma, A. Hydrogenation of Pyrene Using Pd Catalysts Supported on Tungstated Metal Oxides. *Appl. Catal., A* **2010**, *387*, 166.
12. Curtis, C. W.; Chen, J. H.; Tang, Y. Hydrodesulfurization of Model Systems Using Slurry-Phase Catalysts. *Energy Fuels* **1995**, *9*, 195.

13. Yang, H.; Wang, Y.; Jiang, H.; Weng, H.; Liu, F.; Li, M. Kinetics of Phenanthrene Hydrogenation System over CoMo/Al₂O₃ Catalyst. *Ind. Eng. Chem. Res.* **2014**, *53*, 12264.

Appendix B: Chapter 3 Supporting Information

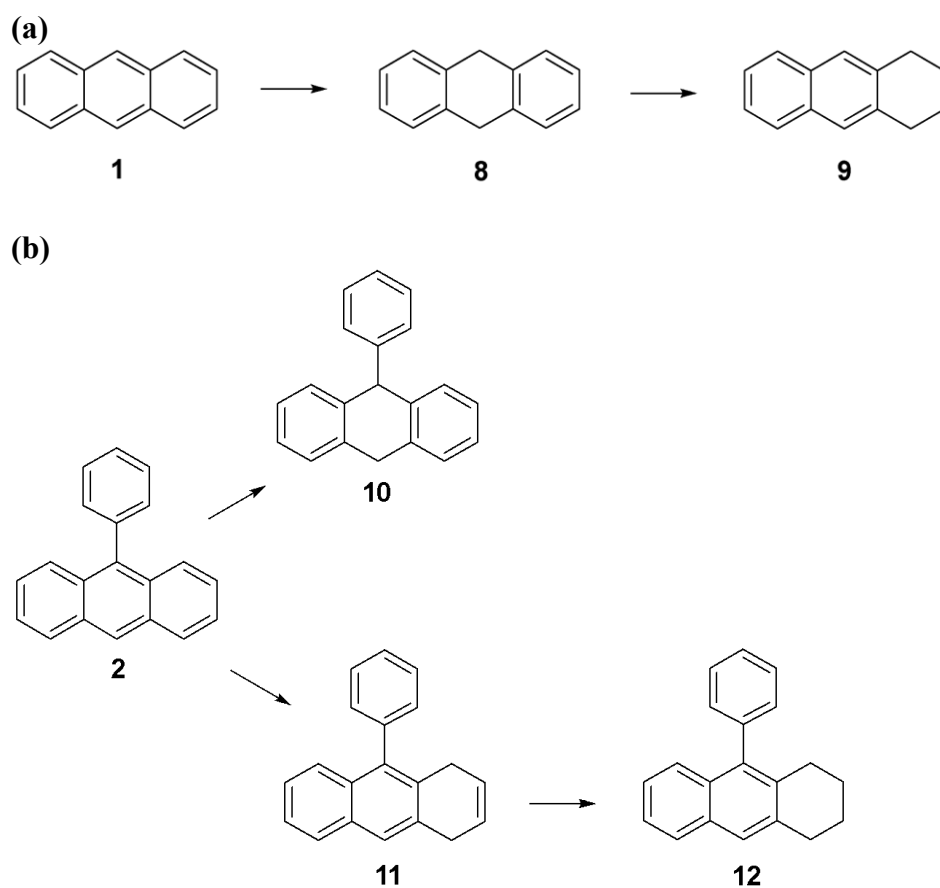


Figure B1. Reaction networks proposed for (a) anthracene and (b) 9-phenylanthracene hydrogenation over unsupported Fe₂S₂(CO)₆. Structures: anthracene (1), 9-phenylanthracene (2), 9,10-dihydroanthracene (8), 1,2,3,4-tetrahydroanthracene (9), 9,10-dihydrophenylanthracene (10), 1,4-dihydrophenylanthracene (11), and 1,2,3,4-tetrahydrophenylanthracene (12).

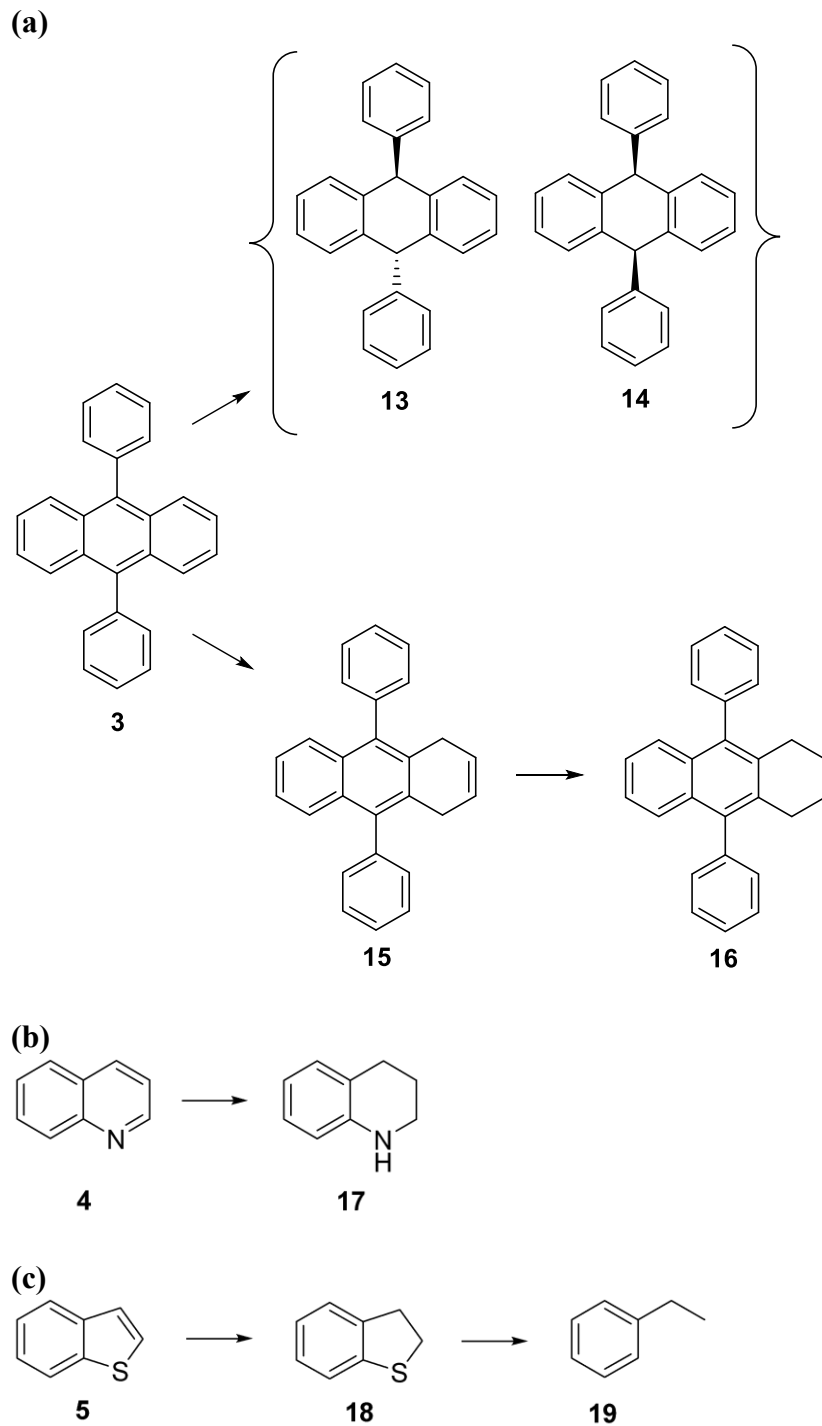


Figure B2. Reaction networks for hydrogenation (a) 9,10-diphenylanthracene (b) quinoline as well as hydrosulfurization of (c) benzothiophene over unsupported $\text{Fe}_2\text{S}_2(\text{CO})_6$. Structures: 9,10-diphenylanthracene (**3**), quinoline (**4**), benzothiophene (**5**), trans-9,10-dihydro-9,10-diphenylanthracene (**13**), cis-9,10-dihydro-9,10-diphenylanthracene (**14**), 1,2,3,4-tetrahydrodiphenylanthracene (**15**), 1,4-dihydrodiphenylanthracene (**16**), 1,2,3,4-tetrahydroquinoline (**17**), 2,3-dihydrobenzothiophene (**18**), and ethylbenzene (**19**).

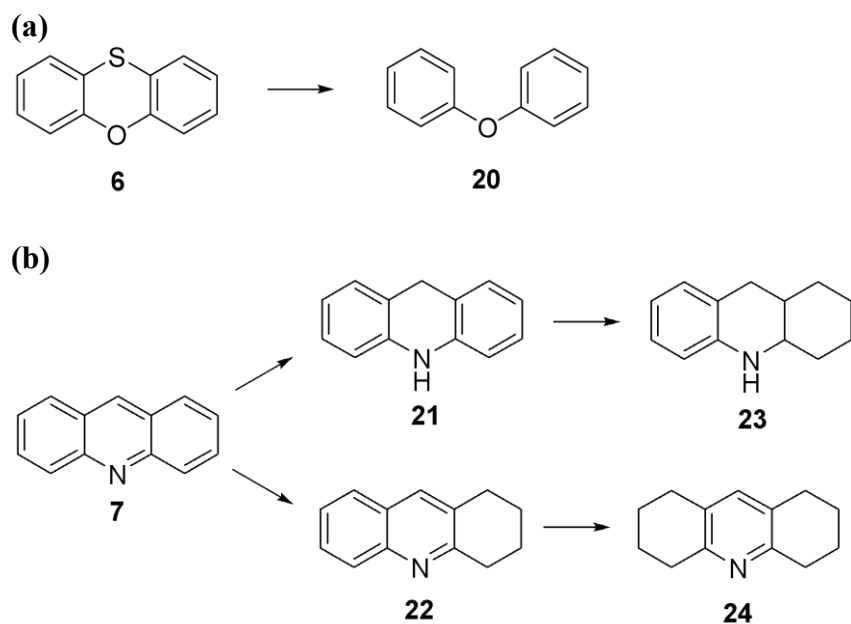


Figure B3. Reaction networks for hydrotreating of (a) phenoxathiin and (b) acridine. Structures: phenoxathiin (**6**), acridine (**7**), diphenyl ether (**20**), 9,10-dihydroacridine (**21**), 1,2,3,4-tetrahydroacridine (**22**), 1,2,3,4,4a,9,9a,10-octahydroacridine (**23**), and 1,2,3,4,5,6,7,8-octahydroacridine (**24**).

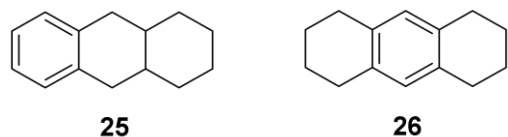


Figure B4. Structures of 1,2,3,4,4a,9,9a,10-octahydroanthracene (**25**) and 1,2,3,4,5,6,7,8-octahydroanthracene (**26**).

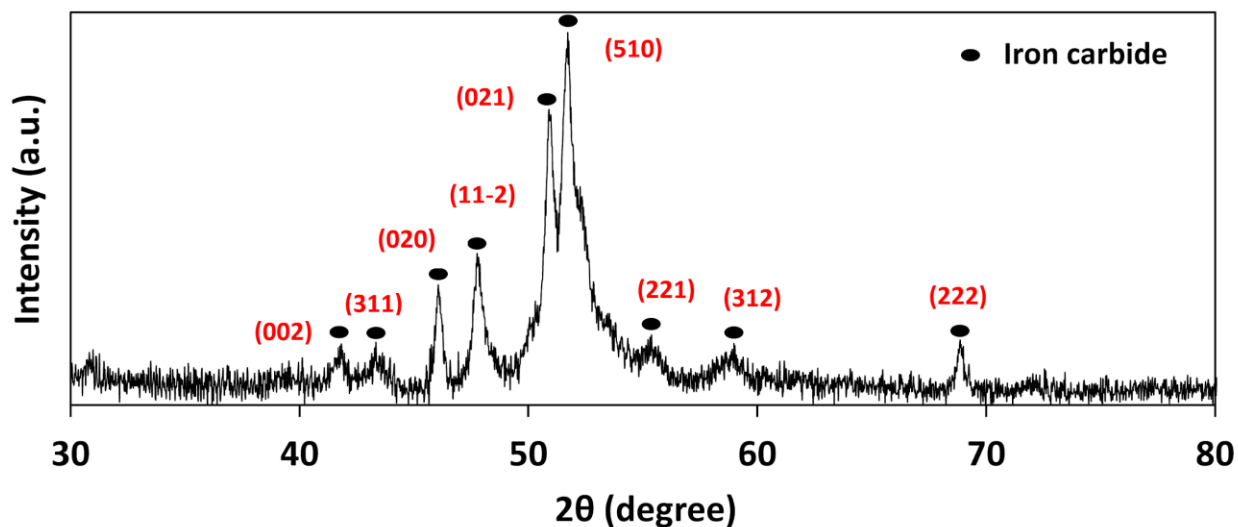


Figure B5. XRD pattern of unsupported catalyst derived from $\text{Fe}(\text{CO})_5$ at 300 °C and 60 min. It is ascribed to iron carbide phase (Jade 9.0 PDF No. 00-036-1248).

References to Appendix B

1. Zawadski, R.; Shih, S. S.; Reiff, E.; Katzer, J. R.; Kwart, H. "Kinetics and Mechanism of Catalytic Hydroprocessing of Components of Coal-Derived Liquids: Tenth and Eleventh Quarterly Reports for the Period August 16, 1981 to February 15, 1982"; Prepared for Office of Fossil Energy, Department of Energy, Washington, DC, 1982.
2. Girgis, M. J.; Gates, B. C. Reactivities, Reaction Networks, and Kinetics in High-Pressure Catalytic Hydroprocessing. *Ind. Eng. Chem. Res.* **1991**, *30*, 2021.